ROYAUME DU MAROC
Université Mohammed V - RABAT - جامعة محمد الخامس - الرباط -
Faculté des sciences كلية العلوم

CENTRE D'ETUDES DOCTORALES - SCIENCES ET TECHNOLOGIES

N° d'ordre: **3499**

PhD THESIS

In order to obtain the: ***DOCTORATE***

Research Structure: Laboratory of Condensed Matter Physics and Interdisciplinary Sciences
Discipline: Condensed Matter Physics
Specialty: Computational Physics and material science

Defended on the 10/07/2021 by:

Younes SBAI

Ab initio and Monte Carlo study of the magnetic and electronic properties of Transition Metal doped DMSs: GaN and GaAs

JURY

Hamid EZ-ZAHRAOUY	PES, Faculty of Sciences, Mohammed V University - Rabat	Président
Lahoucine BAHMAD	PES, Faculty of sciences, Mohammed V University– Rabat	Superviseur
Mohammed AGGOUR	PES, Faculty of sciences, Ibn Tofail University - Kénitra	Examinateur / Rapporteur
Bousselham KABOUCHI	PES, Faculty of sciences, Mohammed V University - Rabat	Examinateur / Rapporteur
Mohammed BENAISSA	PES, Faculty of sciences, Mohammed V University - Rabat	Examinateur / Rapporteur
Rachid MASROUR	PES, Faculty of sciences Dhar El Mahraz, Sidi Mohamed Ben Abdelaah University – Fés	Examinateur / Rapporteur
Abdelilah BENYOUSSEF	PES, Academy Hassan II of Sciences and Techniques - Rabat	Invité d'honneur

Academic year : **2020/2021**

Faculté des Sciences, avenue Ibn Battouta, BP. 1014 RP, Rabat –Maroc
☎ 00212(05) 37 77 18 76 00212(05) 37 77 42 61; http://www. fsr.um5.ac.ma

DEDICATION

I would like to dedicate my thesis work to my family and special friends.

I have a deeply felt gratitude to my mother for her support, motivation and patience, and my gratitude goes also to my brothers and sister.

I would like to thank a special group of friends for their push and motivational words they gave me all the time.

I am grateful to every person who supported me throughout this road.

I appreciate you all.

ACKNOWLEDGEMENTS

It’s been an absolute honor for me to carry out this PhD thesis at the previously called Laboratory of Magnetism and High Energy Physics (LMPHE) and newly called Laboratory of Condensed Matter Physics and Interdisciplinary Sciences (LMCSi), in our beloved Faculty of Science, Mohammed V University – Rabat, under the supervision of Professor **Lahoucine BAHMAD**.

I would like to begin by giving all praises and thanks to Allah, the Almighty, for his unlimited and uncountable blessings in my whole life, in the ups and downs and especially throughout my research work. It hasn’t been easy.
At this moment, I would like to thank all people who made this thesis possible, my family for their patience with me and friends for their help and support.

This PhD thesis has been a huge experience for me not just in scientific research but in life in general, I began this PhD thesis as a person and finished it as a different person. I learned a lot in Life. It has been an unforgettable experience for me.

I want to express my deepest sense of Gratitude (with a capital and bold g) to my supervisor Professor **Lahoucine BAHMAD**, who offered his continuous advice and encouragement throughout the course of this thesis. He supervised my work from the beginnings. During my bachelor degree, then my master degree, and now in my doctorate. I thank him for the systematic guidance and great effort he put into training me in the scientific field.

I would like to express my very sincere gratitude to Professor **Hamid EZ ZAHRAOUY**, our laboratory director from the Faculty of Sciences Rabat, for being the president of the jury of my thesis defense and for his help and support during my thesis.

I’m really thankful to Professor **Mohammed AGGOUR** from the Faculty of Sciences Kenitra, for accepting to be (examinateur/ rapporteur) in my thesis. For accepting to review the thesis, beside the precious time he gave me and for being member of the committee of my PhD defense, and not to forget his valuable remarks.

I extend my gratitude to Professor **Bousselham KABOUCHI** from the Faculty of Sciences Rabat, for being (examinateur/ rapporteur) in my thesis and for his time, the remarks he gave me and for accepting to review my thesis.

I would like to thank Professor **Mohammed BENAISSA** from the Faculty of Sciences Rabat, for accepting to be (examinateur/ rapporteur) in my thesis, and for his willingness to review and evaluate my thesis and his precious time.

I present also my thankfulness and appreciation to Professor **Rachid MASROUR** from the Faculty of Sciences Dhar el Mahraz, Fés, for accepting to be (examinateur/ rapporteur) in my thesis, for the time he gave me, for his review of my PhD thesis and being a member of the jury.

And last but not least, I am especially thankful and grateful to my co-supervisor Professor **Abdelillah BENYOUSSEF** from the Faculty of Sciences Rabat, for accepting to be an honorable guest in my PhD defense. For his countless hours of reflecting, reading, encouraging, and most of all his patience throughout the entire process. And not to forget his Positive Energy he conveys and his valuable remarks.
He is the example of a hard worker and respected professor who never hesitate to bring his help to any student.

Résumé

La spintronique connait actuellement un avancement qui vise à améliorer les nouvelles hétérostructures semi-conductrices pour augmenter la densité des composants, améliorer les performances et baisser les prix. L'objectif est de fusionner des matériaux magnétiques avec des semi-conducteurs afin de trouver des matériaux pouvant fonctionner à une température supérieure à la température ambiante et d'avoir un couplage d'échange ferromagnétique. Dans cette thèse, nous avons réalisé, d'une part, une étude théorique utilisant des calculs Ab initio via le code (AkaiKKR) basée sur la méthode (DFT) avec les deux approximations LDA et GGA. Les principaux matériaux utilisés dans nos calculs sont le Nitrure de Gallium (GaN) et l'Arséniure de Gallium (GaAs), les deux dopé avec des métaux de transition (Mn, Fe and Ni) dans le but d'étudier leur propriétés électroniques, magnétiques et magnéto-optiques. Pour GaN, les DOS et les diagrammes de bands d'énergie ont été calculés, le ferromagnétisme a été observé avec un comportement half- métallique pour une concentration de 5% de Mn avec un gap direct. Tandis que pour GaAs les DOS ont été calculé aussi ainsi que les états magnétiques et la stabilité magnétique du matériau pour différents pourcentages de dopage, la rotation de Faraday a été aussi observé pour le dopage avec le fer (Fe). Confirmant ainsi ces deux DMS comme candidats principaux pour les applications spintroniques.

Mots-Clés : DMS; Calcules Ab initio ; Simulation Monte Carlo ; Propriétés magnétiques ; DOS ; structures de bandes ; Ferromagnétisme.

Abstract

There is currently a huge advancement in the spintronic field aimed at improving new semiconductor heterostructures in order to increase the components density, improve the performance and lower the prices. The objective is to fuse magnetic materials with semiconductors in order to find new materials that can operate above room temperature and have a ferromagnetic exchange coupling. In this thesis, we carried out a theoretical study using Ab initio calculations via (AkaiKKR) code based on the (DFT) method with the two approximations LDA and GGA. The main materials used in our calculations are Gallium Nitride (GaN) and Gallium Arsenide (GaAs), both doped with transition metals (Mn, Fe and Ni) so as to study their electronic, magnetic and magneto-optical properties. For GaN, the DOS and energy band diagrams were calculated and plotted, ferromagnetism was found with half-metallic behavior for a concentration of 5% (Mn) with a direct gap. While for GaAs the DOS were calculated as well as the magnetic states and the magnetic stability of the material for each (Fe) and (Ni) doping concentrations. The Faraday rotation was also observed for Ga(Fe)As. Thus, asserting these two DMSs as main candidates for spintronic applications.

Keywords: DMSs; Ab initio calculations; Monte Carlo simulation; Magnetic properties; DOS; Band Structures; Ferromagnetism.

Résumé (detailed)

Le domaine de la spintronique connait actuellement un avancement qui vise à améliorer les nouvelles hétérostructures semi-conductrices pour augmenter la densité des composants, améliorer les performances et baisser les prix. L'objectif est de fusionner des matériaux magnétiques avec des semi-conducteurs afin d'intégrer, dans un même appareil, des fonctions de mémoire, de détection et de traitement de signaux.

Le but des études actuelles sur la science des matériaux est de trouver des matériaux pouvant fonctionner à une température supérieure à la température ambiante et d'avoir un couplage d'échange ferromagnétique entre les impuretés magnétiques. Dans ce cadre, les méthodes de calcul structurel, par exemple les méthodes ab initio, sont très précieuses et utiles pour le développement de ces matériaux et leurs applications en spintronique et nanotechnologie. Ces méthodes sont utilisées pour calculer les propriétés structurelles, mécaniques, électriques et magnétiques du matériau ciblé en vue d'industrialisation de ses matériaux.

Dans cette thèse, nous avons réalisé, d'une part, une étude théorique utilisant des calculs Ab initio de premier principe via la méthode Korringha Kohn Rostoker (KKR) (KKR-CPA) basée sur la théorie de la fonctionnelle de la densité (DFT) que nous décrirons plus en détail ci-dessous. , à côté des différentes approximations utilisées dans les calculs. Afin d'étudier les propriétés électroniques et magnétiques de deux des plus importants semi-conducteurs magnétiques dilués (DMS) dopés avec des atomes de métaux de transition (TM). Les DMS sont très utiles et beaucoup plus intéressants lorsqu'ils sont dopés avec des impuretés magnétiques (TM), ce qui en fait des matériaux très importants pour le développement de dispositifs spintroniques. Les principaux matériaux utilisés dans nos calculs sont le nitrure de gallium (GaN) et l'arséniure de gallium (GaAs), tous deux sont des semi-conducteurs à bande interdite directe III-V. Le premier matériau est du GaN que nous avons dopé au Manganèse (Mn), pour différentes concentrations d'impuretés magnétiques, nous avons calculé la Densité d'Etats (DOS) pour chaque concentration de dopage. Il montre un comportement semi-métallique et un état ferromagnétique en particulier pour $Ga_{0.95}$ $Mn_{0.05}$ N. En plus de cela, l'aimantation et la susceptibilité suivant la température ont été calculées à l'aide d'une simulation Monte Carlo pour différentes tailles de système, afin d'étudier l'effet de taille. De plus, la température de transition

a été déduite de la susceptibilité. Le second matériau est du GaAs dopé au fer (Fe) et au Nickel (Ni), nous avons étudié l'effet de chaque rapport d'impuretés magnétiques insérées dans la structure, sur les propriétés magnétiques et électroniques du matériau et les phénomènes de rotation de Faraday en tant que magnéto- propriété optique. Nous avons trouvé l'état magnétique et calculé leur énergie associée. Nous donnons également l'état magnétique stable pour le matériau dopé. Les propriétés électroniques telles que la densité d'états (DOS) sont en bon accord avec les données théoriques. Ainsi, GaN et GaAs, lorsqu'ils sont dopés avec la concentration correcte et précise d'impuretés magnétiques, sont des semi-conducteurs très intéressants et d'énormes candidats pour les applications spintroniques et les cellules photovoltaïques également.

Cette thèse sera répartie en quatre chapitres; le premier présentera un aperçu général du domaine de la spintronique et ses applications. Ainsi qu’une présentation sur les semi-conducteurs magnétiques dilués: leurs types, propriétés, avantages et pourquoi le choix de ces matériaux dans ce travail.

Le deuxième chapitre portera sur les méthodes de calcul utilisées dans notre travail, avec les différentes approximations et structures manipulées dans ces calculs et simulations.

Le troisième chapitre sera consacré à l'étude Ab initio des propriétés magnétiques et électroniques du GaN dopé au Mn à côté de la simulation Monte Carlo du système. Tandis que dans le quatrième chapitre on va traiter le cas de GaAs co-dopé avec Ni et Fe, donnant ainsi les états magnétiques et la stabilité magnétique aussi avec une vue sur la Rotation de Faraday.

Enfin, nous clôturons la thèse par une conclusion générale et éventuelles perspectives.

List of Content:

Dedications
Acknowledgments
Résumé
Abstract
Résumé (detailed)
List of contents
Abbreviations
Figures and tables
General Introduction

Chapter 1: The Spintronic field: Applications and DMS

I.1. Introduction: Spintronic ……………………………………………….........................5

I.2. Applications and Technologies………………………………………………………...8

I.2.1. Giant magneto-resistance GMR…………………………………………………......8

I.2.2. Tunneling magneto-resistance TMR…………………………………………….....10

I.2.3. Magnetic random access memories MRAMs……………………………………….12

I.2.4. Spin field effect transistor……………………………………………………….....14

I.2.5. Spin torque oscillators ………………………………………………………………15

I.3. Diluted magnetic semiconductors (DMSs)…………………………………………….15

I.4. DMSs synthesis methods ……………………………………………………………...16

I.5. DMS types: A variety of DMS materials……………………………………………....19

I.6. Benefits of the II-VI and II-V based DMSs……………………………………………20

I.7. The studied materials……………………………………………………………….. 21

I.7.1 Gallium Nitrid GaN…………………………………………………………………….21

I.7.2 Gallium Arsenid GaAs………………………………………………………………25

I.8. Outlook on the magnetic interactions in DMSs…………………………………………..27

I.8.1. Direct exchange interaction……………………………………………………….....28

I.8.2. Indirect exchange interaction…………………………………………………………29

I.8.2.1 Double exchange interaction……………………………………………………30

I.8.2.2 Super exchange interaction……………………………………………/.....31

I.8.3 Ruderman- Kittel- Kasuya- Yoshida (RKKY) Interactions…………………………...32

I.8.4 Zener model……………………………………………………………………………33

I.8.5 Magnetic polarons model……………………………………………………………...33

I.10. Presentation of different magnetic behaviors……………………………………………....34

I.10.1 Diamagnetism……………………………………………………………………….35

I.10.2 Paramagnetism……………………………………………………………………...36

I.10.3 Ferrimagnetism……………………………………………………………………..38

I.10.4 Ferromagnetism…………………………………………………………………….39

I.10.5 Antiferromagnetism………………………………………………………………...40

I.11. Conclusion……………………………………………………………………………...41

Chapter 2: Calculation Methods: Ab initio and Monte Carlo:

II.1. Ab initio method: …...43

II.1.1. Introduction ……………………………………………………………………......43

II.1.2. Concept of the Density functional theory (DFT)………………………………………..44

II.1.2.1. The N-body problem……………………………………………………...45

II.1.2.2. The Born-Oppenheimer approximation………………………………………...46

II.1.2.3. The Hohenberg-Kohn theorems……………………………………………...47

II.1.2.4. The Kohn-sham arstaz equations…………………………………………………48

II.1.2.4.a. Solving the kohn-sham equations………………………………………49

II.1.2.5. The Hartree-Fock approximation……………………………………………….50

II.1.2.6. The exchange-correlation-energy……………………………………………….51

II.1.3. Ab initio Approximations……………………………………………………………..52

II.1.3.1. The Local Density Approximation (LDA)……………………………….......52

II.1.3.2. The Generalized Gradient Approximation (GGA)……………………...……53

II.1.3.3. The approximations of the local density and the generalized gradient with the Hubbard correction (LDA + U and GGA + U) …………………………………………………….…53

II.1.3.4 The Linearized augmented plane wave method……………………………….…...54

II.1.3.4-a. Definition of the Linearized Augmented Plane Wave (LAPW) method…………………………………………………………………………………………54

II.1.3.4-b. Definition of the Linearized Augmented Plane Wave with Local orbitals (LAPW+LO) method……………………………………………………………………………55

II.1.3.4-c. Insight on the Full Potential Linearized Augmented Plane Wave (FP-LAPW) method……………………………………………………………………………………………...56

II.1.4. The Calculation code_ AKAIKKR……………………………………………………….....57

II.1.4.1. Outlook on the AKAI code……………………………………………...……57

II.1.4.2. Studied Materials and Calculation details………………………………………58

II.1.4.2-a. Gallium Nitride (GaN) case………………………………………......58

II.1.4.2-b. Gallium Arsenide (GaAs) case……………………………………….59

II.1.4.3. The coherent potential approximation KKR-CPA method……………..…60

II.1.4.3-a. Presentation…….……………………………………………………..60

II.1.4.3-b. The idea behind the Coherent potential approximation (CPA)…………60

II. 2. Monte Carlo simulation………………………………………………………………………61

II.2.1. Introduction…………………………………………….......................................61

II.2.2. Simulation Models…………………………………………………………..…63

II.2.2-a. Structures and geometries……………………………………………….64

II.2.2-b. Ising Model……………………………………………………………...65

II.2.2-c. Heisenberg Model……………………………………………………..…67

II.2.3. Markov chain and Importance sampling…………………………………………......69

II.2.4. Metropolis Algorithm…………………………………………………………….…70

II.2.5.a- presentation……………………………………………………………………...70

II.2.5.b- Application in Monte Carlo method…………………………………………..…71

II.2.5. Critical properties…………………………………………………………………...73

II.2.6. Implementation and practical details…………………………………………….…74

II.2.7. Conclusion……………………………………………………………………………...76

Chapter 3: Ab initio study of the electronic, magnetic properties and phase transitions in Ga (Mn) N with Monte Carlo Approach:

III.1. Introduction…………………………………………………………………………...…78

III.2. Crystal structure and Calculation Methods………………………………………………...80

III.3. Results and discussions……………………………………………………………………81

III.3.a. Band structures and density of states……………………………..…………………………81

III.3.b. Monte Carlo simulation……………………………………………………………………88

III.4-conclusion………………………………………………………………………………..…94

Chapter 4: Ab initio investigation of (Fe, Ni) doped GaAs : Magnetic, electronic properties and Faraday rotation:

IV.1. Introduction……………………………………………………………………………………96

IV.2. Crystal structure and Calculation Methods…………………………………………………….97

IV.3-Results and discussions…………………………………………………………………...99

IV.3.a. Density of states…………………………………………………………………………99

IV.3.b. Magnetic stability and Faraday rotation………………………….…………………..…105

IV.4. Conclusion……………………………………………………………………………….107

General conclusion………………………………………………………………………………….108

References…………………………………………………………………………………………...111

List of publications……………………………………………………………….…………121

List of Abbreviations

DMS Dilute magnetic semiconductor

TM Transition metal

MTJ Magnetic tunnel junction

HM Half metal

FM Ferromagnetic

DLM Disordered local moment

AFM Antiferromagnetic

Tc Curie temperature

DOS Density of States

TDOS Total Density of States

PDOS Partial Density of States

GMR Giant Magnetic resistance

TMR Tunnel magnetic resistance

RAM Random Access Memory

MRAM Magnetic Random Access Memory

RKKY Ruderman-Kittel-Kasuya-Yoshida

DFT Density functional theory

APW approximation plane wave

LAPW Local approximation plane wave

FP-LAPW Full potential- local approximation plane wave

KKR Korringa Kohn Rostoker

CPA Coherent potential approximation

PBE Perdew-Burke-Ernzerhof

LDA Local Density Approximation

GGA Generalized Gradient Approximation

LSDA Local spin density approximation

MBJ Modified Becke and Johnson

LDA + U Local Density Approximation with Hubbard correction

GGA +U Generalized Gradient Approximation with Hubbard correction

MP Møller–Plesset Perturbation Theory

2D Two Dimensional

3D Three Dimensional

LEDs Light-Emitting Diodes

LMTO Linear Muffin-Tin Orbitals

List of Figures and Tables

Figure I.1: Spintronic field illustration

Figure I.2: The operating concept of Spintronics

Figure I.3: The operating principal of the GMR, with the Variation of the GMR's resistance as a function of the Magnetic field. Also (a) is the Parallel magnetization and (b) as the Antiparallel magnetization.

Figure I.4: Illustration of the alternatively stacked layers of Fe-Cr, beside the Magnetization direction of Ferromagnetic layers.

Figure I.5: The Tunnel Magnetoresistance operating model with parallel and antiparallel cases.

Figure I.6: Magnetic random access memory

Figure I.7: Schematic illustration of the spin field-effect transistor.

Figure I.8: Spin-torque device

Figure I.9: Illustration representing (A) a magnetic semiconductor, (B) a non-magnetic semiconductor material, and (C) a diluted magnetic semiconductor.

Figure I.10: Representation of the "ion implant" process.

Figure I.11: step by step representation of the CVD method.

Figure I.12: Representation of the Molecular Beam Epitaxy principal on the substrate.

Figure I.13: Representation of different DMS's Types.

Figure I.14: The evolution of the size of transistors following Moore's law.

Figure I.15: The crystal structures of GaN. (a) Wurtzite Structure; (b) Blende Structure; (c) Salt Mine Structure.

Figure I.16: Illustration of the hexagonal wurtzite-type crystal structure.

Figure I.17: The Zinc blend crystal structure of GaAs, with atoms position.

Figure I.18: (a) Direct band gap vs (b) indirect band gap, such as "E" is the energy and "k" refers to the momentum from the brillouin zone)**.**

Figure I.19: Direct exchange interaction without any nonmagnetic atom.

Figure I.20: Indirect exchange interaction between two magnetic ions **i** and **j** via a non-magnetic ion **k**, as illustrated by **a)** Kramers in 1934 and **b)** Pratt in 1955.

Figure I.21: Double exchange mechanism between Mn ions.

Figure I.22: The super exchange mechanism between magnetic elements (transition metals).

Figure I.23: Graphical illustration the indirect exchange interaction RKKY, giving the variation of the spin density of conduction electrons following the distance (d).

Figure I.24: Magnetic polarons. The electron forms a hydrogenoid orbit and couples with the magnetic ions of the system.

Figure I.25: Diamagnetic materials with spin behavior and H as magnetic field.

Figure I.26: illustration of Paramagnetic materials.

Figure I.27: Paramagnetism while the magnetic moments of each atom align with the external magnetic field (in blue).

Figure I.28: The magnetic moments in one direction do not have the same intensity as those in the other one.

Figure I.29: Presentation of spin behavior in a ferromagnetic material, both in presence and absence of magnetic field.

Figure I.30: The magnetic moments of an atom are reversed with that of the neighboring atom.

Figure II.1: Different calculation methods based on DFT.

Figure II.2: schematic representation of the auto-coherent cycle corresponding to the resolution of Kohn-Sham equations.

Figure II.3: Interstitial and spherical regions.

Figure II.4: Idea of CPA method.

Figure II.5: Monte Carlo method modeling.

Figure II.6: C_{point} representation

Figure II.7: Various 2D spatial lattices used in Monte Carlo, cellular automaton and percolation simulations also.

Figure II.8: Field lines of two magnetic dipoles.

Figure II.9: Flowchart representing the basic steps in a Monte Carlo simulation for a simple spin model.

Figure III.1: The density of states (DOS) for GaN without any transition metal impurities.

Figure III.2: The band structure (E-k curve) for non-doped GaN (1Ry =13.605 ev).

Figure III.3: Total d and p state projected density of stat (DOS) of Mn, doped GaN.$Ga_{0.95}Mn_{0.05}N$, the total DOS is denoted by a thick solid black line,3d-states of Mn by a blue line and 2p-states of N by a Green line.

Figure III.4: The Band structure (E-k curve) in the case $Ga_{0.95}Mn_{0.05}N$ for up spins $Ga_{0.95}Mn_{0.05}N$**Up** and down spins $Ga_{0.95}Mn_{0.05}N$**dn.**

Figure III.5: Total d and p state projected density of stat (DOS) of Mn, doped GaN, for different concentrations of Mn impurities, x(Mn)=0.10, x(Mn)=0.15 and x(Mn)= 0.20.

Figure III.6: The Band structure (E-k curve) for $Ga_{0.90}Mn_{0.10}N$, $Ga_{0.85}Mn_{0.15}N$, $Ga_{0.80}Mn_{0.20}N$ for up spins and down spins.

Figure III.7: The DOS of GaN doped with various concentrations of Mn plotted simultaneously.

Figure III.8: a) The Wurtzite-unit-cell-3D and b) The Wurtzite-unit-cell that we have obtained using "XCrySDen".

Figure III.9: The wurtzite structure of GaN with the 3 coupling interactions between atoms.

Figure III.10: The ground state phase diagram in the plan (J,H) for an Ising system corresponding to our spin configuration.

Figure III.11: a) The magnetization and b) The susceptibility as a function of the temperature for different size ranges L= 4 to L= 30.

Figure III.12: the magnetization M_s and magnetic susceptibility χ_s versus the temperature plotted simultaneously.

Figure IV.1: GaAs zinc blende structure where Ga atoms are presented in Blue color and As atoms in purple one via "XCrySDen"

Figure IV.2: Density of states by GGA approximation for the pure GaAs without any doping impurities.

Figure IV.3: Total and Partial density of states for the case of $Ga_{1-x}Ni_xAs$ for various doping concentrations: a)x=0.01, b)x=0.02, c)x=0.03, d)x=0.04, e)x=0.05, f)x=0.06, g)x=0.07.

Figure IV.4: Total and Partial density of states for the case of $Ga_{1-y}Fe_yAs$ for various doping concentrations: a) y=0.01, b) y=0.02, c) y=0.03, d) y=0.04, e) y=0.05, f) y=0.06, g) y=0.07.

Table IV.1: The Values of the ferromagnetic and Dlm energy for 0.01≤x(Ni)≤0.07 in the case of $Ga_{1x}Ni_xAs$.

Table IV.2: The Values of the ferromagnetic and Dlm energy for 0.01 ≤y(Fe)≤0.07 in the case of $Ga_{1y}Fe_yAs$.

General introduction

It's always a challenge for scientist and researchers in the industry around the world to develop new technologies and materials to have a better performance in nanotechnology devices. This is why the researches and studies of the specific properties of new materials in solid physics are the keys to the industrial development. The research activities focus on the application's domains and specially micro-electronics, energy, nanomaterials, ect.

The electrons have a charge and a spin but, for a long time, charge and spin have been used separately. Classical electronics ignore the spin and move the electrons by acting only on their charge. The spin appears through its macroscopic manifestation, the magnetization of a magnetic material, used to store information. Under the impetus of several recent discoveries, a new electronic emerges associating control of spin and charge currents in new devices that can be integrated into the high density circuits of microelectronics. Magnetic RAM memories are a prime example. This "Spin Electronics" or "Spintronics", now in full expansion, is evolving towards hybrid nanodevices combining semiconductors and ferromagnets, and promises applications for recording, electronics, optoelectronics and quantum information…

The development of the spin valve, that followed the discovery in 1988 of the giant magnetoresistance (GMR) ferromagnetic multilayers, was one of the first experimental achievements of a spin-dependent electrical transport. A magnetic multilayer is a stack of alternately ferromagnetic and non-magnetic metal layers, cobalt and copper, for example. Through the effects of spin-dependent transport, the resistance of such a multilayer strongly depends on the relative orientation of the magnetizations of neighboring ferromagnetic layers, it is the GMR effect. The "spin valve" is, for its part, a sophisticated multilayer, working in current parallel to the plane of the layers, and designed to optimize a sensor type operation.

Hence, So far two main effects of spintronics are: Giant Magnetoresistance (GMR) and Tunnel Magnetoresistance (TMR). These discoveries, which can be considered as the starting point of the domain, will lead to the development of Random Access Magnetic Memories (MRAM) and which makes it possible to replace the current RAM memories, thus the integration of this new science in technology research means a lot, since all the reading heads of the current hard drives are based on the TMR

The Magnetic Tunnel Junctions (MTJ) is the second type of spintronic device that will soon have important applications. The resistance of the MTJ depends on the relative orientation of the magnetizations of the electrodes. For alloy electrodes, the relative change in resistance between the parallel and antiparallel orientations of the magnetizations exceeds 50% at room temperature. This change of resistance is called TMR for Tunnel Magneto-Resistance. The MTJ is the first spintronic device in vertical current (current perpendicular to the layers). This vertical geometry makes it possible to insert it into circuits of very high density of microelectronics. Thus, small size MTJs (a few hundred nanometers) are at the basis of the new type of memory circuits, MRAM (Magnetic Random Access Memory).

The development of spintronic aims at improving the new semiconductor hetero-structures to increase the density of components, improve the performance and lower the prices. The goal is to combine magnetic materials and semiconductors to integrate, in a same device, memory functions, signal detection and processing.

However, there is a number of the factors that control the competitiveness, at the microscopic scale, of the realization of these new devices, the most important one is the injection of spin polarized electrons in a semiconductor from a metal. The raison is the difference in conductivity between the two materials and that of the compatibility with semiconductor technology. It's here when the Diluted Magnetic semiconductors take part, by the injection of polarized spins taken from a DMS into the semiconductor, thus a part of the semiconductor ions are replaced by the magnetic ones, making it more interesting and useful.

Diluted magnetic semiconductors (DMS) are very interesting especially when doped with a small concentration of magnetic impurities, which are transition metals, inducing ferromagnetic DMSs. In particular, DMS based on III–V and II–VI semiconductors, such as GaN, ZnO, GaAs…,In this doping there is an induced polarization coming from the exchange coupling of the valence band electrons of the semiconductor and 3d band electrons of the transition metal.

The goal of the actual material science researches is to find materials that can operate in a temperature which is above room temperature 350K, and to have a Ferromagnetic exchange coupling between the magnetic impurities.

Structural calculation methods, for example the ab initio methods, can be very valuable and useful for the development of these materials and their applications in spintronic and nanotechnology. These methods are used to calculate the structural, mechanical, electrical, and magnetic properties of the material.

These methods provide the predictability and the possibility of being able to treat any element or atomic system, and they are likely to replace the very expensive experiments or even unrealizable to the current experimental level in laboratories. More specifically, the ability to predict new materials and calculate their basic physical, magnetic and chemical properties is quite remarkable based on the structural properties: atom distributions in space, atom positions, mesh parameters, crystal symmetry….

We aim in this theoretical study to investigate, by mean of Ab initio calculations and Monte Carlo simulation, the electronic, structural and magnetic properties of the two of the most interesting and promising diluted magnetic semiconductors GaN and GaAs.

This thesis is divided into three chapters; the first chapter will present a general overview on the field of Spintronic and Its wide range of applications. Beside, we'll give a presentation on the Diluted Magnetic Semiconductors: description, types, properties, advantages, and why the choice of these materials in this work.

The second chapter will focus on the computational methods employed in our calculations, with the different approximations and structures manipulated in the calculations and simulations.

The third chapter will be devoted to the investigation of the Magnetic and electronic properties of Mn doped GaN via Ab initio calculations beside Monte Carlo simulation of the system. While the fourth chapter will treat the case of GaAs single doped and co doped with Ni and Fe, giving the magnetic states and magnetic the stability beside the Faraday rotation property.

Finally we close out the thesis with a conclusion and an overview.

Chapter I

The Spintronic field: Applications and DMS

I.1. Introduction: The Spintronic

The today's research on current technologies aiming to improve the miniaturization as well as the speed of the components highlights the limits of classical electronics. That is the raison why multiple projects are studying a new kind of electronics: spintronics or spin electronics, which uses the spin of electrons to process or store information.

Electronics uses the properties of electrons, elementary particles discovered by Joseph John Thomson in 1897. What's interesting is that the electron is also characterized by a spin. The notion of spin of the electron was discovered in 1921 thanks to the experiment of Stern and Gerlach which made it possible to quantify the component of the magnetic moment of an atom.

Spintronics proposes to use the spin of the electron in addition to its charge to guide the electrons and create currents. In the 1930s, Sir Nevill Mott, Nobel Prize in Physics, suggested that the spin of the electron is involved in electrical conduction.

This idea was taken up by Albert Fert, scientific director at CNRS / Thalès, in the 70s. He showed the influence of the spin on the mobility of electrons in magnetic metals such as iron and nickel.

So the spintronics describe devices that take advantage of the "spin", as mentioned before. It's a quantum-mechanical property of an electron that takes only two values: spin-up and spin-down. But why did we require spintronic science? It's because the electronics wasn't enough. Electronics are based, only, on the exploitation of the electrical charge carriers in the semiconductor, but the spintronic introduces the spin that can be manipulated via small magnetic fields.

On the atomic scale, by sandwiching a non-magnetic layer of a material between two magnetic layers, where each of the layers was just a few atoms thick, and by applying small magnetic fields, the current flowing through the sandwich could significantly be changed. The reason was that within the magnetic layers, the electrical current, which was composed of negatively charged electrons, became "spin-polarized", which means that all the spins of electrons became oriented either "up" or "down," depending on the magnetic orientation of these layers.

Nowadays, scientific research focuses on the development of devices based on new materials to address the integration of spintronics in semiconductor technologies. But the complexity of the

issue requires a different approach to overcome physical difficulties. Namely, we must electrically inject spin polarized carriers in the semiconductor section.

Also, researchers faced a problem in such materials which is the fact that the spin of the electron remains stable only over a distance of the order of 0.1 μm on average and beyond, it reverses. This distance is defined as the spin relaxation distance.

It was therefore necessary to wait for the arrival of ultra-vacuum molecular beam epitaxy (MBE) in the mid-1980s to highlight the spintronics. It is now possible to pass electrons through thin layers of metal having a thickness of the order of a nanometer without their spin being reversed.

Then, Albert Fert and team were able to bring out giant magnetoresistance (GMR) in 1988. This has paved the way for multiple possibilities; its use has increased the storage capacity of computer hard drives. Hence, Albert Fert and Peter Grünberg were awarded the Nobel Prize in Physics in 2007 for their discovery.

In recent years, spin electronics is looking for new materials to meet the demand of technological challenges that drive the realization of new devices. Among them, the diluted magnetic semiconductors or DMSs, which are now the subjects of many studies as we'll see below.

The realization of such devices is a serious problem because of the great difference in conductivity during polarized spin injection in a semiconductor from a metal. Solutions based on new materials such as diluted magnetic semiconductors in which a part of the semiconductor is replaced by magnetic ions, which could be a solution to the problem.

Let's recap via the next illustration:

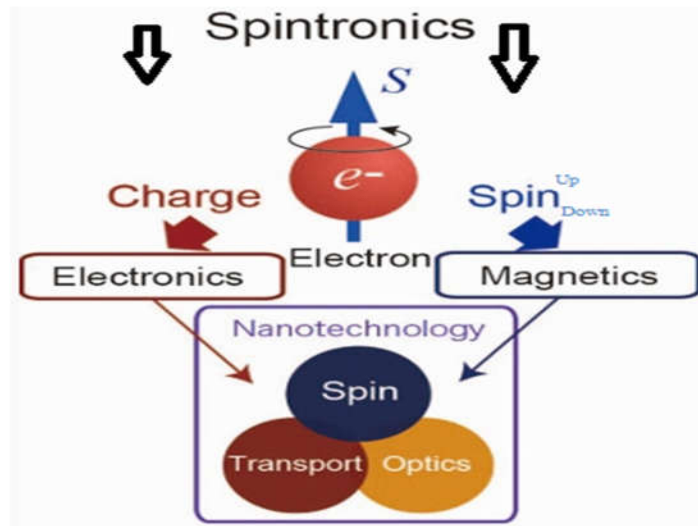

Figure I.1: Spintronic field illustration.

We ought to note that the purpose of spintronics is the use of spin as a new degree of freedom: ⇒New phenomena ⇒new components (MRAM, Logic gates, RF components,…). As illustrated in **Figure I.1 [1]**, the merge of the spin and charge of electrons give rises to new applications in Nanotechnology, Data Transport and also in Optics domain.

We can simplify the concept of spintronics as follow: It's when we have a flow of electrons with Up and Down spins and we interrupt their path by a layer of magnetized material, like Iron (Fe), in order to stop or slow either the spin (up/down) electrons, Hence, we favor a direction over the other.

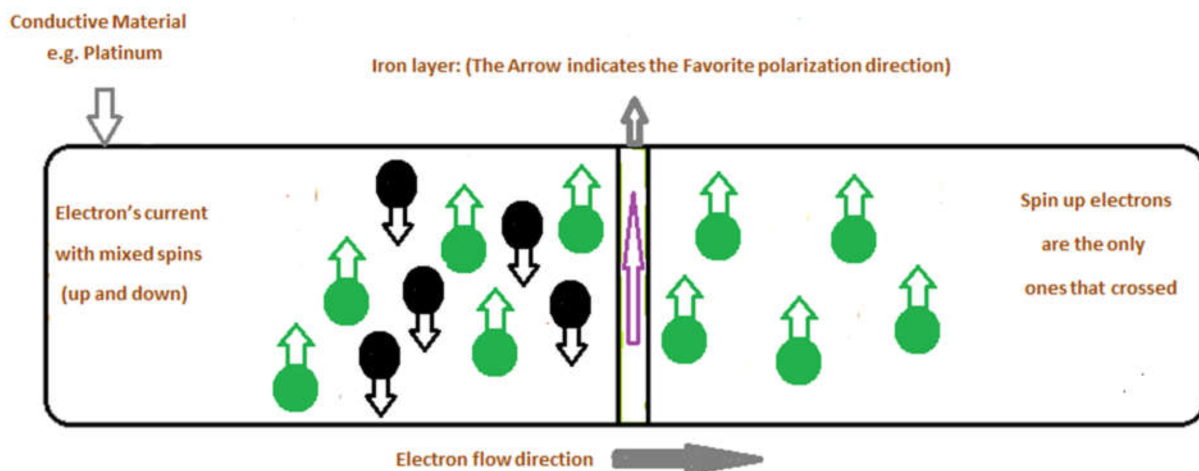

Figure I.2: The operating concept of Spintronics.

Figure I.2 schematizes this concept as seen above, we have as example Platinum as a conductive material, and then there is a layer of Iron as ferromagnetic material with a spin up orientation and a passing electron current. As noticed, the up spin electrons with a spin orientation parallel to the polarization direction of Iron passed through, while the down spin electrons were blocked by the magnetic layer. This concept paved the way to the birth of Giant Magnetoresistence (GMR), which we'll elucidate below.

I.2. Applications and Technologies:

I.2.1.The Giant MagnetoResistance (GMR):

It was in 1988 that two solid-state physicists, Albert Fert **[2]** and Peter Grünberg **[3]**, discovered that an alternation of ultrathin layers of a magnetic metal and a non-magnetic metal, e.g. iron and chromium, **Figure I.3,** with a thickness of a few atoms for each layer, showed a very strong fall in its resistivity, **Figure I.4** under the action of a magnetic field, and the macroscopic magnetizations of the successive magnetic layers, switch from an antiparallel state to an aligned parallel state. The effect was already known for a long time but not with such amplitude, which is why it was called giant magnetoresistance or GMR.

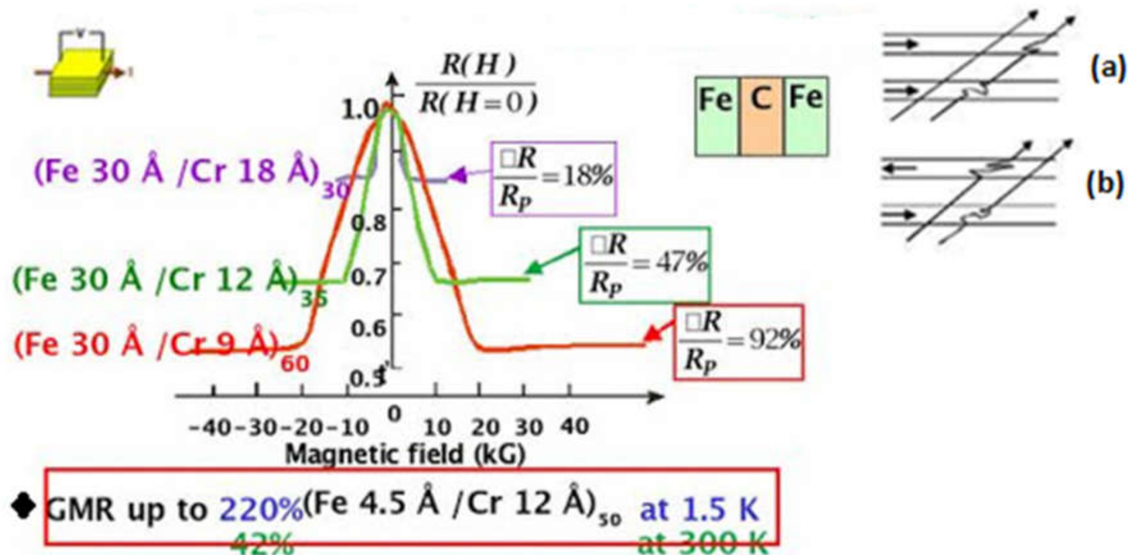

Figure I.3: The operating principal of the GMR, with the Variation of the GMR's resistance as a function of the Magnetic field. Also (a) is the Parallel magnetization and (b) as the Antiparallel magnetization **[4]**.

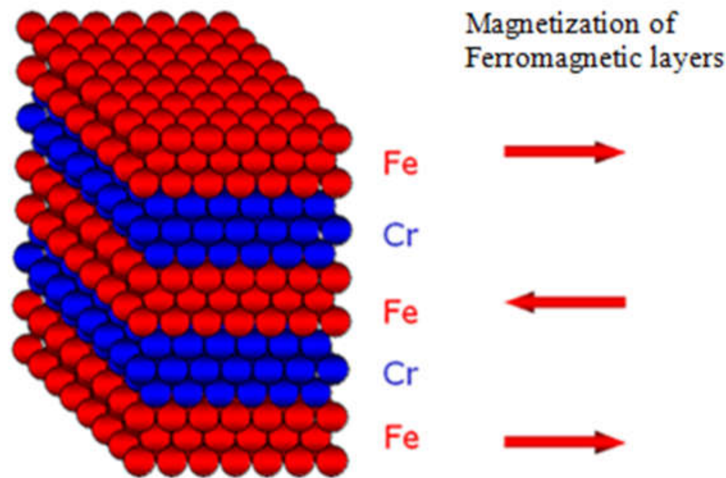

Figure I.4: Illustration of the alternatively stacked layers of Fe-Cr, beside the Magnetization direction of Ferromagnetic layers.

In order to illustrate the operating principle of the GMR effect, we give two configurations characterized by a stack of two ferromagnetic layers to Parallel magnetization (**Figure I.3.a**) and antiparallel (**Figure I.3.b**) separated by a layer non-magnetic conductor **[5]**. The electrons that participate in the electrical conduction may have a parallel spin (majority ↑) or opposite (minority ↓) compared to the magnetization of the layers. The trajectories of the electrons are determined by their spin because the diffusion phenomena are strong in the case of a spin opposite the magnetization and weaker in the opposite case. In the configuration with parallel magnetization layers, the majority spin electrons (e^{up}) pass through the almost non-scattering structure (green arrow), while the minority spin electrons (e^{down}) are more strongly scattered (red arrow). In the antiparallel configuration, the electrons are all scattered and thus the strength of the structure is higher.

In addition, without an external magnetic field, the magnetization axes of the successive ferromagnetic layers are opposite and the resistance is at maximum, while in the presence of a magnetic field, the magnetization axes of the ferromagnetic layers are progressively aligned in the axis of the applied magnetic field and therefore the electrical resistance of the structure decreases.

Hence, very small variations in the intensity of magnetic fields became measurable. Practical applications were almost immediate with the technology of recording and reading magnetic information on hard disks. Indeed, it is by magnetizing a small region of these disks that an

alternation of magnetizations in a perpendicular direction "high" or "low" allows to record a series of binary information. The smaller these areas are, the higher the information density, and therefore the storage capacity of the hard disks, is important. In return, the magnetization is becoming weaker and it becomes more and more difficult to read. Using the GMR effect, the storage capacity has been multiplied by 100!

I.2.2.The tunnel Mangetoresistance (TMR):

Hereafter is the tunnel magnetoresistance (TMR) effect which is close to the giant magnetoresistance. This effect has been noticed in systems consisting of two ferromagnetic electrodes (free layer and trapped layer) separated by a thin insulating layer (called tunnel barrier) whose thickness is of the order of one nanometer. The trapped layer acts as a reference layer, its magnetization being frozen either by coupling with a strongly antiferromagnetic layer, or because of its harder magnetic character (higher coercive field). The other ferromagnetic layer retains the possibility of changing its orientation according to that of the applied magnetic field.

In 1975, after the first experiments of Tedrow et al. on the tunnel transport Spin-dependent **[6]**, Jullière [**7]** observes tunnel magnetoresistance in a Fe / GeOx / Co (GeOx, amorphous germanium oxide) low-temperature tri-layer. The effect disappears by applying a low voltage or by raising the temperature.

Based on previous related works, Jullière developed a model based on two hypotheses to account for this TMR effect. The first hypothesis is that the spin of the electron is preserved during tunnel transport. The second is that the probability of electron transmission across the barrier is proportional to the density of states at the Fermi level in the receiving electrode. The number of electrons able for passage is proportional to the density of states at the Fermi level in the emitting electrode. The current for each spin channel is hence proportional to the product of the state densities at the Fermi level of the two electrodes.

Figure I.5 represents a schematic illustration of the Jullière model. Such as the densities of states of majority and minority spin electrons ($\boldsymbol{n}_\uparrow$ and $\boldsymbol{n}_\downarrow$) are represented by parabolas shifted in energy. This shift induces what Jullière defines as the polarization P of ferromagnetic materials:

$$\boldsymbol{P} = \frac{\boldsymbol{n}_\uparrow - \boldsymbol{n}_\downarrow}{\boldsymbol{n}_\uparrow + \boldsymbol{n}_\downarrow} \qquad \textbf{\textit{I.1}}$$

Let's analyze this in details:

In a parallel configuration of the magnetizations of the two ferromagnetic materials, **Figure I.5.a)**, the density of state of majority spin electrons in the Fermi level is important in the emitting electrode F1 and in the receiving electrode F2. As a result the corresponding resistance is small $r_{\uparrow}$ for this spin channel, whereas the Fermi state density of state of minority spins in Fermi level is low in both electrodes, the tunnel resistance $R_{\downarrow}$ in this case is important. As a result, the current is mainly due to the majority spin channel. Hence, the total resistance of the magnetic tunnel junction in the parallel state is given by:

$$\boldsymbol{R_{\uparrow\uparrow} = \frac{r_{\downarrow} . R_{\uparrow}}{r_{\downarrow} + R_{\uparrow}}} \qquad \textit{\textbf{I.2}}$$

In the configuration of antiparallel magnetizations **Figure I.5.b)** the density of states at Fermi level of the majority or minority spin electrons is as weak in the emitting electrode F1, as it is in the receiving electrode F2. The two channels conduct equivalently and generally in a lower rate than in the case of parallel magnetizations. As a result, the tunneling resistances of the majority spins R ↑ and minority spins R ↓ are average. Hence, the total resistance of the magnetic tunnel junction in the antiparallel state is:

$$\boldsymbol{R_{\uparrow\downarrow} = \frac{R_{\downarrow} . R_{\uparrow}}{R_{\downarrow} + R_{\uparrow}}} \qquad \textit{\textbf{I.3}}$$

Moreover, the low resistance $r_{\uparrow}$ makes $R_{\uparrow\uparrow}$ lower than $R_{\uparrow\downarrow}$. A shift of magnetizations configuration from a parallel state to an antiparallel state consequently causes a variation of electric current through the tunnel barrier.

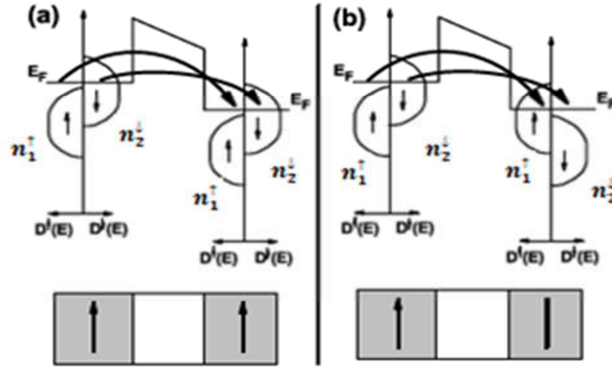

Figure I.5: The Tunnel magnetoresistance operating model with parallel and antiparallel cases.

We can then conclude that the tunnel magnetoresistance (TMR) effect is specified as the relative variation of the resistance of the system between its two extreme values:

$$\boldsymbol{TMR} = \frac{R_{\uparrow\downarrow} - R_{\uparrow\uparrow}}{R_{\uparrow\uparrow}} = \frac{G_P - G_{AP}}{G_{AP}} = \frac{(n_1^{\uparrow} n_2^{\uparrow} + n_1^{\downarrow} n_2^{\downarrow}) - (n_1^{\uparrow} n_2^{\downarrow} + n_1^{\downarrow} n_2^{\uparrow})}{n_1^{\uparrow} n_2^{\downarrow} + n_1^{\downarrow} n_2^{\uparrow}} = \frac{2P_1P_2}{1 - P_1P_2} \qquad \textit{I.4}$$

Previously, it wasn't evident to have a stable TMR at ambient temperature, which is why it took a long time and exactly twenty years (1995) before that Moodera et al. **[8]** observed a consistent TMR at ambient temperature measured on a CoFe / Al_2O_3/ Co or NiFe / Al_2O_3 / Co type junction. The attained TMR was 11.8% at 295 K **[8]**.

Since then, the improvement of the deposition processes as well as the intense research carried out on new types of tunnel barriers have made it possible to obtain TMR of the order of 1000% **[9]** at low temperature, and 500% at room temperature **[10]**.

I.2.3. Magnetic random access memories MRAMs:

The access time to a piece of information (a bit) in a hard disk is long, a thousandth of a second. Also, when we turn on our computer and open a program, various software is read on the disk and loaded into RAM (Random Access Memory), memories based on very fast access semiconductors (billionth of a second). These RAMs are certainly fast access but unfortunately "volatile", which means that the stored information dies as soon as one turns off the computer and even, for some RAM, must be re-entered every thousandths of a second. A new type of memory, called MRAM (Magnetic Random Access Memory) appeared already as non-volatile

memories. Note that, MRAMs utilize the spintronic phenomenon observed in components called "magnetic tunnel junctions", see the figure below.

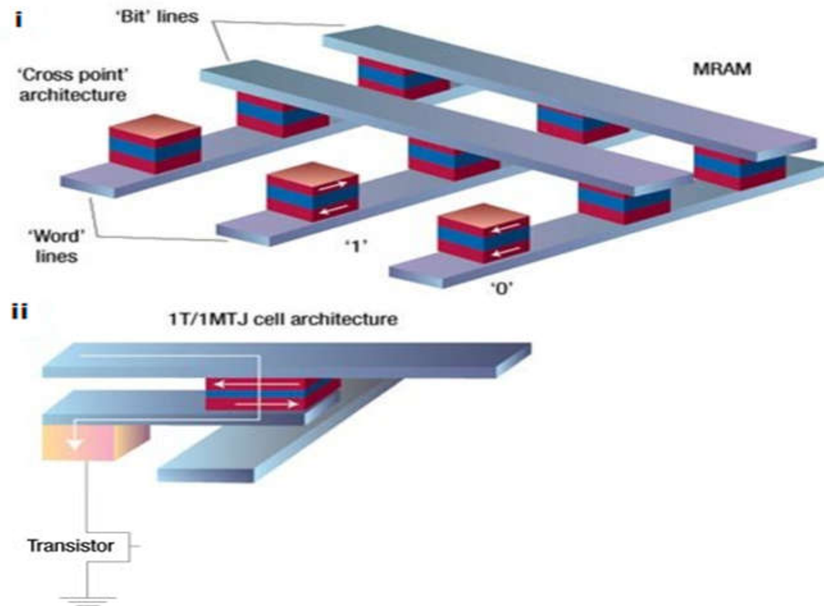

Figure I.6: Magnetic random access memory **[11].**

The above **Figure I.6.i** represents the MRAM operational principle; the change of state is done by flipping the spin of the electrons (by tunnel effect in particular). In the basic cross-point architecture. The binary information 0 corresponding to the parallel configuration (weak resistance) and 1 corresponding to the antiparallel configuration (strong resistance),is recorded on the two opposite orientations of the magnetization of the free layer of magnetic tunnel junctions (MTJ), which are connected to the crossing points of two perpendicular arrays of parallel conducting lines. For writing, current pulses are sent through one line of each array, and only at the crossing point of these lines is the resulting magnetic field high enough to orient the magnetization of the free layer. For reading, the resistance between the two lines connecting the addressed cell is measured.

To remove the unwanted current paths around the direct one through the MTJ cell addressed for reading, the usual MRAM cell architecture has one transistor per cell added, resulting in more complex 1T/1MTJ cell architecture such as the one represented in **Figure I.6.ii**.

Spintronics is now developing considerably and other interesting phenomena are appearing. Some will allow extremely fast switching of MRAM components **[11]**. Others are very promising for the generation of microwave waves. There should also be a gradual fusion between classical electronics and spintronics in hybrid components combining semiconductors and magnetic materials or in components based on magnetic semiconductors. Long-term perspectives also concern the quantum computer.

I.2.4. Spin field effect transistor:

The spin field-effect transistor or (SpinFET) is a one of the advanced semiconductor spintronics devices promising a performance superior to that achieved with normal transistor technology. **Figure I.7** present an illustration of the SpinFET. These transistors are composed of two ferromagnetic contacts that sandwich the semiconductor region, namely, source and drain. These contacts contain mostly spin-polarized electrons and play the role of polarizer and analyzer **[12]**. The ferromagnetic source contact injects spin-polarized electrons into the semiconductor. Because of the non-zero spin-orbit interaction the electron spin processes in his way through the channel. At the drain contact, only the electrons with spin aligned to the drain magnetization, can easily leave the channel and then have the majority contribution to the current. Thus, the total current through the device depends on the relative angle between the magnetization direction of the drain contact and the electron spin polarization at the end of the semiconductor channel. There is current modulation is achieved by tuning the strength of the spin-orbit interaction in the semiconductor region and thus the degree of the spin precession. Basically, the strength of the spin-orbit interaction in the channel depends on the effective electric field and can be controlled by the voltage applied to the gate.

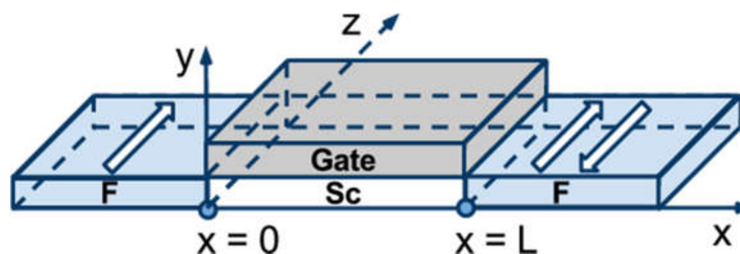

Figure I.7: Schematic illustration of the spin field-effect transistor **[13].**

I.2.5. Spin torque oscillators:

Also called “spin-flip transistor” is a magnetoelectronic thin-film transistor that can display negative differential resistance and gain. This transistor works by the modulation of the source-drain current in a spin valve by the magnetization of a third electrode, which is rotated by the spin-torque created by a control spin-valve. Moreover, for this device to be more interesting and practical, it requires ferromagnetic materials with small polarizations, and the transistor operates smoothly at room temperature.

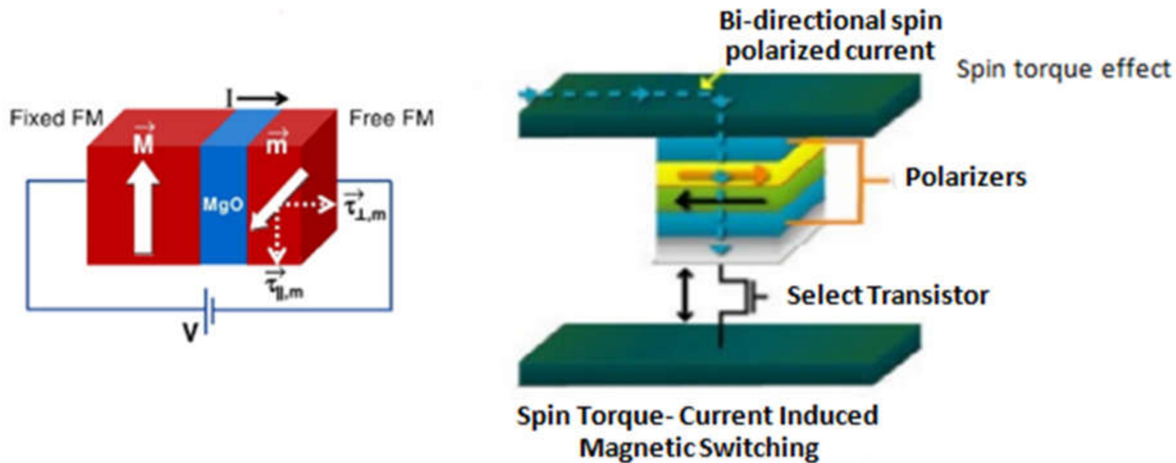

Figure I.8: Spin-torque device.

Spin-torque device has three terminals composed of an antiparallel spin-valve in which the conducting channel is in contact with a ferromagnetic base; see **Figure I.8 [14].**

As we mentioned, the base magnetization direction is the one responsible for the modulation of the source-drain current that affects the spin accumulation in the conducting channel **[15,17]** the magnetization in spin valves can be switched by an electric current **[16,18]** Due to its characteristics, the spin-flip transistor was proposed as an MRAM element, in which the base magnetization is switched by the spin-torque due to the induced spin accumulation.

I.3. Diluted Magnetic Semiconductors (DMSs):

For the advancement of spintronics, the research of new materials was required, ones that exhibit half-metallic behavior and ferromagnetism at room temperature. Hence, DMSs are the solution, these materials are non-magnetic semiconductors in nature, in order to be magnetic, a DMS need to be doped with a small concentration of magnetic impurities, usually Transition-Metals (TM) (see **Figure I.9**). They offer an easy integration with existing semiconductors and also a high

spin-polarization. However, there is a huge challenge in solid-state science in the way of the discovery and understanding of such materials. Indeed, one of the critical unanswered scientific questions recently raised, “Is it possible to create magnetic semiconductors that work at room temperature?”.

The DMS challenge is appealing because it requires both magnetic and electronic doping. The interaction between magnetic dopant spins and free carriers must be engineered to achieve thermally robust dopant spin carrier coupling.

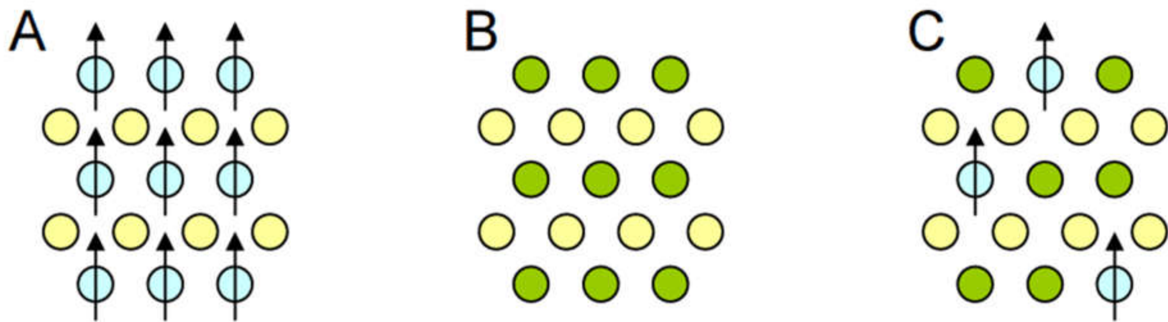

Figure I.9: Illustration representing (A) a magnetic semiconductor, (B) a non-magnetic semiconductor material, and (C) a diluted magnetic semiconductor **[19].**

I.4. DMS’s synthesis methods:

In the experimental field of condensed matter physics, there are various synthesis methods dedicated to elaborate a Diluted Magnetic Semiconductor and introduce a certain concentration of magnetic elements in a semiconductor. Amidst these DMSs synthesis methods:

- *The implant*, which principal is bombarding our substrate with ionized magnetic atoms having a kinetic energy that we control experimentally. The interesting benefit here is that, after the implantation, we can entirely control the obtained phase with the desired amount of magnetic impurities. Nevertheless, this method has a drawback, because this is no smooth way to implement these magnetic elements, the roughness of the introduction of the magnetic impurities creates defects in our substrate. Consequently, the quality of the material decreases significantly. This is not what we want in the industry. Hence, we have to remove these defects by annealing, which is done near the thermodynamic equilibrium. Unluckily, some intermetallic precipitates are created in the process.

Hence, as shown in **Figure I.10** Ions are pumped from the source then it goes through an analyzing magnet and passes after that within an accelerator in order to enhance ion's speed, so as this ions wave is focused in order to be deposed or planted finally in the wafer

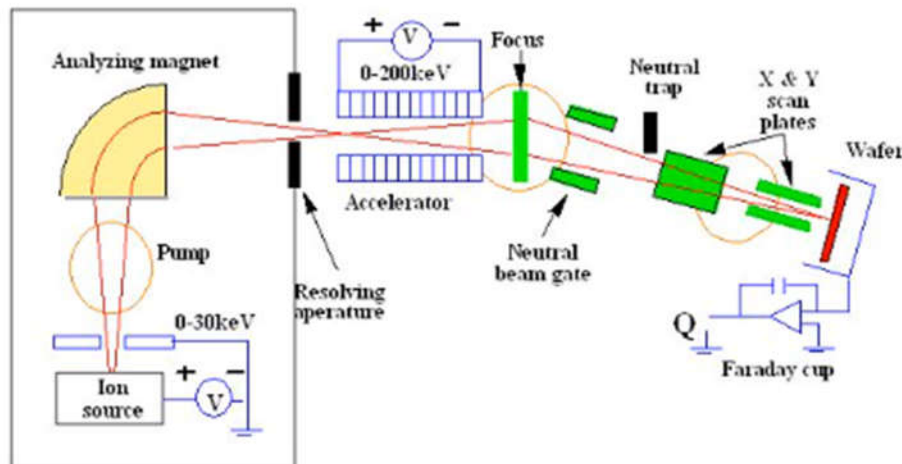

Figure I.10: Representation of the ion implant process.

Hence this ion implantation method is favored due to: its large spectrum of doses 10^{11} to $10^{16}/cm^2$, its highly accurate dose control, low temperature process, and its wide choice of masking materials.

- ***The chemical vapor deposition*** or ***CVD*** is also one of the most commonly utilized synthesis methods, especially in the industry of Nano-wires. This method involves chemical processes to insert the magnetic elements in the substrate. It has two advantages: Less material defects and needs no vacuum. This results in great quality materials and gives high production rhythm.

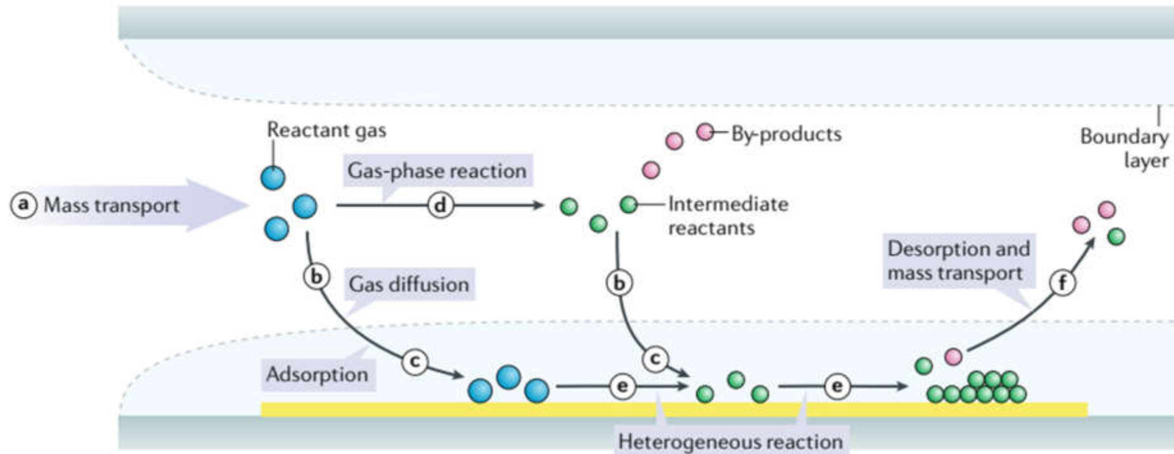

Figure I.11: step by step representation of the CVD method **[20].**

As shown in **Figure I.11**, we start with (step a) in which reactant particles or reactant gas (blue circles) are conducted into the reactor. Here, we have two likely paths for the reactant gas, either by direct diffusion via the boundary layer shown in (step b) and then it's adsorbed on the substrate (step c). Or by creating intermediate reactants (green circles) and by- products (red circles) using the gas-phase reaction (step d) after which, it's deposited by diffusion and adsorption on the substrate (step b and c). On the other hand, the surface diffusion and heterogeneous reactions in (step e) occur at the substrate’s surface prior to the formation of thin films or coatings. At the end, the by-products and unreacted species are desorbed from the surface and extracted from the reactor as escapements in (step f). Hence, this is the CVD process.

- ***The Molecular Beam Epitaxy*** or ***MBE***: The Molecular Beam Epitaxy was originally developed for the crystal growth of semiconductors. It is an ultra-vacuum technology (P <10-6 mbar) based on the sequential evaporation of the elementary constituents placed in Knudsen effusion cells. The principle of molecular beam epitaxy as schematized in **Figure I.12 [21]** is as follows: we want to create a certain configuration of atomic layers on a substrate. The atoms which will constitute these layers are bombarded on the substrate (where they will be fixed) in the form of a gas flow at high speed. We play on the alternation of the emitted atoms and on the exposure time of the substrate to the flux in order to create the desired nanostructure.

In the aim to obtain epitaxial growth, several parameters are important: very low deposition rate (approximately 5 nm / hour), particular growth conditions (temperature of the substrate, ultra-vacuum, etc.), monocrystalline substrates ... **[21].**

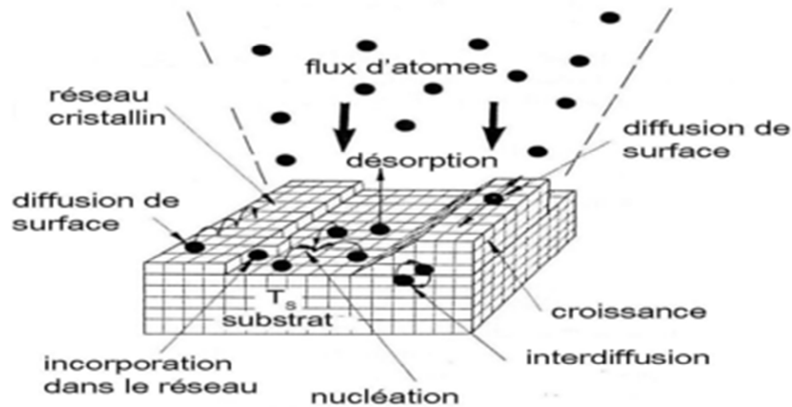

Figure I.12: Representation of the Molecular Beam Epitaxy principal on the substrate.

I.5. DMS types: A variety of DMS materials:

Based on the host semiconductor matrix, we can distinguish different types of DMS:

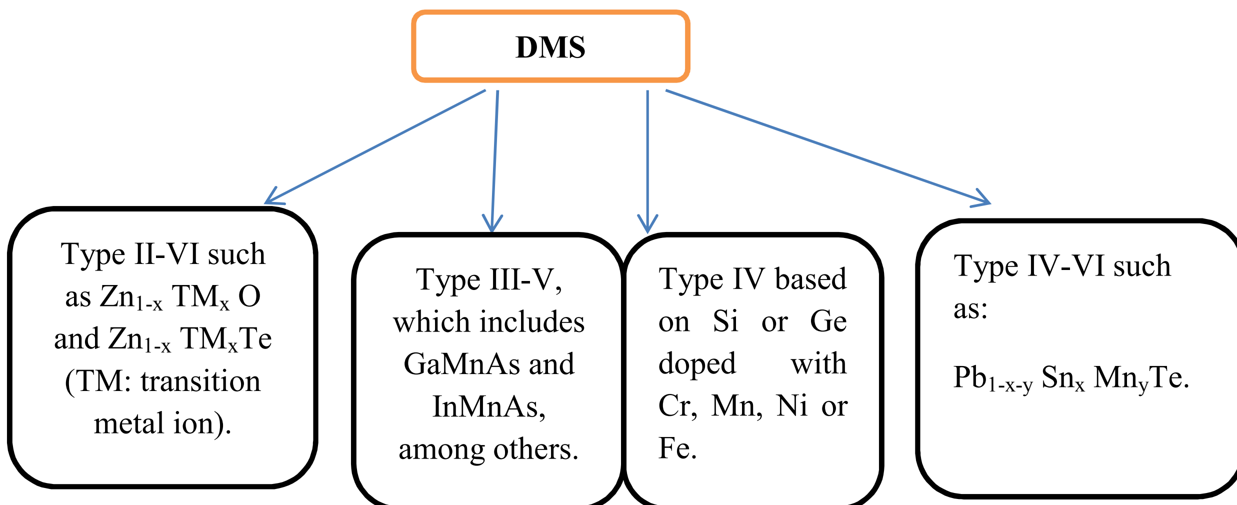

Figure I.13: Representation of different DMS's Types.

To start with these DMSs types, as shown in **Figure I.13**, we have DMSs based on type **IV** semiconductors: among this family of DMS there is silicon Si doped with magnetic impurities,

e.g. Ni, Co, Mn, and germanium Ge doped with magnetic ions, e.g. Cr, Mn **[22]**. Then, there are DMSs based on type **IV-VI** Semiconductors: These DMS are composed by cations of column IV and anions of column VI of the periodic table. They have a complex crystallographic structure and high carrier density, the ferromagnetic state can be stabilized, $Pb_{1-x-y}Sn_xMn_yTe$**[23]**. After that, there is the type of DMSs based on **II-VI** semiconductors: The II-VI DMSs have two stable structures, either zinc blende or wurtzite, formed by cations of column II (Cd, Hg, Zn) and anions of column VI (Se, S, Te...) of the periodic table. They have an antiferromagnetic spins coupling making the super-exchange the dominant type of magnetic interaction in these DMSs, but we report Ferromagnetic appearance mediated by holes carriers **[24]**. And last but not least, we've the **III-V** family of DMS: This type of DMSs is composed of a mixture of cations of column III and anions of column V of the periodic table. For instance, in manganese (Mn) DMS III-V, the magnetic ions Mn^{2+} are acceptors **[25]**. The ferromagnetic coupling carried by the carriers is the dominant one. Also the type of doping and the magnetism induced are strongly related, and we report a ferromagnetism phase mediated by holes as carriers **[26,27]**.

I.6. Benefits of the II-VI and III-V based DMSs:

Till today, scientists have known a considerable number of DMSs, but it was in the 80s that the prime DMSs were identified; they're the II-VI semiconductors alloys, e.g, $Cd_{1-x}Mn_xTe$ and $Zn_{1-x}Mn_xTe$ **[28].** their magnetic study revealed a spin-glass behavior and sometimes weak ferromagnetism with low Curie temperatures (Tc) that are in the order of a few Kelvin (K) **[29],** hence it was inadequate for spintronic applications, ones demanding the ferromagnetism at room temperature. On the other hand, recent studies revealed ferromagnetism with high Curie temperature in Mn doped III-V semiconductor $Ga_{1-x}Mn_xAs$ **[30,31]** and $In_{1-x}Mn_xAs$ **[32].** Also a Tc of 173 K was reached for Mn doped GaAs employing low temperature annealing techniques that proved very promising **[33,34].**

These materials attract a huge interest in research on spin electronics because their intrinsic advantages: Firstly, a long lifespan (up to 100 ns) of polarized carriers allowing their transport over several hundred nanometers;

Secondly, a high efficiency in both polarization and spin injection. Thirdly, they have a location of carriers within heterostructures in quantum wells or quantum dots. Add to that all the

possibilities that band engineering offers for these materials: gap, mesh parameter and constraint adjustment, as needed.

These materials also have some interesting magnetic properties: The existence of a ferromagnetic phase, beyond the ambient temperature. The importance of their “Landé” factor, which quantifies the coupling between the spin properties and the external magnetic field, ensures a consistent Zeeman splitting. The spin-dependent properties, such as the giant Faraday rotation, are thus amplified and a rather weak magnetic field may be sufficient to completely polarize the carriers at the Fermi level.

I.7. The studied materials:

I.7.1. Gallium Nitrid (GaN):

In the beginning of electronic technology, engineers have been on a mission to find the ideal switch, one that will convert, with rapidity and efficiency, raw electrical energy into a controlled, useful current of electrons. As a candidate, first came the vacuum tube but it was inefficient, since they generated heat that stands for loss in energy, and their large size and high cost, created limits to their use. Next, in the late ‘50s, the transistor gained expanded use; with its small size and better efficiency, creating new markets unreachable by vacuum tube technology.

Silicon rapidly became the "chosen one" material for the semiconductor transistor, not only because of its fundamentally superior electrical properties. The fast rise of the silicon transistor in integrated circuits, continued throughout the 70’s and 80’s.

Moreover, the silicon-based power MOSFET was the core of the rise predicted by “Moore’s Law” – which called for a doubling of the transistor’s performance with a lowering cost approximately every 18 months, as shown in **Figure I.14**.

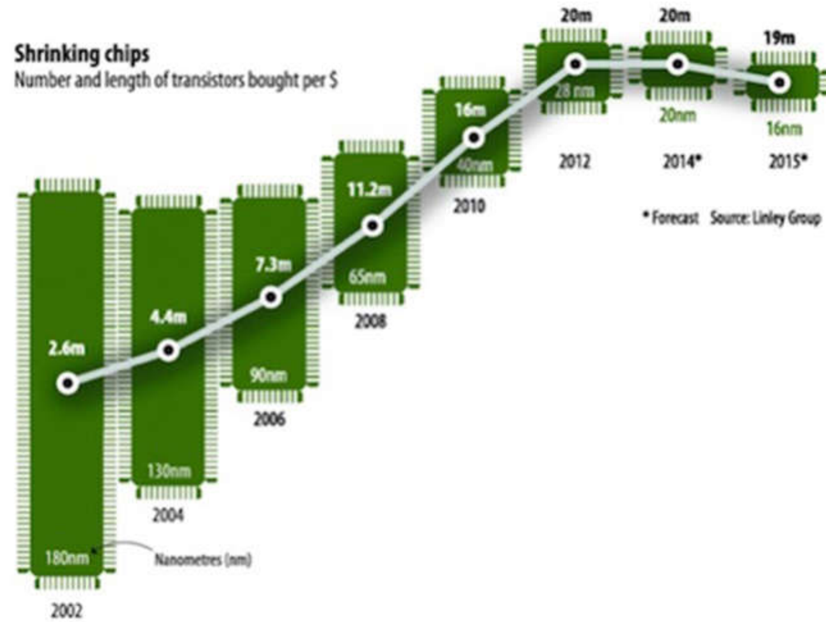

Figure I.14: The evolution of the size of transistors following Moore's law **[35].**

Now the vacuum tube, silicon power MOSFETs reached their limit in delivering better performance at a constantly decreasing cost. GaN presents the main candidate to take electronic performance to the next level and also gives a chance to reactivate a positive momentum of Moore's Law. GaN's ability to conduct electrons more than 1000 times more efficiently than silicon, while being able to be manufactured at a lower cost than silicon has now been well established. Silicon is out of gas, and a new, higher performing semiconductor material is emerging, GaN is on the rise.

Gallium nitride (GaN) is a III/V direct bandgap semiconductor, with a wide band gape of 3.4 ev, this material is very interesting and has three kinds of structures: hexagonal wurtzite, cubic blende and salt mine (NaCl-type compound square structure), which are shown in **Figure I.15**, the wurtzite structure is the most stable one presenting better atomic disposition, its large gape offers various opportunities for the application in many domains- optoelectronic, frequency-doubling, solar cells…

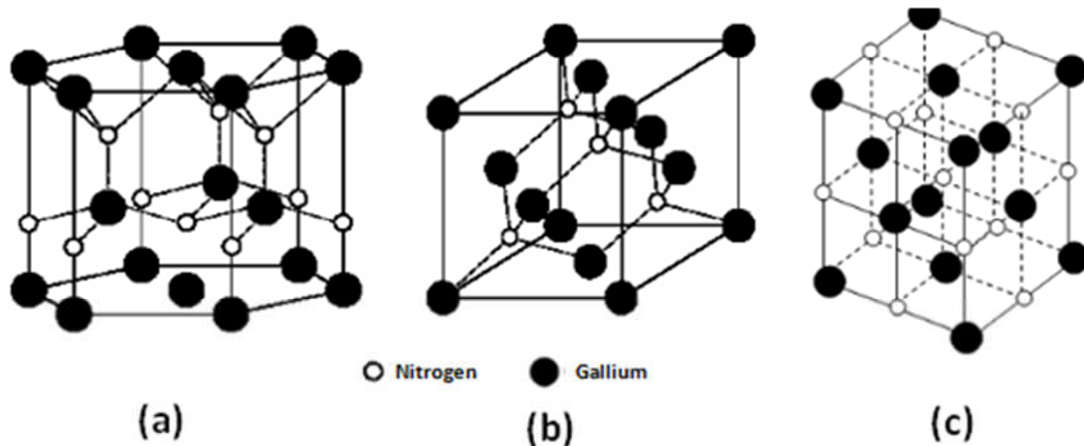

Figure I.15: The crystal strcutures of GaN. (a) Wurtzite Structure; (b) Blende Strcuture; (c) Salt Mine Structure.

In our study we worked with the Wurtzite structure of GaN, **Figure I.16**, because it's the most stable one.

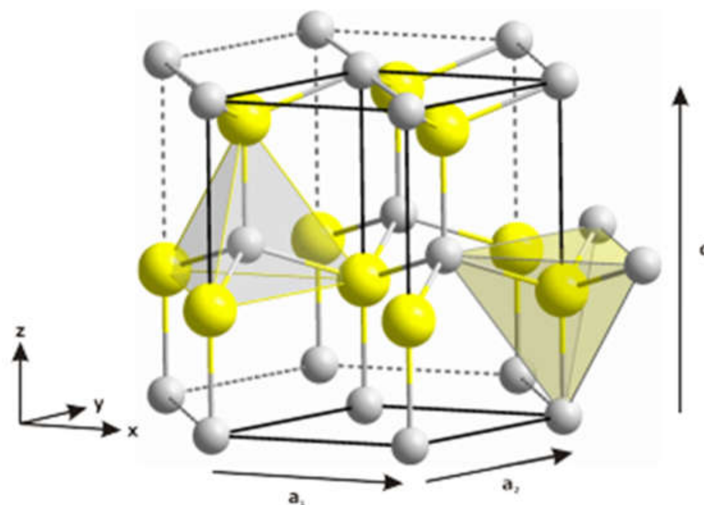

Figure I.16: Illustration of the hexagonal wurtzite-type crystal structure. The unit cell (black box) has a four-atomic basis with the cations (grey) located at the positions (0, 0, 0) and (1/2, 1/2, 1/2), the anions in (yellow) are located at the positions (0, 0, 3/8) and (1/2, 1/2, 1/2). Each atom is tetrahedrally coordinated, which is showed by two polyhedral. Each one of two atom types constitutes a sublattice which is hexagonally close packed.

As there is no more important evolution in silicon power devices, gallium nitride is set to take over, in speed, temperature and power. GaN presents the technology that will enable us to incorporate essential future innovations where efficiency is highly required.

Material science community huge interest in GaN comes from its unique material and electronic properties. We can sum up five essential characteristics that GaN devices offer: a high operating temperature, high current density, strong dielectric strength, a high speed switching and they're low on-resistance. These characteristics stems from the unique properties of GaN, which, compared to silicon, offers ten times higher electrical breakdown characteristics, three times the bandgap, and exceptional carrier mobility.

Thanks to its properties, GaN systems have successfully developed transistors presenting an attainable on-resistance lower than silicon (Si). Add to that, GaN's negligible charge storage, which offered unprecedented efficiencies in power switching circuits, beside the small size and very low heat losses.

Here we give some other technical advantages:

Due to material limitations, Silicon (Si) technology is being cut out in higher power applications. The totality of power electronic systems in the upcoming years will take full advantage of the wide band gap devices such as GaN. These are some the advantages;

- 80% reduction in system volume and weight
- Increased output power
- Improved transient characteristics and switching speed
- Reduced heat sink requirements
- Lower voltage drop for unipolar devices
- Reduced electrical noise due to virtually zero recovery charge
- Reduced electrical noise from smaller system packages

The Age of GaN is Underway ,With the increase in transistor and Integrated Circuit (IC) performance made possible by GaN materials, now is the time for innovative power design engineers to take advantage of GaN attributes: lower on resistance giving lower conductance losses, faster devices yielding less switching losses, less capacitance resulting in less losses when charging and discharging devices, less power needed to drive the circuit, smaller devices taking up less space on the printed circuit board, lower cost.

I.7.2. Gallium Arsenide (GaAs):

Gallium arsenide (GaAs) is a chemical compound belonging to the family of III-V semiconductors, because gallium and arsenic are respectively in columns III and V of the periodic table of elements, and thus have three and five valence electrons. Gallium arsenide has a crystalline structure of the blende type, considering that the gallium atoms follow a face centered cubic (CFC) type structure, the arsenic atoms occupy 4 of the 8 tetrahedral sites of this mesh (and vice versa), as shown in **Figure I.17.**

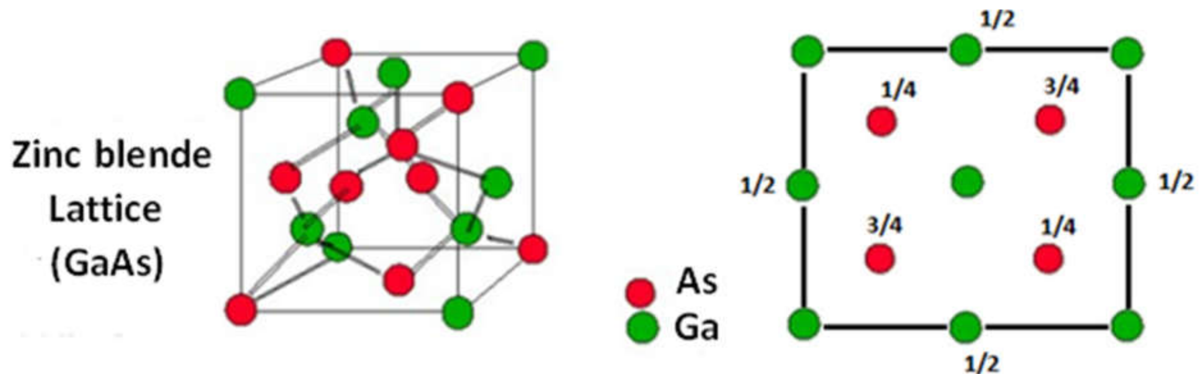

Figure I.17: The Zinc blend crystal structure of GaAs, with atoms position.

It is a semiconductor material used in particular for producing microwave components and opto-electronic components, enabling transistors made of gallium arsenide to function at frequencies over 250 GHz, infrared light emitting diodes and photovoltaic cells.

Gallium arsenide devices are not sensitive to heat because of their wide band gap. Also, these devices typically have less noise than silicon devices, especially at high operating frequencies.

There are various applications of gallium arsenide, namely, in the manufacturing of devices such as monolithic microwave integrated circuits, microwave frequency integrated circuits, infrared light-emitting diodes, actually, GaAs diodes are used to detect X-rays. GaAs is also used in solar cells, laser diodes and optical windows.

The direct band gape of GaAs, unlike many other semiconductors, gives him the ability to emit light with high efficiency, to be resistant to radiation damage enabling its use in optical windows and space electronics in high power applications.

It is also used as an electrical substrate and offers natural isolation between circuits and devices. This makes it suitable for millimeter wave and microwave ICs.

As interesting application also, in astronomy missions, in fact, solar cells based on GaAs power the "Opportunity and Spirit rovers" that are exploring the surface of Mars. In addition, a number of solar cars make use of GaAs in solar arrays.

GaAs is also highly resistant to radiation damage, which lends GaAs to satellite and space applications.

Analysts predicted the GaAs Wafer Market will reach $650M+ by 2017. Primarily, due to demand for handsets and LEDs in lighting and automotive domains. Solar cells for high-concentration photovoltaic (HCPV) will also add to the development of the GaAs substrate market.

The two biggest bonuses to Gallium Arsenide over Silicon in terms of device performance are:
1) Much higher Electron mobility , that is, you can shoot electrons across a transistor faster, get higher gain and higher bandwidth out of transistors, and get better n-type conduction with a lower doping level.

2) Direct band-gap, **Figure I.18**, allowing for direct on-chip generation of light for signaling and detection.

Note that, a semiconductor's band gap is defined as the energy difference between the bottom of the conduction band (CB) and the top of the valence band (VB). **Figure I.18** illustrates the difference between a direct and an indirect band gap. In the first one (a) the top of the VB and the bottom of the CB have the same momentum value, while for the indirect one (b) the respective momentum values are different.

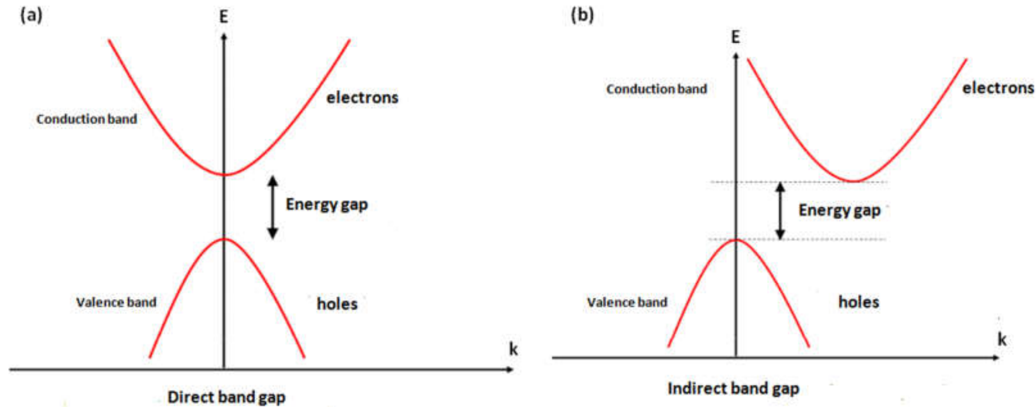

Figure I.18: (a) Direct band gap vs (b) indirect band gap, such as "E" is the energy and "k" refers to the momentum from the brillouin zone) **[36].**

In fact, there are a number of technologies where GaAs is applied that silicon technology just can't stand up to. For instance, RF/Microwave amplifiers. In consumer electronics, a GaAs-based Heterojunction bipolar transistor is likely at the heart of your high-end Wi-Fi receiver and transmitter, and is almost certainly at the heart of your cell phone's receiver and transmitter.
In our work we have studied the magnetic and electronic properties of these two materials. The atomic interaction plays the main role in DMSs properties. Next, we give the different type of interactions that we can have in diluted semiconductor materials.

I.8. Outlook on the magnetic interactions in DMSs:

When we incorporate magnetic impurities into a semiconductor to make it a diluted magnetic semiconductor, there are different magnetic interactions that occur between the magnetic impurities. Since the most wanted type of magnetism in DMSs is ferromagnetism. The origin of ferromagnetism in a material so far is not totally clear, but several models are available to convince the scientific community. These magnetic interactions are exploited to explain how this ferromagnetism is mediated.

The origin of ferromagnetism in a material so far is not totally clear, but several models are available to convince the scientific community. In this paragraph we will present some origins that stabilize ferromagnetism in some of these materials. .

For most systems, beside these interactions, it is necessary to proceed more precisely, for example, by identifying the local coupling spins in the exchange interactions. This identification is based on a theoretical model inspired by the Hamiltonian and the comparison with the experimental observations. Our approach is based on the density functional theory that provides us very precious information on the magnetism of the DMS.

I.8.1. Direct exchange interaction:

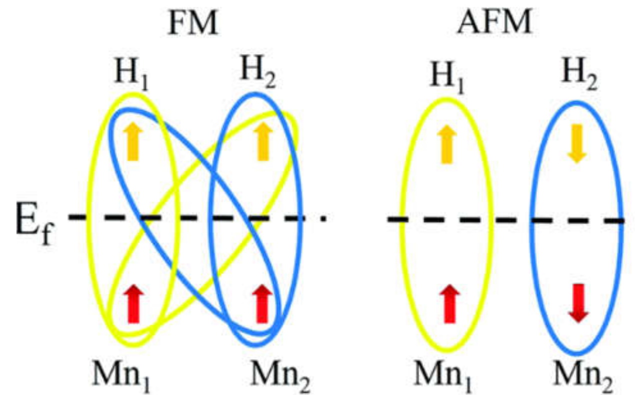

Figure I.19: Direct exchange interaction without any nonmagnetic atom.

This interaction occurs when there is direct overlap of electrons of the nearest neighbors of these magnetic atoms in **Figure I.19 [37]**, meaning a direct interaction between the magnetic impurities in the DMS without an intermediary ion. This interaction can also be understood based on Pauli's principle and the Coulomb energy, the Coulomb energy decreases if the spins of the electrons are parallel, because for the alignment of parallel spins this energy is minimal compared to the antiparallel alignment. In the case of DMS, the average distance between magnetic impurities is much greater than the nearest neighbor distance, so that the mechanism describing this interaction is a short-range magnetic one.

The Hamiltonian describing the interaction is as follow:

$$\boldsymbol{H_{dd} = \sum_{i \neq j} j(R_i - R_j) S_i . S_j} \qquad \textit{I.5}$$

Where: j (R_i- R_j) is the coupling between the Spins S_i and S_j located in the sites R_i and R_j respectively.

I.8.2. Indirect exchange interaction:

This exchange interaction occurs between localized, transition metals (3d) or rare earth (4f), magnetic ions via a non-magnetic element. See **Figure I.20.**

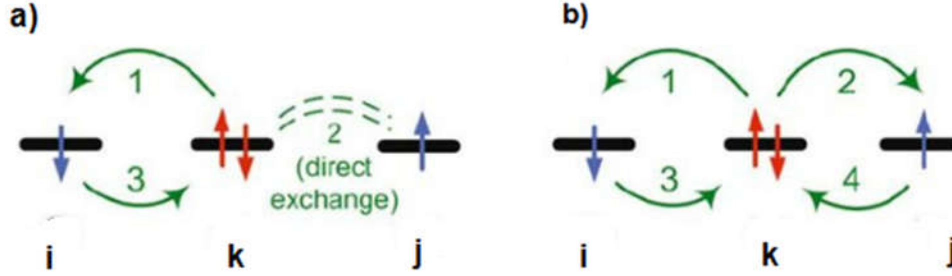

Figure I.20: Indirect exchange interaction between two magnetic ions **i** and **j** via a non-magnetic ion **k**, as illustrated by **a)** Kramers in 1934 **[38]** and **b)** Pratt in 1955 **[39].**

The Hamiltonian of this coupling exchange type is:

$$\boldsymbol{H_{ap-d} = -\frac{1}{2}\sum_i \sum_{n,k,k'} J_n^{sp-d}(k,k') e^{i(k-k').R_1} \times S_i.\sum_{\mu\vartheta} C^{+}_{nk\mu}\sigma_{\mu\nu}C_{nk'\mu}} \qquad \textbf{\textit{I.6}}$$

With:

$$\boldsymbol{J_n^{sp-d}(k,k') = \int d^3r d^3r' \frac{\varphi_k^*(r)\varphi_0^*(r)\varphi_0(r')\varphi_{k'}(r)}{|r-r'|}} \qquad \textbf{\textit{I.7}}$$

Here are the meanings of each element in the equation **(I.6)**:

$J_n^{sp-d}(k,k')$: Represents the exchange integral between the carriers (electrons or holes) of the conduction or valence band respectively, with (n, k) and (n, k') adding S_i as spin of the magnetic impurity.

$\varphi_k^*(r)$: Defines the Bloch wave function of the (electron or hole) of the conduction band where n=c or valence band with n=ν.

$\varphi_0(r)$: Taken as the wave function of the magnetic ion's 3d level.

$C_{nk\mu}^{+}$: Refer to the creation operator of an electron or a hole in the conduction or valence band, with k as a wave factor.

$C_{nk'\mu}$: Stands for the annihilation factor of an electron or a hole located either in the conduction or in the valence band, with μ as a wave factor.

$\sigma_{\mu\nu}$: The Pauli matrices vector.

I.8.2.1. Double exchange interaction:

The double exchange mechanism is type of interaction in which an electron is exchanged between two magnetic elements via a nonmagnetic ion, oxygen for example. The two magnetic element in interaction are identical but with different valence.

This model was introduced by Zener **[40,41]** in 1951 to explain ferromagnetism in manganites (perovskites of general formula $A_X^{III}\ B_{1-X}^{II}$ Mn$O_{3-\alpha}$) as $La_{0.75}r_{0.3}$Mn$O_{3-\alpha}$**[42].**

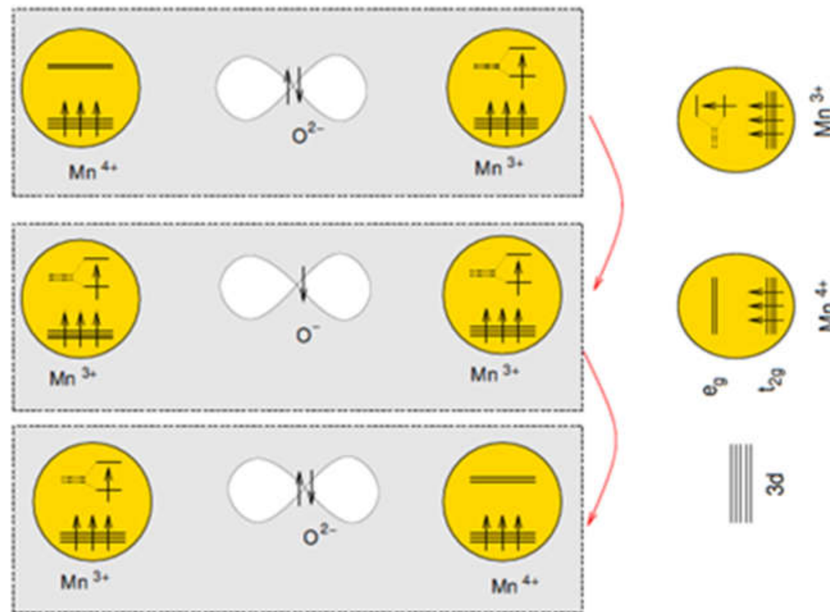

Figure I.21: Double exchange mechanism between Mn ions.

For instance, let's take a 180 degree interaction of Mn-O-Mn where Mn "e_g" orbitals are directly interacting with the O "2p" orbitals, and there is a one electron difference between the two Mn ions. In the ground state, electrons on each Mn ion are aligned according to the Hund's rule.

As shown in **Figure I.21**, the process is as follow: when oxygen (O) gives up its spin-up electron to Mn^{4+}, its vacant orbital can then be filled by an electron from Mn^{3+}. At the end of the process, an electron has moved between the neighboring metal ions, retaining its spin.

there are various theoretical studies that consider the double exchange mechanism as the one responsible for the ferromagnetism and ferromagnetic stability in DMS, when the Fermi energy is placed in the t_{2g} band of the majority impurity as in the case of (Ga, Mn)N, and (Zn, Cr)O.

I.8.2.2. Super exchange interaction:

The super-exchange is an interaction that occurs between two second neighbor magnetic elements (cations), 3d state, through a non-magnetic element (anion), normally oxygen. This coupling is generally antiferromagnetic [**43]**, providing exchange carriers in the DMS. It differs from direct exchange for which there is a coupling between cations that are immediate neighbors without involving an intermediate anion, as seen in **Figure I.22**, which is an illustration of a super exchange interaction between Transition Metal ions, via non-magnetic element playing the role of ligand (L). The d band is half-filled for each ion in interaction, as stated by Goodenough-Kanamori (GK) rules **[44]**, when we have the angles of 180° and 90°, we get an antiferromagnetic and ferromagnetic spin alignment of the TM ions, respectively. Note that the one factor differing from both cases is the location of the two electrons of L, if they are in the same orbital or not, which provoke separate tendencies of spin alignments for those two electrons (L) in interaction with the TM.

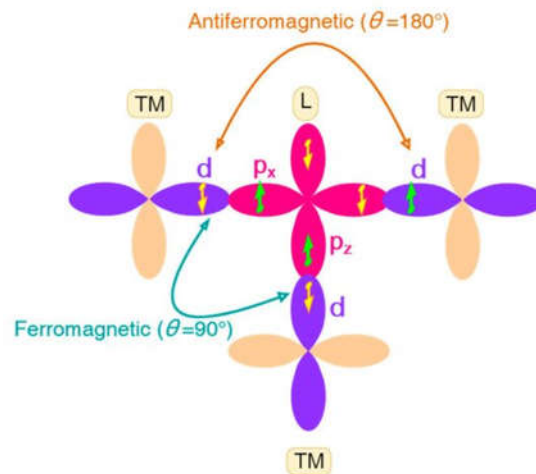

Figure I.22: The super exchange mechanism between magnetic elements (transition metals) **[44]**.

In some compounds such as Rb_2CrCl_4 **[45]** a crystal lattice distortion (Jahn-Teller effect) leads the super-exchange to produce a ferromagnetic coupling. Indeed, the complete description of the super-exchange involves the orientation and the occupation of the orbitals of the metal. The different possible configurations lead to either antiferromagnetic or ferromagnetic interactions.

I.8.3. Ruderman-Kittel-Kasuya-Yoshida (RKKY) Interactions:

The RKKY interaction, carried out via electrons in the conduction band, is a very strong indirect exchange interaction between the localized moments carried by the orbitals of the inner layer.

An electron spin interacts with a conduction electron, which interacts with another electron spin thus creating a correlation of energy between the two spins. The spin of the conduction electron is oriented in the environment of the magnetic ion and its polarization decreases with the displacement from the magnetic ion in an oscillating way [**46,47**]. Thus, the sign of the coupling depending on the electron density in the free electron gas and the distance between two magnetic ions, it is alternately ferromagnetic and antiferromagnetic (**Figure I.23**). This type of interaction requires the presence of free charge carriers (traveling electrons or hole).

This model was then applied to explain the ferromagnetic /antiferromagnetic coupling between two thin layers of a ferromagnetic metal separated by a thin layer of a non-magnetic metal. Depending on the thickness of the non-magnetic layer there is a ferromagnetic or antiferromagnetic coupling between the two layers **[48-50]**.

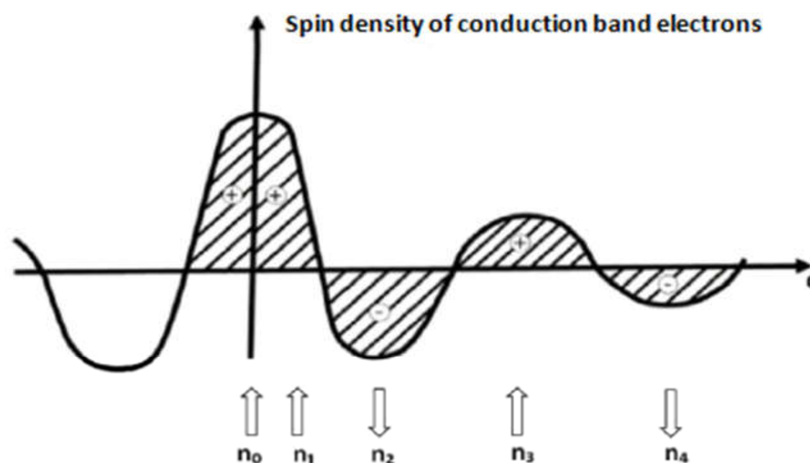

Figure I.23: Graphical illustration the indirect exchange interaction RKKY, giving the variation of the spin density of conduction electrons following the distance (d) **[50].**

The two signs (+) and (-) represent the polarization of the conduction electrons as a function of the distance d from the magnetic ion located at site n_0. The up and down ↑and ↓ represent the orientation of the magnetic moments.

I.8.4. Zener model:

The origin of the ferromagnetism in the Mn doped III-V DMS is still on debate in the scientific community, but there are some theoretical studies that attributed the ferromagnetism observed in these materials to the Zener model. In this context, the addition of manganese into these semiconductors creates a p-type doping, meaning more hole carriers than electrons. Furthermore, there is a p-d exchange coupling between the delocalized valence band holes and the localized Mn^{2+} ions. Therefore, this exchange interaction will antiferromagnetically couple the holes with the Mn ions and as a result, induce a ferromagnetic phase **[51,52].**

On the other hand, In RKKY interaction we neglect the spin-orbit and carrier-carrier interactions, we can notice that there is a similitude between Zener model and RKKY interaction. Thus Zener model suits perfectly the doped III-V DMS. Adding to that, in various theoretical works **[53-56]**, Zener model is used to describe the magnetic properties of semiconductors ferromagnetic.

We question the origin of the ferromagnetism in Mn doped III-V semiconductors such as GaAs or InAs as for II-VI tellurides. In this context, the carriers (holes) density is important in the induction of ferromagnetism phase, in this point we can see the advantage of III-V semiconductors over the II-VI type, since for the III-V DMS manganese doping, introduces both carriers and spin, while for II-VI semiconductors it is necessary to co-dope in order to have sufficient holes density.

I.8.5. Magnetic polarons model:

It's not an easy task to apply the Dietl et al. model , since this model needs the presence of free carriers (holes), but what about when these holes are localized around the ions?, yes ,the model doesn't work. In this case f localized holes; there interaction with the magnetic impurities causes the formation of magnetic polarons. In systems where the holes concentration is very low compared to magnetic ion density, a magnetic polaron is formed by a localized hole and a large number of magnetic impurities around this ‘hole’ (**Figure I.24**) **[57]**.

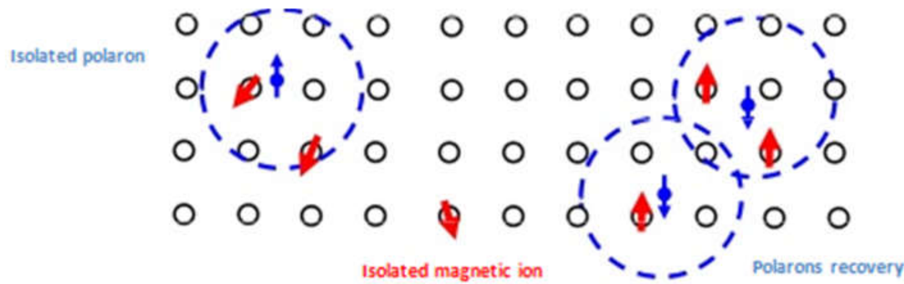

Figure I.24: Magnetic polarons. The electron forms a hydrogenoid orbit and couples with the magnetic ions of the system **[57].**

Therefore, antiferromagnetic interactions occur between the localized hole and the Mn ions and a ferromagnetic interaction between polarons. It is possible to define an effective radius of the polaron R_p which depends on the temperature, the exchange interaction between the hole and the ion Mn and a characteristic length of the whole wave function. When the temperature decreases, R_p increases and for sufficiently low temperatures, there is a recovery of polarons (percolation). The ferromagnetic interaction between the polarons dominates the antiferromagnetic interaction between the manganese ions and a ferromagnetic phase is established.

An interesting model was developed relaying on the properties of magnetic polarons in the aim to explain the ferromagnetism phase in ZnCoO **[58]**. We show that the existence of a band of impurities close to the conduction band and 3d levels of Co is a result to the formation of polarons of radius large enough to ensure their percolation. TM ions, in general, or Co ions, in this case, align with the internal magnetic field due to these magnetic polarons.

I.10. Presentation of different magnetic behaviors:

In the Free State, an atom is magnetic if it carries a permanent magnetic moment represented by a constant module vector. Note that, every material substance is formed of a set of atoms that can be either non-magnetic or magnetic; in the latter case, the direction and sometimes the modulus of the magnetic moment may depend on the particular environment of each atom (nature and position of the neighboring atoms, temperature, and applied magnetic field).

We'll now briefly present the main types of magnetic behavior. These main types of magnetism are: ferromagnetism **[59]**, paramagnetism and antiferromagnetism. Beside other types such as, ferrimagnetism and diamagnetism.

I.10.1 Diamagnetism:

In the majority of materials, diamagnetism is a weak magnetic behavior. However, in a superconductor it is not, since a powerful quantum effect repulses the magnetic field totally, except a thin layer at the surface.

Historically, the discovery of diamagnets was in 1778, when Sebald Justinus Brugmans observed that bismuth (Bi) and antimony (Sb) were repelled by magnetic fields. In 1845, the term "diamagnetism" was pointed out by Michael Faraday, when he experimentally concluded that each material responded (in either a diamagnetic or paramagnetic way) to an applied magnetic field.

Generally, diamagnetism is a quality related to all materials. It regularly makes a rather weak contribution to the material's response to a magnetic field. Nevertheless, for materials exhibiting other forms of magnetism, e.g. ferromagnetism or paramagnetism, the diamagnetic par can be insignificant.

For no-physicists, a diamagnetic material is the one said to be non-magnetic, such as, water and wood beside the majority of organic compounds (petroleum and some plastics), and also various metals involving Copper (Cu), not to forget the heavy ones having a large number of core electrons, namely, Mercury (Hg), Gold (Au) and Bismuth (Bi).

In addition, diamagnetic materials possess a relative magnetic permeability that is less than or equal to 1, and consequently a magnetic susceptibility that is less than 0, since the susceptibility by definition is:

$$\boldsymbol{\chi_{\upsilon} = \mu_{\upsilon} - 1} \qquad \textit{I.8}$$

That's why this type of materials is repelled by magnetic fields. However, the diamagnetic effect isn't observed in everyday life because it's such a weak property within materials. For instance, the magnetic susceptibility of diamagnets such as water is ($\chi_{\upsilon} = -9.05 \times 10^{-6}$). The strongest diamagnetic material is Bismuth ($\chi_{\upsilon} = -1.66 \times 10^{-4}$, while pyrolytic carbon may have a susceptibility of $\chi_{\upsilon} = -4.00 \times 10^{-4}$ in one plane **[60]**.

This type of magnetism is characterized by a negative low amplitude relative susceptibility. Diamagnetism is due to an orbital movement of the electrons, caused by the applied field. This movement can be assimilated to a microscopic current which behavior would be comparable to that of a solenoid induced current. According to Lenz's law, the induced current opposes the field that produces it, which is consistent with the fact that χ_r is negative, see **[61]** for more details.

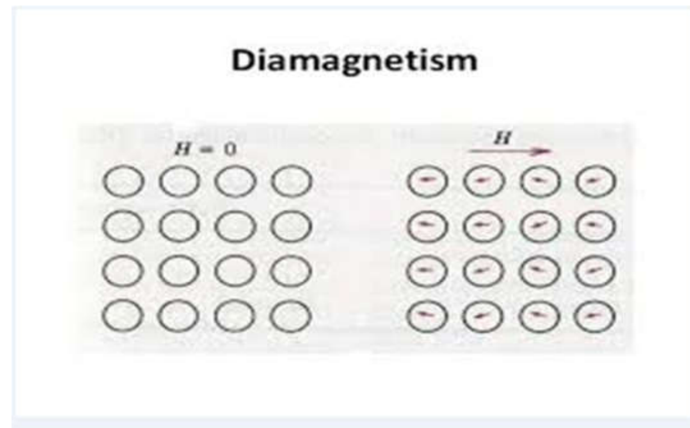

Figure I.25: Diamagnetic materials with spin behavior and H as magnetic field **[61].**

They create an induced magnetic field in a direction opposite to an externally applied magnetic field. See **Figure I.25**, the spins are repelled by the applied magnetic field, and the permanent dipoles are absent in diamagnetic materials.

I.10.2. Paramagnetism:

Paramagnetism is characterized by a positive low amplitude relative susceptibility, which is to say between 10^{-6} and 10^{-3}. It is found in substances whose atoms have a permanent magnetic moment and these moments are not coupled together. Under the action of a magnetic field, these moments tend to align, see **Figure I.27**. However, the resulting polarization remains very weak, because the effect of the thermal agitation, which randomly orients the magnetic moments, remains preponderant.

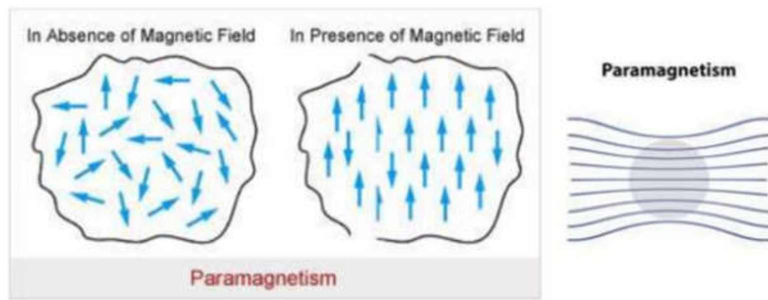

Figure I.26: illustration of Paramagnetic materials **[62]**.

As seen in the **Figure I.26** above, they exhibit magnetism when the external magnetic field is applied. This type of materials loses magnetization in the absence of an externally applied field. Also, they are weakly attracted towards magnetic field. The degree of magnetization is proportional to the strength of the applied field, and the magnetization is parallel to the field.

The usual magnetism, which allows a magnet to lift paper clips, is paramagnetism: it is the magnetism of iron and steel, but also nickel or cobalt **[62].**

Its process is quite simple but it is still necessary to dive in the heart of the matter. In atoms like those of iron, some electrons, those located on the periphery and don't participate in the atomic bonds, are adjustable (one speaks about magnetic moment of the electron, which we could describe as the meaning of the magnet represented by the electron).

When an iron sample is subjected to a magnetic field, these electrons all align in the same direction as the field lines of the magnetic field as illustrated here:

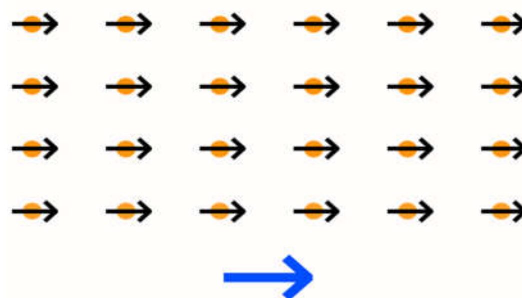

Figure I.27: Paramagnetism while the magnetic moments of each atom align with the external magnetic field (in blue).

As a result, the magnetic field of the material and that of the magnet are added. The material and the magnet are then attracted to each other. This allows a trombone to remain "stuck" to a magnet.

In addition, you may have noticed that if you use a relatively powerful magnet, you can create a kind of "snake" with the paper clips: the first trombone is glued to the magnet, but the other trombones can stick to the previous one. As a result, we can stick two or three thereafter, depending on the strength of the magnet.

This is due to the fact that each trombone, in the presence of the magnet, becomes a magnet too (because of the electrons being all aligned). When the magnet is removed, the electrons return to a random orientation and the magnetization disappears.

I.10.3. Ferrimagnetism:

The ferrimagnetism is considered at the intermediary between paramagnetism (all the electrons are oriented in the same direction) and antiferromagnetism (the electrons are oriented in two opposite directions). We find in this case that: the magnetic moments of the electrons are well opposed two by two. However, those following the direction of the external magnetic field (blue arrow) are stronger than those in the opposite direction. See **Figure I.28**, the total magnetic moment in one direction is therefore greater than that in the other direction and as a result, the total magnetic moment of the sample is not zero:

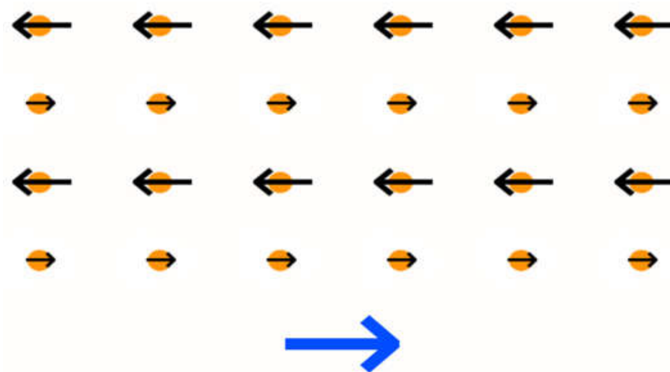

Figure I.28: The magnetic moments in one direction do not have the same intensity as those in the other one.

The ferrimagnetic materials have anisotropic properties, which means that the orientation of the crystals used is important in the studies related to these materials. This is used in the field of

paleomagnetism **[63]**, where ferrimagnetic rocks capture terrestrial magnetism from the time of their formation. The study of these rocks makes it possible to deduce that the earth's magnetic field is regularly reversed over the years. Conversely, one can also date a rock by analyzing the magnetic field recorded in it. Such as, some minerals contain a record of the direction and intensity of the magnetic field when they form. This record provides information on the past behavior of the Earth's magnetic field.

These ferrimagnetic materials also have an interest in nanotechnologies **[64]**: their global magnetic moment being "controllable" under the effect of heat, some forms of memory could use ferrimagnetic elements with a laser based reading and writing heads. The goal is to have memory modules much faster than the memories which record data using electrical voltages only **[65] [66]**.

I.10.4. Ferromagnetism:

Ferromagnetism is considered as the Main mechanism generated by some materials such as Iron (Fe)... in order to create permanent magnets, or to be attracted to magnets. In physics, we have various types of magnetism, but Ferromagnetism (involving ferrimagnetism) stands out as the strongest type. Such as, it is the only type of magnetism that generates forces strong enough to be sensed and is the one getting credit for the common phenomena of magnetism experienced in real life.

Actually, this type of magnetism results from the alignment of permanent magnetic moments, these moments being oriented parallel to each other by a mutual interaction called “ferromagnetic coupling”. The ferromagnetic materials therefore also have a spontaneous polarization. What has been said for ferrimagnetic materials, concerning the return to a random distribution of magnetic moments under the effect of a rise in temperature, also applies here (**Figure I.29**). The ferromagnetic materials also have a Curie temperature T_C, over which they become paramagnetic, beside their susceptibility following the Curie-Weiss law.

If we take the previous (diamangnetic) case, where we stick paper clips to a magnet, but now we use a very powerful magnet (neodymium magnet for example), then the paper clips retain a small residual magnetization even when the magnet is removed.

As a result, the electrons in the material remain oriented in the same direction as the magnet has them, even when the magnet is removed. This is called ferromagnetism.

In this case, the material has become a permanent magnet itself and it will retain this magnetization until it is removed (by heating the material, for example). In fact, the material is subdivided into small regions, called Weiss micro-domains. The orientation of the electrons in each of these regions is identical, but each domain has a random orientation. In total, the sample in its entirety is not magnetized as long as one does not apply an external magnetic field.

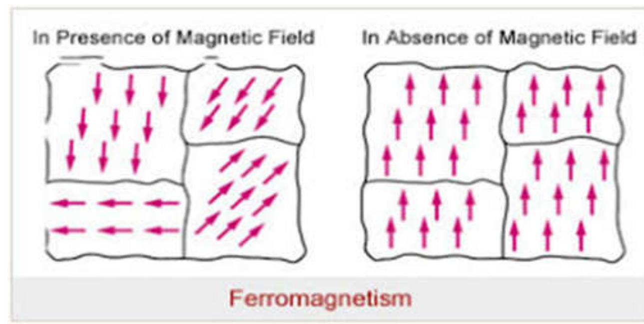

Figure I.29: Presentation of spin behavior in a ferromagnetic material, both in presence and absence of magnetic field **[67]**.

There is a large number of studies, in material sciences, regarding ferromagnetism since its interesting and powerful characteristics **[67-70].**

I.10.5. Antiferromagnetism:

As we mentioned in ferromagnetic materials, the electrons are all oriented in the same direction as the external magnetic field (blue arrow). While, in antiferromagnetism, the orientation is inverted from one atom to the other, as shown in **Figure I.30**, forming a zero global magnetic moment:

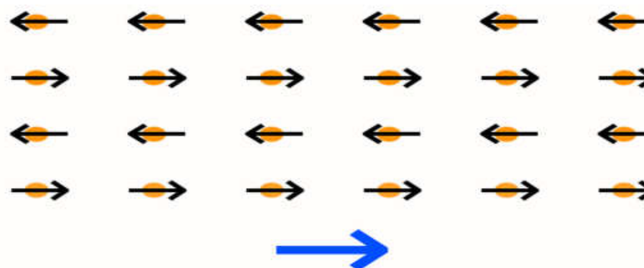

Figure I.30: The magnetic moments of an atom are reversed with that of the neighboring atom.

Macroscopically, this material reacts like a non-magnetic material (it is neither attracted nor repelled by a magnet), but magnetic phenomena intervene all the same at the microscopic level.

Note that, the antiferromagnetic materials are below a certain temperature (called Neel T_N) and are usually paramagnetic above. In addition to the intrinsically antiferromagnetic materials, ferromagnetic layer assemblies separated by an insulator sometimes also exhibit antiferromagnetic behavior. These devices are widely used in electronics and mechanics, because of particular electronic behavior **[71-73].** These constructions with antiferromagnetic behavior are used on the read heads of the hard disks, in the magnetic random access memory (Magnetic Random Access Memory, or MRAM) and more generally in other forms of electromechanical microsystem (or MEMS).) which include the accelerometers and hall sensors that are found in smartphones today **[74-76].**

I.11. Conclusion:

In this chapter we gave an introduction regarding the Spintronic domain and its importance in the industry besides different spintronic technologies and applications such as the GMR, TMR, MRAM, Spin field transistor and spin torque oscillators… where the exploitation of the spin is the main driving force in these technologies. Also we introduced the DMSs materials, their synthesis methods, their characteristics and their types, namely, DMSs based on the II-VI, IV-VI, III-V and IV semiconductors. Moreover, we elucidated the importance of our two main DMS of choice: GaN and GaAs, and their advantages in the spintronic applications, then we gave the different types of magnetic interaction governing the magnetism in DMS materials, beside some important magnetic behaviors observed in semiconductors (Ferromagnetism, Paramagnetism, antiferromagetism,…). Next we'll present the calculation methods and approximations used in our work.

Chapter II

Computational Methods: Ab initio and Monte Carlo

II. 1. Ab initio method:

II.1.1. Introduction:

In Condensed Matter physics, Studies based on ab initio calculations make it possible to predict and to explain the electronic structure and the nature of the magnetic interactions in Semiconductors, namely, GaN, GaAs with MTs. In the doping process, to simulate doping concentrations close to the experimental concentrations, supercells formed of a large number of atoms are required. The calculation results for TM-doped DMS were obtained using different implementations of the electronic structure, usually using density functional theory (DFT) in which the total energy of an N-system electrons is described as a function of electronic density.

Since solving Schrödinger equation is so difficult except for the case of hydrogen we resorted to the simulation methods such as the Monte Carlo method, molecular dynamics method, and also the methods for calculating the electronic structure called « Ab initio » (meaning « from the very beginning »), and which are used at zero temperature and constant pressure.

In this chapter we are going to present the theoretical foundations of the ab initio method used in this work. We first start with the fundamental quantum approximations introduced to solve the Schrödinger equation for a complex system, we then introduce the concept of density functional theory (DFT), which is based mainly on Hohenberg and Kohn's (1964) theorems and Kohn and Sham's (1965) approach. We explain how the exchange-correlation potential can be processed through different approximations (LDA, GGA).Then we describe the different possible choices for the basis of the wave functions and for the shape of the potential, more particularly the Linearized Augmentation + Local Orbital Waveforms coupled to the Total Potential (FP) and the KKR method based on the functions of Green.
The ab initio methods that rely on DFT can model materials reliably and quantitatively and process large systems **[77-79]**. In this way they allow comparison with the experimental results.

In this chapter, we will present the bases on which the DFT is based, by discussing the different levels of approximations needed to solve the Schrödinger equation. In particular, the approximations used in our Ab intio calculations**.**

II.1.2. Concept of the Density functional theory (DFT):

The density functional theory (DFT) is one of the most widely used quantum methods in the fields of solid state physics and quantum chemistry for the determination of the physical and quantum gradients of a system (and particularly the systems) containing a large number of electrons), such as its electronic structure, its ionization energy, etc. This is a so-called first principle method. Indeed, it is based on the foundations of quantum mechanics and involves only a limited number of input data. For a given system with several bodies, it makes it possible to solve the Schrödinger equation without the introduction of parameters adjusted by the experiment.

Here we give the Schrödinger equation:

Time dependent:

$$\hat{H}\Psi = E\Psi \qquad \text{II.1}$$

Precisely:

$$\hat{H}\boldsymbol{\Psi}(\{\mathbf{R_1}\},\{\mathbf{r_i}\},\mathbf{t}) = \mathbf{i}\,\frac{\partial\boldsymbol{\Psi}(\{\mathbf{R_1}\},\{\mathbf{r_i}\},\mathbf{t})}{\partial\mathbf{t}} \qquad \text{II.2}$$

With:

$$\hat{H} = \sum_i -\frac{\nabla^2}{2M_i} + \sum_i -\frac{\nabla^2}{2} + \hat{V}(\{R_1\},\{r_i\}) = m_e = e = 1 \qquad \text{II.3}$$

Giving:

e: The elementary charge

m_e: The mass of the electron

$\{R_1\}$: represents the variables that describe the nucleuses

$\{r_1\}$: represents variables describing the electrons

V: stand for the operator of potential energy considering all interactions in the system, namely, between the electrons, the nucleus, or between the two of them.

There are different methods within the DFT, some of these calculation methods are schematized on **Figure II.1**, and we'll detail a number of these methods in the upcoming section.

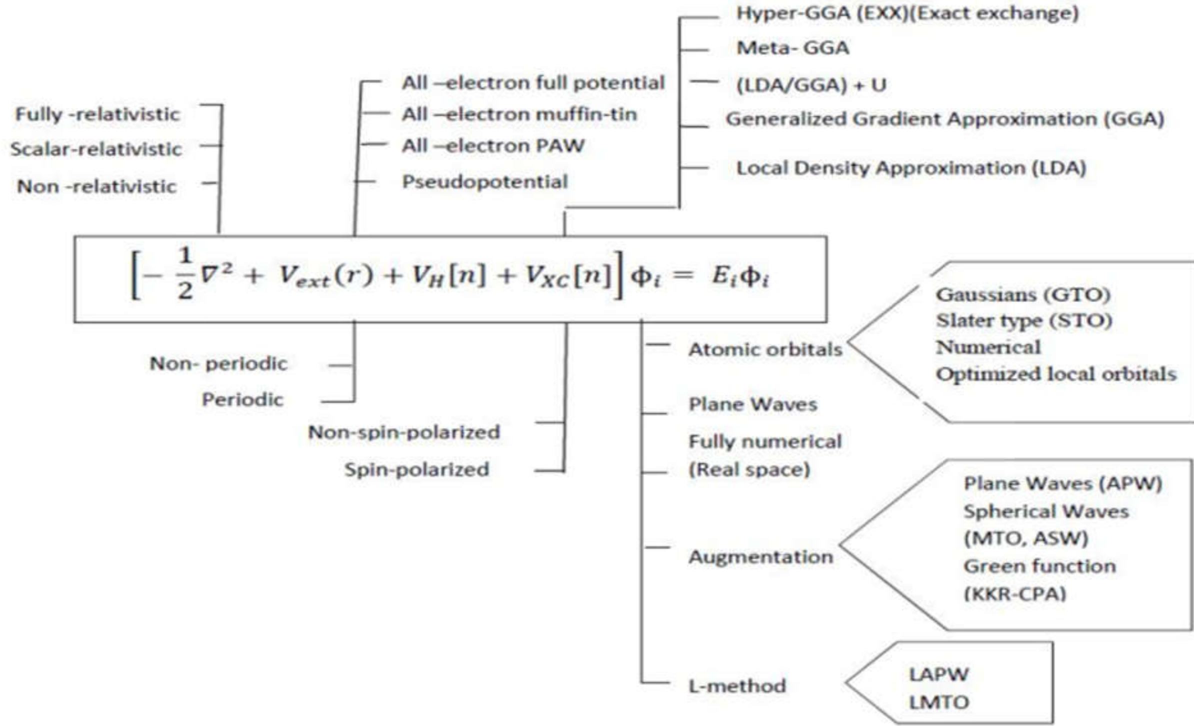

Figure II.1: Different calculation methods based on the DFT.

II.1.2.1. The N body problem:

Unlike the Hartree-Fock method where the energy of the system is a functional function of the wave function Ψ, the DFT expresses energy as a functional the electron density ρ. This method allows a great simplification of the resolution of the Schrödinger equation. Here, the N electrons (3N spatial coordinates) are replaced by the total electronic density which depends only on 3 spatial variables. The principle of the DFT is to reformulate a quantum problem to N body, into a one body problem (spin function) with electronic density as variable.

A solid, in condensed matter, is mixture of positively charged heavy particles (nuclei) and negatively charged light particles (electrons). If we have N nuclei, we are confronted with a problem of (N + ZN) particles in electromagnetic interaction. It's a multi-body problem. Here is the Hamiltonian for such system:

$$\hat{H}_T = \hat{T}_n + \hat{T}_e + \hat{V}_{n-n} + \hat{V}_{n-e} + \hat{V}_{e-e} \qquad \textbf{\textit{II.4}}$$

Where $\hat{T}_n$ and $\hat{T}_e$ are the kinetic energies of electrons and nuclei, $\hat{V}_{n-n}$ is the potential energy of nuclei-nuclei interaction, $\hat{V}_{n-e}$ as the potential energy of electron-nuclei interaction and

$\hat{V}_{e-e}$ for the potential energy of electron-electron interaction. Unfortunately, we can exactly calculate the eigenvalues of equation ***II.4*** only for the hydrogen systems. In the case of a polyelectronic system, it's nearly impossible to have an analytical solution of the Schrödinger equation, because of the electronic interactions. Therefore, in order to find acceptable approximated eigenstates, we need to make approximations. Let's present one of these solution approximations, the Born-Oppenheimer approximation.

II.1.2.2. The Born-Oppenheimer approximation:

All methods of solving the Schrödinger equation are based on this approximation, in which its authors (Born and Oppenheimer) assume that there is a large difference in mass between nuclei and electrons and a difference in time scale between electronic and nuclear movements. As a result, it is possible to decouple the movement of the nuclei from that of the electrons and to write the wave function as the product of two wave functions, a nuclear one and an electronic one in the equation ***II.5***:

$$\boldsymbol{\psi}(\vec{\boldsymbol{r}},\vec{\boldsymbol{R}}) = \boldsymbol{\psi}_{\boldsymbol{nucl}}(\vec{\boldsymbol{R}})\boldsymbol{\psi}_{\boldsymbol{elec}}(\vec{\boldsymbol{r}},\vec{\boldsymbol{R}}) \qquad \textit{II.5}$$

Where $\psi_{nucl}(\vec{R})$ is the wave function associated with the nuclei and $\psi_{elec}(\vec{r},\vec{R})$ is the wave function related to the electrons, with the nuclei fixed in the position $\vec{R}$. The total energy is then written as the sum of a nuclear and electronic contribution:

$$\boldsymbol{E} = \boldsymbol{E}_{\boldsymbol{nucl}}(\vec{\boldsymbol{R}}) + \boldsymbol{E}_{\boldsymbol{elec}}(\vec{\boldsymbol{R}}) \qquad \textit{II.6}$$

This approximation is known as the adiabatic approximation of Born-Oppenheimer **[80]**.The position of the nuclei then becomes a parameter and the problem consists in solving the electronic Schrödinger equation in the field of the supposedly fixed nuclei.

$$\hat{H}_{\boldsymbol{elec}}\boldsymbol{\psi}_{\boldsymbol{elec}}(\vec{\boldsymbol{r}},\vec{\boldsymbol{R}}) = \boldsymbol{E}_{\boldsymbol{elec}}(\vec{\boldsymbol{R}})\boldsymbol{\psi}_{\boldsymbol{elec}}(\vec{\boldsymbol{r}},\vec{\boldsymbol{R}}) \qquad \textit{II.7}$$

$$[\boldsymbol{T}_{\boldsymbol{e}} + \boldsymbol{V}_{\boldsymbol{ee}}(\vec{\boldsymbol{r}}) + \boldsymbol{V}_{\boldsymbol{nn}}(\overrightarrow{\boldsymbol{r}}) + \boldsymbol{V}_{\boldsymbol{ne}}(\vec{\boldsymbol{r}} + \vec{\boldsymbol{R}})]\psi_{elec}(\vec{r},\vec{R}) = E_{elec}(\vec{R})\psi_{elec}(\vec{r},\vec{R}) \qquad \textit{II.8}$$

There are various methods exist for solving equation ***II.6***, these methods are widely used in quantum chemistry to treat atoms and molecules, but they are less accurate for solids. DFT is a more modern and probably more powerful method. Its history dates back to the first half of the 20th century, but was formally established in 1964 by Hohenberg and Kohn's two theorems.

These authors demonstrated that all aspects of the electronic structure of a non-degenerate ground state system are completely determined by its electron density $\rho(\vec{r})$ instead of its wave function.

II.1.2.3. The Hohenberg and Kohn theorems:

In the First principle method, the DFT is based on the following two theorems of Hohenberg and Kohn **[81]**:

a. The electronic density $\rho_0(\vec{r})$, associated with the fundamental level of an N system electrons interacting in an external potential $V_{ext}(\vec{r})$, uniquely and rapidly determines this potential. As a result, all the properties of the system and in In particular, the total energy of the ground state is determined from $\rho_0(\vec{r})$. The functional state of the total energy of the ground state is written as follows:

$$\boldsymbol{E[\rho(\vec{r})] = F[\rho(\vec{r})] + \int \rho(\vec{r})V_{ext}(\vec{r})d\vec{r}} \qquad \textit{II.9}$$

Taking $\int \rho(\vec{r})V_{ext}(\vec{r})d\vec{r}$ as the interaction nuclei-electrons, $F[\rho(\vec{r})]$ is a functional density of $\rho(\vec{r})$ independent of external potential $V_{ext}(\vec{r})$; it contains the kinetic and coulomb contributions to energy:

$$\boldsymbol{F[\rho(\vec{r})] = T[\rho(\vec{r})] + V_{ee}[\rho(\vec{r})] = T[\rho(\vec{r})] + E_{Hartree}[\rho(\vec{r})] + E_{xc}[\rho(\vec{r})]} \qquad \textit{II.10}$$

Where T $[\rho(\vec{r})]$ is the kinetic energy of the electronic system, $V_{ee}[\rho(\vec{r})]$ is the electron-electron interaction that includes Hartree's energy $E_{Hartree}[\rho(\vec{r})]$ (the electron-electron Coulomb repulsion) and the exchange and correlation energy $E_{XC}[\rho(\vec{r})]$.This functional is not exactly known because the expressions of kinetic energy T $[\rho(\vec{r})]$ and the exchange and correlation energy $E_{XC}[\rho(\vec{r})]$ are not exactly known.

b. Let's take an external potential and a fixed number of electrons, the fundamental state of the system is the overall minimum of the functional $E[\rho(\vec{r})]$ and the density of the ground state $\rho_0(\vec{r})$is the density which minimizes this functional.

$$\left[\frac{\partial E[\rho(\vec{r})]}{\partial \rho(\vec{r})}\right]_{\rho(\vec{r})=\rho_0(\vec{r})} = 0 \qquad \textit{II.11}$$

The functional F $[\rho(\vec{r})]$ is taken as universal for any multi-system of electrons. If this functional is known, then it will be relatively easy to use the variational principle to determine total energy and density of the ground state for a given external potential. Unfortunately, Hohenberg and Kohn's theorem gives no indication on the form of F $[\rho(\vec{r})]$.

II.1.2.4. The Kohn-Sham arstaz equations:

In condensed matter, the Kohn-Sham theory **[82]** is based on the hypothesis that it is possible to reproduce the ground-state density of a system composed of N interacting particles by an auxiliary system consisting of independent particles. The real system formed by interacting electrons is replaced by a set of fictitious and independent particles evolving in an effective potential. All the N-body interactions being contained in a functional exchange and correlation depending on the electron density given by:

$$\boldsymbol{\rho(\vec{r}) = \sum_{i=1}^{N} |\psi_i(\vec{r})|^2} \qquad \textit{II.12}$$

The "variational" principle was applied for the ground state energy and the density given the functional $E_{Vext}(\rho(\vec{r}))$. Therefore the energy functional is written as:

$$\boldsymbol{E_{Vext}[\rho(\vec{r})] = T_0[\rho(\vec{r})] + V_H[\rho(\vec{r})] + V_{xc}[\rho(\vec{r})] + V_{ext}[\rho(\vec{r})]} \qquad \textit{II.13}$$

The variable T_0 stands for the kinetic energy of the system without interaction, V_H is the term of Hartree (the classic Coulomb interaction between electrons). V_{xc} the term introducing the effects of exchange and correlation, and finally V_{ext} includes the Coulomb interaction of electrons with nuclei and nuclei between them. The Hartree's term and kinetic energy play an important role in describing the states of free electrons.

These variables are the most important in the treatment of electron interaction. The difference between the real kinetic energy and that of the non-interacting electrons as well as the difference between the real interaction energy and that of Hartree are taken into account in the energy of exchange and correlation.

Meanwhile, The Schrödinger equation is written as follows:

$$\boldsymbol{\left[-\frac{\hbar^2}{2m_e}\overrightarrow{\nabla_i}^2 + V_H(\rho(\vec{r})) + V_{XC}(\rho(\vec{r})) + V_{ext}(\rho(\vec{r}))\right]\psi_i(\vec{r}) = E_i\psi_i(\vec{r})} \qquad \textit{II.14}$$

Where: **i**= 1,…, N.

Thus the exchange and correlation potential is given by the derived functional:

$$\boldsymbol{V_{xc}(\rho(\vec{r})) = \frac{\partial V_{xc}[\rho(\vec{r})]}{\partial \rho(\vec{r})}} \qquad \textit{II.15}$$

Consequently, to determine the fundamental state of the system, we must solve, in a self-consistent manner, Kohn-Sham equations ***II.13***. The sum of the three terms $V_H + V_{HC} + V_{ext}$ constitutes an effective potential V_{eff} taken as local, since it depends only on r. This method is very accurate, but for practical calculation, the exchange and correlation energy, which is a density functional, it requires the introduction of other approximations.

II.1.2.4 .a. Solving Kohn-Sham equations:

To solve the Kohn-Sham equations, one must choose a basis to represent the electronic density ρ (r), the potential V (r) and the orbitals of Kohn-Shamφ_i. The process of resolution is done iteratively using an auto coherent cycle of iterations. This is accomplished by injecting the initial density of charge ρ_{in} to diagonalize the secular equation:

$$\mathbf{(H-\varepsilon_i S)=0} \qquad \textit{II.16}$$

With H representing the Hamiltonian matrix and S is the recovery matrix.

After that, the new density of charge ρ_{out} is constructed with the eigenvectors of this secular equation using the total charge density that can be obtained by summation over all occupied orbitals. If we do not obtain the convergence of the calculations, we mix the densities of charges ρ_{in} and ρ_{out} as follows:

$$\boldsymbol{\rho_{in}^{i+1} = (1-\alpha)\rho'_{in} + \alpha\rho'_{out}} \qquad \textit{II.17}$$

Taking i as the i_{th} iteration and α as a mixing parameter. Thus the iterative procedure can be continued until convergence is achieved. When the convergence is reached, the energy of the ground state of the system is accessed. This entire procedure is shown below, in **Figure II.2**.

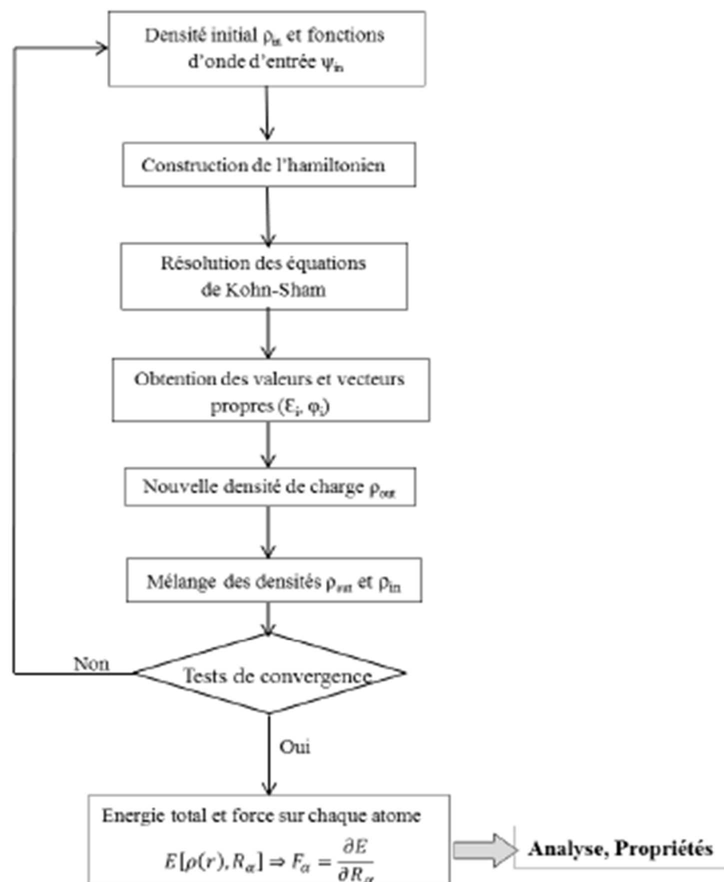

Figure II.2: schematic representation of the auto-coherent cycle corresponding to the resolution of Kohn-Sham equations **[82].**

The previous algorithm calculates the energy and electronic density in the state fundamental of the atomic configuration with a fixed geometry (shape and volume). If the atomic set is not in mechanical equilibrium, forces are exerted on the atoms. They can be calculated from the Hellmann-Feynman theorem.

In a practical way, it is enough to recover the value of the forces on the atoms at the end of each self-coherent electronic cycle and to use conjugated gradient or Verlet algorithms to minimize the energy and determine the optimal geometry or else perform molecular dynamics calculations.

II.1.2.5. The Hartree-Fock approximation:

Since the electron-electron interaction creates a sort of complexity in their studies, the Hartree-Fock approximation was proposed to resolve this problem taking into consideration the supposition of free electrons. Hence, the electrons are taken as independent and each electron is

surrounded by a number of other electrons which creates a field in which the electron can progress. In this case, every electron evolves in an orbital, so we can write the total wave function as follow:

$$\boldsymbol{\Psi}(\{\boldsymbol{R_1}\},\{\boldsymbol{r_i}\},\boldsymbol{t}) = \boldsymbol{\Psi_1}(\{\boldsymbol{r_i}\}) \ldots\ldots \boldsymbol{\Psi_{Ne}}(\{\boldsymbol{r_{Ne}}\}) \qquad \textit{II.18}$$

It's a product of orthogonal wave functions of one particle. So as we are discussing the electron-electron interaction, one should not forget about the Pauli principal, and unfortunately this principle does not apply well within this approximation, so the solution based on the Harthree-Fock approximation was to take the wave function of N electrons as a Slater determinant such as the elements of the determinant have one electron each **[83,84].** Consequently, every electron is under the influence of two fields, an external field generated by the nucleuses, and another field created by the surrounding electrons and it's named Hartree potential.

The goal is still the same and it's to reach an exact solution for the Schrödinger equation. In this aim, There are various methods in quantum chemistry founded on the Hartree-Fock approximation to deal with atoms and molecules but still doesn't give precise results for solids.

II.1.2.6. The exchange-correlation energy:

The fact that the DFT gives no information on the form of the functional exchange-correlation, the approximation introduced for its determination must be applicable for different systems. The interactions between electrons give rise to three kinds of effects:

The first one is the exchange effect, also called Fermi correlation, which results from the anti-symmetry of the total wave function. It corresponds to the fact that two electrons of the same spin have a zero probability of being in the same place. This effect is directly related to Pauli's principle and absolutely does not involve the charge of the electron. The Hartree-Fock approximation takes it into account naturally, because of the anti-symmetry of the Slater determinant representing the wave function Ψ.

The second one is the coulomb correlation which is due to the charge of the electron. It is connected to the repulsion of electrons in $1 / |r-r'|$. Unlike the exchange effect, it is spin independent. This effect is neglected by the Hartree-Fock theory.

The third effect emanates from the fact that the electronic wave functions are formulated in terms of independent particles. This is the 'self-interaction 'correction **[85]**, which must lead to a correct count of the number of electron pairs.

On the other hand, to apply Kohn-Sham's approach, the exchange-correlation term is required, Moreover, the correction of the kinetic energy term. Indeed, even if the density of the fictitious system considered is the same as that of the real system, the determined kinetic energy is different from the real energy, because of the artificial independence of the wave functions.

The calculation of energy and exchange-correlation potential is based on a number of approximations, which we'll introduce next.

II.1.3. Ab initio Approximations:

II.1.3.1. The Local Density Approximation (LDA):

We have used this approximation in our work. The Local Density Approximation (LDA) is based on the assumption that the electron density varies slowly in space and therefore the exchange-correlation terms depend only on the local value of ρ (r); that is, it treats a non-homogeneous system as locally homogeneous.

The exchange-correlation functional$E_{xc}(\rho(\vec{r}))$ is thus replaced by that of a homogeneous gas of density electrons ρ (r):

$$\boldsymbol{E_{xc}^{LDA}[\rho(\vec{r})] = \int \rho(\vec{r})\varepsilon_{xc}[\rho(\vec{r})]d\vec{r}} \qquad \textit{II.19}$$

Taking $\varepsilon_{xc}[\rho(\vec{r})]$ as the exchange-correlation energy for a uniform gas of electrons, with ρ(r) as a density.

The exchange-correlation functional can be divided into two terms, one term of the exchange and another representing the correlation.

$$\boldsymbol{E_{xc}^{LDA}[\rho(\vec{r})] = E_{x}^{LDA}[\rho(\vec{r})] + E_{c}^{LDA}[\rho(\vec{r})]} \qquad \textit{II.20}$$

With the Dirac exchange functional gives $E_x^{LDA}(\rho(\vec{r}))=-\frac{3}{4}(\frac{3}{\pi}\rho(\vec{r}))^{1/3}$.

There are some studies, namely, quantum Monte Carlo calculations **[86,87]** in which precise values of $E_c^{LDA}[\rho(\vec{r})]$ have been obtained. These values were then interpolated by Vosko, Wilk

and Nusair (VWN) **[88]** and by Perdew and Zunger **[89]** and Hedin-Lundqvist **[90]** to arrive at a form analytics of $E_c^{LDA}[\rho(\vec{r})]$.

Recall that the LDA approximation only describes the ground state of electronic systems but not the excited states. The bandwidths of forbidden energies of semiconductors and insulators are underestimated in this approximation. For some systems with strong correlation effects (f-band or narrow-band), the LDA does not adequately describe the properties of the system. Especially, Mott-Hubbard insulating-type transition metal compounds or charge transfer insulators are predicted metal.

II.1.3.2. The generalized gradient approximation (GGA):

The Generalized Gradient Approximations (GGA), which we've employed in our work, provides an improvement over the LDA approximation. In the local approximation, the exchange and correlation potential depends only on density$\rho(\vec{r})$. Whereas, in the GGA approximation, the potential is expressed as a function of the local electronic density$\rho(\vec{r})$ and its gradient $\nabla\rho(\vec{r})$ **[91]**.

$$\boldsymbol{E_{xc}^{GGA}[\rho(\vec{r})] = \int \rho(\vec{r}) f[\rho(\vec{r}).\nabla\rho(\vec{r})] d\rho(\vec{r})} \qquad \textit{II.21}$$

$f[\rho(\vec{r}), \nabla\rho(\vec{r})]$ as the exchange-correlation function depending on the electronic density and its gradient.

In Ab initio calculations, we find several versions of the GGA, but the most frequently used in theoretical works are those introduced by Perdew and Wang (PW91) **[92]** and Perdew, Burke and Ernzerhof **[93].** In many cases, the GGA approximation provides better results than the LDA for total energies, cohesive energies, equilibrium volumes, and incompressibility modules **[94].** However, the forbidden band widths of insulators and semiconductors remain far too low. Systems with high correlations (narrow or narrow bands) are poorly described.

II.1.3.3. The local density and generalized gradient approximations with the Hubbard correction (LDA + U and GGA + U):

In the TM-doped or Rare earth-doped systems in which there are highly localized d or f orbital systems, the effective intra-site Coulomb repulsion between localized electrons, represented by U (Hubbard's term) is strong in front of the bandwidth. The LDA method is then insufficient and

the intra-atomic correlations must be taken into account. Mott Hubbard's insulators, such as the transition metal compounds of the end of the 3d series, of rare earths, or of actinides, are in fact obtained in LDA metal.

This incorrect description of high correlation systems comes from the fact that in the LDA method, the charge density is defined by an average occupancy on all orbitals of the same orbital quantum number l. The effective mono-electronic potential which is a functional of the charge density is therefore identical for all the orbitals having the same value of l. This violates Hund's second rule associated with orbital polarization and responsible for local moments.

In more details, the Strong intra-site Coulomb interactions screened between d electrons have been introduced using the approach known as the DFT + U method that combines the DFT (LSDA or GGA with spin polarization) method with a Hubbard Hamiltonian:

$$\hat{H}_{\text{Hubbard}}=\frac{U}{2}\sum_{m,m',\sigma}\hat{n}_{m,\sigma}\hat{n}_{m',-\sigma}+\frac{(U-J)}{2}\sum_{m\neq m',\sigma}\hat{n}_{m,\sigma}\hat{n}_{m',\sigma} \qquad \textit{II.22}$$

Where $\hat{n}_{m,\sigma}$ is the operator that gives the number of electrons occupying an orbital that has the quantum magnetic number m and spin σ at a particular site. U is the spherically averaged Hubbard parameter, which describes the energy cost of placing an extra electron on a particular site. J represents the screened exchange energy. U depends on the spatial extension of the wave functions and the screening. J is an approximation of the exchange parameter of Stoner. Parameters U and J characterize the intrasite Coulomb repulsion. In addition to that, in this approach U and J do not interfere separately but by their difference (U_{eff} = U- J).

The Hamiltonian of Mott-Hubbard has the contributions of energy already accounted for by the functional DFT. After subtracting the twice-counted terms from the energy given by the classical DFT method, the energy of the functional DFT + U in spin polarization is obtained:

$$E_{DFT+U}=E_{DFT}+\frac{(U-J)}{2}\sum_{m\sigma}(\hat{n}_{m,\sigma}-\hat{n}^{2}{}_{m\sigma}) \qquad \textit{II.23}$$

II.1.3.4. Linearized augmented plane wave method:

II.1.3.4-a. Definition of the linear augmented plane wave (LAPW) method:

The LAPW was first introduced by Andersen in the aim to resolve the problems brought by the APW base and especially the problem of non-linearity **[95]**. This method is also considered as an

improvement of the APW given by Slater. Its principle evolves Taylor series expansion which is performed for the radial function around the energy E_0 where we can determine the function $u_l^\alpha(r', E)$:

$$\mathbf{u}_l^\alpha(\mathbf{r}', \mathbf{E_k}) = \mathbf{u}_l^\alpha(\mathbf{r}', \mathbf{E_0}) + (\mathbf{E_0} - \mathbf{E_k})\left[\frac{\partial u_l^\alpha(r', E)}{\partial E}\right]_{E=\mathbf{E_0}} \qquad \textbf{\textit{II.24}}$$

And

$$\left|\frac{\partial u_l^\alpha(r', E)}{\partial E}\right|_{E=E_0} = \dot{u}_l^\alpha(r', E_0) \qquad \textbf{\textit{II.25}}$$

Hereafter, we use the given equations ***II.24*** and ***II.25*** to get the expression for the LAPW basis:

$$\psi_K^k(r, E) = \begin{cases} V^{-1/2} e^{i(k+K)r} & Region(I) \\ \{A_{lm}^{\alpha,k+K} u_l^\alpha(r', E_0) + B_{lm}^{\alpha,k+K} \dot{u}_l^\alpha(r', E_0)\} * Y_{lm}(r') & r < R_{MT}^\alpha \end{cases} \qquad \textbf{\textit{II.26}}$$

Where:

$B_{lm}^{\alpha,k+K}$: As coefficient which is determined by the continuity of Ψ_K^k(r, E).

E_0: Is an Energy value.

E_0 is taken close to the center of the band p of the studied energy, this, when we investigate a proper state with character p. So that we find the energy difference E_0- E_k as minimum as possible. Hence, LAPW method is very practical, providing all the valence bands energies based only on an energy value of E_0.

R_{min}^α: As the minimum radius of the atomic sphere.

K_{max} : represents the maximum value of ||K||.

Normally, the R_{min}^α K_{max} is taken between 7 and 9. Consequently, the electronic density for spin up and down can also be calculated by integrating the square of the wave function in the sampled Brillouin zone.

II.1.3.4-b. Definition of the Linear Augmented plane wave with Local orbitals LAPW+Lo method:

The application of the Augmented plane wave with Local orbitals (LAPW+Lo) method is significant in the case of various electronic state studies, namely, "semi-core" states despite that

this type have a small contribution in the atomic bounding and the electronic hybridizations **[96]**. Hence, in order to resolve this issue, the next equations are used to implement the local orbitals into the LAPW method:

$$\psi_{lm}^{LO} = [A_{lm}u_l(r, E_{1,l}) + B_{lm}\dot{u}_l(r, E_{1,l}) + C_{lm}u_l(r, E_{2,l})]Y_{lm}(\hat{r}) \quad II.27$$

There are two purposes, the first one is to have a better linearization of the LAPW method and the second one is to be able to treat the semi-core and valence states in the calculation. Thus, was the need to add other basic functions, namely, "local orbital" functions **[97]**, having a linear fusion of two radial functions corresponding to two different energies (3s and 4s…) with their derivatives.

In addition, the coefficients A_{lm} , B_{lm} and C_{lm} are calculated using the condition that ψ_{lm}^{LO} have to be standardized besides having a slope at the edge of the sphere.

II.1.3.4-c. Insight on the Full Potential Linearized Augmented Plane Wave (FP-LAPW) method:

Note that, in order to study the electronic behavior of studied atomic systems, the plane wave is accurate to describe the free electrons when they are distant from the core, but when the electrons are very close to the core, they are assimilated as a free atom, another method is used in this case, which is the spherical functions.

The spheres in this method can be illustrated as shown in **Figure II.3**, there are two regions: spherical muffin tin and interstitial region, these two regions are treated differently. Thus, two approaches are applied: in one hand, the spherical functions inside the muffin tin spheres where the solutions of Schrödinger equation are radial and angular, in the other hand, the plane wave in the interstitial region.

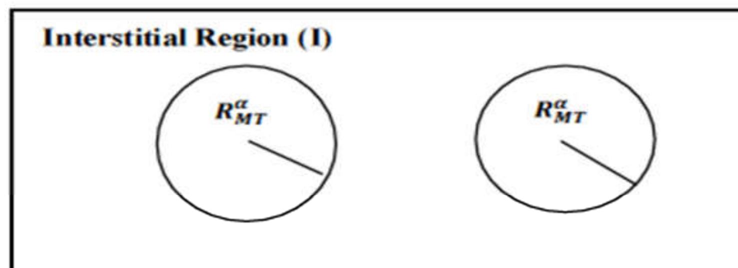

Figure II.3: Interstitial and spherical regions.

Here's where this method is interesting: the FP-LAPW or full-potential linearized augmented-plane wave method, enables a self-consistent solution of the Schrödinger equation (Kohn-Sham) within the unit cell involving the muffin tin sphere and the interstitial area. In addition, the potential and the density in the muffin tin spheres are both described by the angular and radial functions, since we've a spherical symmetry. However, in region (l), the unit cell is described by plane waves.

II.1.4. The Calculation code_ AKAIKKR:

II.1.4.1. Outlook on the AKAI code:

The AkaiKKR (MACHIKANEYAMA) is a program package designed and made by Akai **[98]** using the Korringa- Kohn-Rostoker method combined with the coherent potential approximation (KKR-CPA) with the parameterization of Moruzzi, Janak and Williams (MJW), and Vosko, Wilk, and Nusair (VWN) **[88], [99]**. This code is exploited to perform first-principles calculation (Ab initio) of electronic structures, of metals, semiconductors and compounds beside the magnetic properties for the DMS, all this within the local density approximation (LDA) or generalized gradient approximation (GGA) of the density functional theory.

AkaiKKR is based on KKR–Green's function method. The code offers unique advantages in the calculations: high speed, high accuracy and compactness. It's a totally electronic method which, unlike the plane-wave cutoff, it does not has any serious truncation errors. In addition, since AkaiKKR is combined with CPA (coherent potential approximation), it makes the code very convenient for both normal ordered crystals and disordered systems, such as impurity systems, random substitutional alloys and mixed crystals. Also, the fact that the method directly calculates the Green's function of the system, it provides a good starting point for first-principles linear response theory, many-body theory, etc.

The package has been continuously developed since late 70th. Each program in the package is written in FORTRAN 77. The package is completely self-contained and does not need any additional libraries. It runs equally well, under different platforms (UNIX, Linux, Mac OS), on a small note PC and a large supercomputer.

We use the LDA technic as approximation since we have a disordered system. This method is the most convenient to study this kind of system. KKR-CPA was developed by Akai and Dederichs for DMSs doped with a transition metal see Refs **[100]** about KKR-CPA method. Also for oxide semiconductors, ZnO based DMSs **[101]**.

We've employed the Generalized Gradient Approximations (GGA) approximation, Perdew–Wang functional, (GGA91) **[92]**, to treat this disordered system since it is one of the most accurate and precise approximation to deal with this disorder.

Hereafter, we introduce the KKR-CPA method with the details.

II.1.4.2.Studied Materials and Calculation details:

II.1.4.2-a. Gallium Nitride (GaN) case:

We have used the AKAI-KKR-CPA code MACHIKANEYAMA2002v08 package designed and made by Akai **[98]** for our GaN system. Within the Korringa- Kohn-Rostoker method combined with the coherent potential approximation (KKR-CPA) with the parameterization of Moruzzi, Janak and Williams (MJW), and Vosko, Wilk, and Nusair (VWN) **[88].** The MJW and VWN functional predict a band gap of approximately 2.72 eV for bulk GaN. This finding is compared with the experimental value of 3.507 eV. We use the LDA technic as approximation since we have a disordered system. This method is the most convenient to study this kind of system. KKR-CPA was developed by Akai and Dederichs for DMSs doped with a transition metal see Refs **[100]** about KKR-CPA method. Also for oxide semiconductors, ZnO based DMSs **[101]**.

The density of states (DOS) were calculated and plotted for $Ga_{1-x}Mn_xN$ for different doping concentrations which are Mn magnetic impurities. For better understanding of the upcoming figures, the syntax "Total" represents the total density of spins up and down, located in the valence and band conduction in the system structure. The Total density must not change from a figure to another. But the partial DOS curves will change, when varying the doping concentrations. These concentrations are x(Mn)=0.10, x(Mn)=0.15 and x(Mn)= 0.20. After the doping operation, the Mn atoms are placed in the Ga sites in the wurtzite structure at any concentration. We've used in our code 250 K-point in the first Brillouin zone and took into account that the magnetic impurities (Mn) replace randomly Ga atoms in the structure. Our system has a wurtzite crystal structure with a = 3.180 Å, and c = 5.166 Å as lattice constants and u= 0.377 **[102]**. Since the unite cell is hexagonal with two lattice parameters, our atoms in this

system are disposed as each Ga atom is encircled by four N atoms on the corners and vice versa as we will see next for more details about the model.

II.1.4.2-b. Gallium Arsenide (GaAs) case:

The first principal calculations (Ab initio) were executed also with the AKAI-KKR-CPA code MACHIKANEYAMA2002v08 package designed and made by Akai. Korringa- Kohn-Rostoker method **[98]** combined with the coherent potential approximation (KKR-CPA).Based on the density functional theory (DFT), the KKR-CPA method was developed by Akai and Dedrichs to trait transition metal alloys, with the parameterization of Vosko, Wilk and Nusair (VWN) **[88]**, e.g. in our case we have GaFeAs and GaNiAs alloys. The host material is GaAs and the transitions metals are Fe and Ni, the doping with these impurities is done randomly since the Fe and Ni atoms in each case replace and take the cation atoms (Ga) sites randomly. Therefore, we have employed the Generalized Gradient Approximations (GGA) approximation, Perdew–Wang functional, (GGA91) **[92]**, to treat this disordered system since it is one of the most accurate and precise approximation to deal with this disorder. In our previous works we have used the local density approximation LDA approximation also.

The density of states (DOS) were calculated and plotted for both systems $Ga_{1-x}Fe_xAs$ and $Ga_{1-y}Ni_yAs$ for different doping concentrations which are the Fe, Ni magnetic impurities. To better understand the upcoming figures, the syntax "Total" represents the total density of spins up and down, located in the valence and conduction bands in the system structure. The Total density must not change from a figure to another. But the partial DOS curves will change, when varying the doping concentrations. These concentrations are x (Fe) =0.01, 0.02, 0.03, 0.04, 0.05, 0.06, 0.07, and y (Ni) = 0.01, 0.02, 0.03, 0.04, 0.05, 0.06, 0.07. As mentioned above, the Fe atoms are placed in the Ga sites inside the structure of GaAs. We've used in our code 300 K-point in the first Brillouin zone. Our system is a III-V direct bandgap semiconductor with a zinc blende crystal structure. With a = b= c= 5.65325 Å, as lattice constants and T_d^2-F43m as a space group. Since we have a zinc blend structure with one lattice parameter, our atoms in this system are disposed as each Ga atom is encircled by four As atoms on the corners and vice versa.

II.1.4.3. The coherent potential approximation (CPA) method:

II.1.4.3-a. presentation:

In material physics, alloys are the center of high importance in material researches. They attracted a lot of interest because the addition of small percentage of atoms in a metal or semiconductor changes the magnetic and mechanical properties. The KKR method calculates the energy band structure of these classes of materials. This is one of the most powerful methods that have brought a deeper understanding of the structure of metals and semiconductors. The application to solids of this method among others allowed the use of Bloch's theorem where the periodicity of the crystal leads to simplifications in the equations.

On the other hand the averaging process in the coherent potential approximation is done on all possible configurations. It applies to disordered alloys that do not present short-range order. The concept of this coherent potential has been developed in the context of multiple diffusions. It was proposed for the first time by Shiba and Soven **[103,104]**.

In condensed matter physics, the coherent potential approximation, denoted as (CPA), is a method consisting on of finding the Green's function of an effective system. It is a very benefiting approach, used in other domains, as, to understand the scattering of sound waves in a material which displays spatial inhomogeneity.

In our case, the CPA is applied to random materials using the muffin-tin approximation to calculate electronic band structure in solids. A variational implementation of the muffin-tin approximation to crystalline solids using Green's functions was suggested by Korringa and by Kohn and Rostocker, and is often known as the KKR method. For random materials, the theory is applied by the introduction of an ordered lattice of effective potentials to replace the varying potentials in the random material. This approach is called the KKR coherent potential approximation.

II.1.4.3-b.The idea behind the coherent potential approximation (CPA):

Let us consider the representation in **Figure II.4** and take a random alloy system which consists of n components, A_1 , A_2 , ... A_n and their concentrations are x_1 , x_2 , ... x_n . Suppose that the

atom A_i is at the origin in the effective medium. Green's function which starts from the origin and comes back to the origin is:

$$G^{i}_{LL'} = \sum_{L''} \widetilde{G}_{LL''}[1-(t_i-\tilde{t})\widetilde{G}]^{-1}_{L''L'} \qquad II.28$$

$G_{LL'}$ and $\tilde{t}$ are the Green's function with t-matrix (coherent t-matrix) of the effective medium, respectively. CPA is an efficient approximation to determine $\tilde{t}$. We use the self-consistent equation:

$$\sum_{i=1}^{n} x_i G^{i}_{LL'} = \widetilde{G}_{LL'} \qquad II.29$$

This equation means that we calculate the Green's function of the medium by taking weighted average of the Green's function where the component atom is placed at the origin in the effective medium.

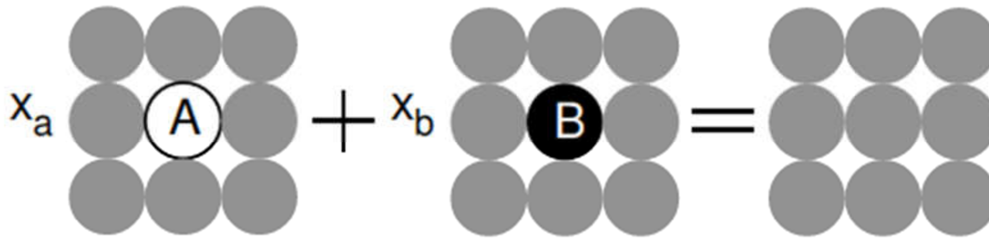

Figure II.4: Schematization of the CPA method

II. 2. Monte Carlo simulation:

II.2.1. Introduction:

Monte Carlo method is one of the most accurate and important numerical methods used in atomic scale calculations and to solve statistical physics problems both in equilibrium and out of equilibrium states **[105].** This method has a strong asset which is the ability to exploit empirical or ab initio results in the simulations in the aim to calculate various properties, namely, thermodynamic and transport properties of systems.

Monte Carlo method is based on simulations that enable us to utilize experimental or ab initio results along with classical statistical mechanics, in order to find out the thermodynamic and transport properties of various systems. Within this method, the change or development in our

system is controlled by a stochastic process based on a sequence of random numbers generated in the simulation by the program **[106]**.

Generally, one can dissemble Monte Carlo models into three defining steps, in the first one; the studied physical problem is represented in an analogous probabilistic or statistical model. In the second one, a high number of arithmetical and logical operations within a numerical probabilistic sampling experiment are used to solve the generated model, and then we have generated a number of data, which leads us to the third step, where the collected data are analyzed using statistical methods and we present and interpret the results, see **Figure II.5**.

More importantly, Monte Carlo method is founded on Metropolis algorithm which stands out as one of the most powerful and known numerical algorithms on the 20th century **[107,108]**. Nevertheless, this method is limited by the computer tie and memory since we need a computer to perform the simulations, and the larger the simulations, the more powerful the computer should be.

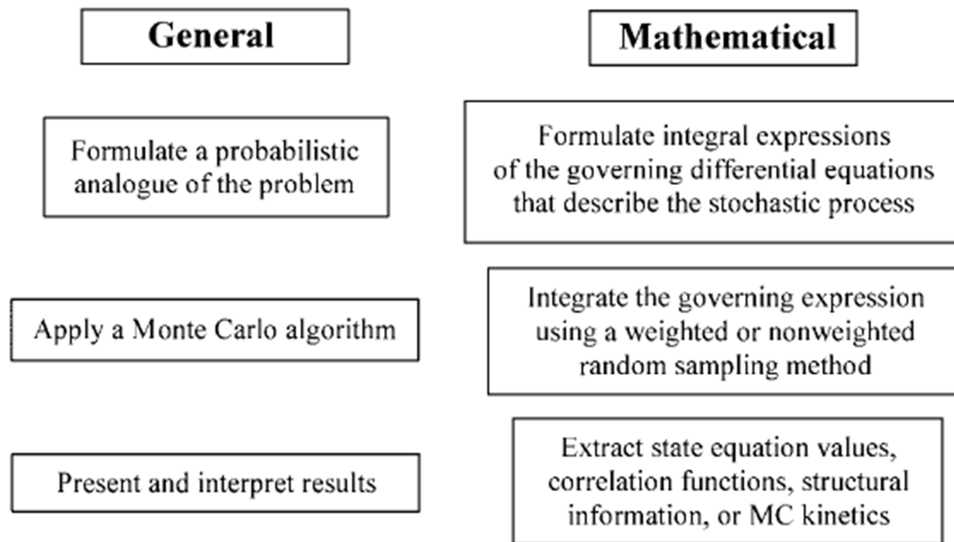

Figure II.5: Monte Carlo method modeling

In Statistical mechanics, one of our priorities is to study and calculate the different properties of condensed matter systems in macroscopic scale. Generally, a physical system can be studied macroscopically and microscopically, the first one is not an easy task, hence, we investigate the microscopic properties of the system and we use the obtained results to describe the macroscopic behavior of that system. Nevertheless, these systems contain a huge number of data, leading us to

a critical problem in these types of systems, which is there composition of a high number of particles with various types. Hence, Monte Carlo method is an example of the numerical computer simulations that are key methods in the aim to investigate and study profoundly the complex physical systems, namely, spin, spin glasses, critical phenomena and order- disorder phase transitions or even in biology problems, protein folding. These magnetic properties and phase transitions of these systems have been highly studied with various techniques as the mean-field approximation **[109,110]**, renormalization group **[111]**, series expansions **[112]** and Monte Carlo simulations **[106]**, **[113]** which stands out as the most precise and powerful method among them.

Hereafter, we have to point out the fact that not every magnetic system has these phase transitions. The presence of phase transition is normally related to different system's parameters, that is to say, the type of interactions between the atoms, the dimension of the space and symmetry of the system. Relating to that, we've mentioned before the order- disorder situation, there is an order parameter related to the type of symmetry that the investigated system has. There is a critical point, see **Figure II.6**, according to which the analysis is based on. Such as, if in one phase above the critical point, it takes a non-zero value, and zero otherwise, this order parameter is considered a good one. For us we're interested in the magnetic systems that have a phase transition, in this case the magnetization is considered as the order parameter.

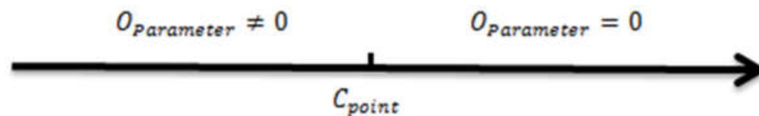

Figure II.6: C_{point} representation

II.2.2. Simulation Models:

In condensed matter physics, a magnetic system is one formed of atoms having a magnetic moment and a spin. But before going into that, one should ask how can we describe a physical system?

Describing a system includes solving it; there are two methods for that:

1. By solving, numerically, the Schrödinger's equation of the system, which includes every data, starting with all possible and complicated interactions to understand quantitatively the behavior of this studied system.

2. By simplifying the system with a representative model that has the system's key parameters, and then from this model we can elaborate an analytic solution or an accurate numerical one.

Within a magnetic system, the magnetic interactions between the ions are the most important source of information. Thus, a variety of Hamiltonians related to magnetic models were given to describe the interactions in these magnetic systems. The spin and lattice model are the two main elements of these magnetic models **[114,116].** In addition, the Hamiltonian is the representation of the energy variation and magnetic coupling in the studied magnetic system, using spin variables and coupling exchange as input.

II.2.2-a. Structures and geometries:

In physics, every system has degrees of freedom which represent the most important parameter that controls the system. Hereafter, we can define the lattice model in two parts; the first one is, as an interval where the degrees of freedom reside on the sites. The second one is, as a space that connects a D-dimensional lattice. Let's take the example of spins system (magnetic system), it's crucial to know which spins are interacting in the system because that controls the magnetism. To do that, those spins most have a position or location, or we have to elaborate a way to connect one spin with the other. Hence, this can be schematized by a geometric structure, composed by line linked lattices.

There are various examples of lattice schematization, as shown in **Figure II.7**, that we can divide in three categories:

(1) A simple lattice, such as cubic, square, triangular or honeycomb).

(2) Complicated regular lattice, namely, diamond, face-centered cubic (FCC), body-centered cubic (BCC) or hypercubic,...

(3) Random lattices, see refs **[115-118]**.

Generally, in the regular lattice, every spin is located on a site. Nevertheless, in the random lattices, some sites in the structure can be empty or simply does not have any spin. In addition, between sites, there is a lattice bond which connects two sites to each other.

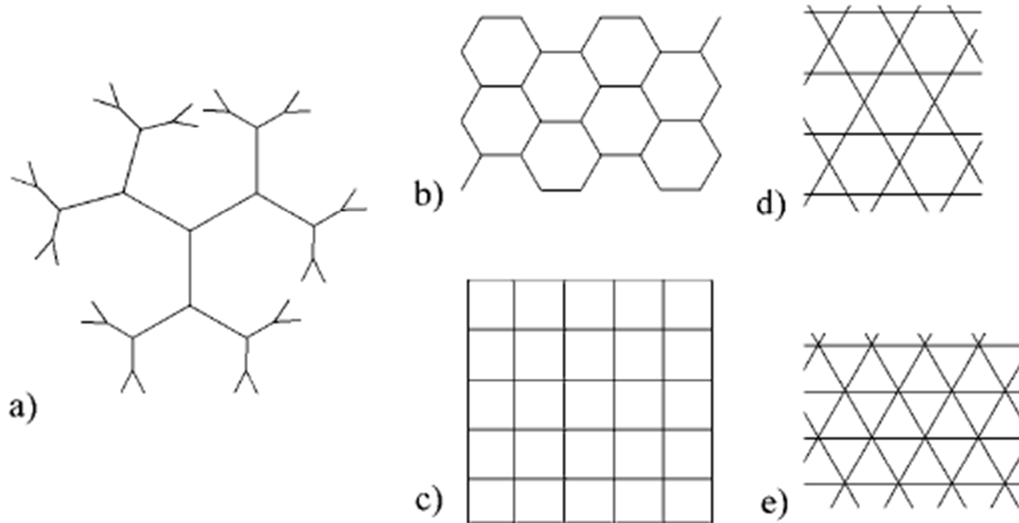

Figure II.7: Various 2D spacial lattices used in Monte Carlo, cellular automaton and percolation simulations also.

(a) Bethe/Cayley lattice (coordination number k = 3) (lattice with no closed circuits; beside the perimeter sites, the other sites have the same number of neighbors);

(b) Honeycomb lattice (k = 3);

(c) Square lattice (k = 4);

(d) Kagom´e lattice (k = 4);

(e) Triangular lattice (k = 6).

II.2.2-b. *Ising* model:

Among the most famous models in solid-state physics and material sciences, spin models are based on degrees of freedom which are located in a discrete spatial lattice and interact locally. Beside different terms of spin interaction that are implemented in the Hamiltonian. In these models, the energy change typically occurs by the flip of particle spins instead of exchanging atoms or displacement. They are very effective when we want to predict the behavior of many-body systems by attributing particles with certain properties to the lattice sites. Amid the classical spin models, there are different types:

-Models with discrete spins:

- Ising model **[119,121]**.
- Potts model **[122,123]**.

- Models with continuous spins:

- The two dimensional unit vectors XY model **[115].**
- Three dimensional unit vectors of the classical Heisenberg model **[117]**.
- N dimensional unit vectors (n-vector model or O(n) model) **[124]**.
- Baxter's vertex models **[120]**.

Note that, the first proposed Ising model was in 1920 by W. Lenz as recognition to his student Ising for being able to explain quantitatively the transition between ferromagnetic and paramagnetic state **[120]**. Ising has developed the model in 1925 **[121]**, where the spin interaction is governed by the Hamiltonian:

$$\mathcal{H} = -J \sum_{<ij>} S_i S_j - h \sum_i S_i \qquad \textit{II.30}$$

Where:

J: stands for the coupling exchange constant, which takes different values depending on the type of magnetism: positive (J>0) in the ferromagnetic state, zero (J=0) in the paramagnetic state and negative (J<0) in the anti-ferromagnetic state.

<ij>: represents the nearest neighbors, so that the lattice sum runs only over all these nearest-neighbors.

Si, Sj: are the spin amplitude values for each site.

In 1944, a solution was analytically found for the two-dimensional square lattice Ising model in vanishing field **[125]**.This is a simpler case, but there is no exact solution for more complicated systems such as, those with 2^+ states of spin, mixed spins or systems with more than two dimensions (2D). Hence, to study these systems, different approaches and approximate methods were proposed to determine their magnetic properties, namely, the magnetization, susceptibility, energy, specific heat, critical temperature, critical exponents and the phase transitions, etc.

In addition, the advancement and the thermodynamic properties of these spin lattice models are generally investigated by randomly flipping the spins of particles that occupies random lattice sites and weighting the resulting energy variation by the use of a Metropolis Monte Carlo sampling approach that we'll elucidate next.

As mentioned before, Monte Carlo method gives the most precise calculations. In what follow we'll explain shortly the basic of this method. There are more studies covering more theoretical concepts related to Monte Carlo algorithm **[105,106]**, **[117, 118]**.

II.2.2-c. *Heisenberg* Model:

The Heisenberg's model treats interactions between spins. This model strongly depends on the sign of the coupling constant; positive for the ferromagnetic state or negative for the antiferromagnetic state, for the purpose of studying the magnetic properties of magnetic materials.

This model makes it possible to directly treat a set of spins in relative interaction which depends on the distance between the close neighbors **[126]**.

Recall that, the spin is the intrinsic kinetic moment of the particle. It is a vector operator with three components $\vec{S}_x$, $\vec{S}_y$, $\vec{S}_z$.

In the case of spin 1/2, we can define the spin operators according to the creations and annihilation operators in the following form:

$$\hat{\mathbf{S}}_{\mathbf{i}} = \frac{1}{2} \sum_{\sigma,\acute{\sigma}} \mathbf{C}^{+}_{\mathbf{i}\acute{\sigma}} \vec{\boldsymbol{\sigma}}_{\sigma\acute{\sigma}} \mathbf{C}_{\mathbf{i}\dot{\sigma}} \qquad \textbf{\textit{II.31}}$$

Where $\vec{\sigma}_{\sigma\acute{\sigma}}$ represent the Pauli's matrices.

$$\boldsymbol{\sigma_x} = \begin{bmatrix} \mathbf{0} & \mathbf{1} \\ \mathbf{1} & \mathbf{0} \end{bmatrix}, \boldsymbol{\sigma_y} = \begin{bmatrix} \mathbf{0} & -\boldsymbol{i} \\ \boldsymbol{i} & \mathbf{0} \end{bmatrix}, \boldsymbol{\sigma_z} = \begin{bmatrix} \mathbf{0} & \mathbf{1} \\ \mathbf{1} & \mathbf{0} \end{bmatrix} \qquad \textbf{\textit{II.32}}$$

Note that, the interaction energy between a magnetic moment and a magnetic field is defined by the following term$-\vec{B}.\vec{M}$. We can represent the two magnetic moments $\vec{M}_1$ and $\vec{M}_2$ by two small magnets which are oriented antiparallel to minimize their energy as in **(Figure II.8)**:

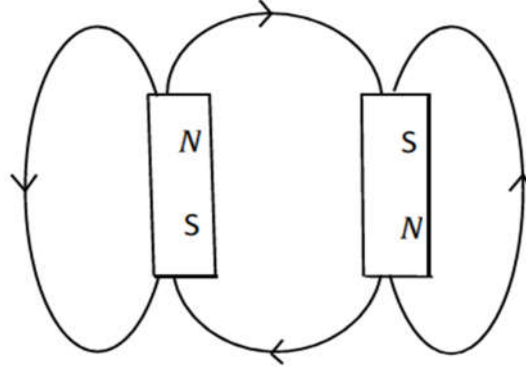

Figure II.8: Field lines of two magnetic dipoles

The Heisenberg Hamiltonian describes a set of interacting magnetic moments in the theory of quantum magnetism.

Where the expression of this Hamiltonian is:

$$\mathcal{H} = \frac{1}{2}\sum_i j_{i,i+1}\vec{S}_i.\vec{S}_{i+1} - \sum_i g_i \mu_B \vec{h} \qquad \textit{II.33}$$

Where:

μ_B: Bohr magneton.

g_i: refers to the gyromagnetic ratio.

$\vec{S}$: The spin operator.

$\vec{h}$: represents the external magnetic field.

$j_{i,i+1}$: The exchange constant. Such as, for $j_{i,i+1} > 0$ the interaction is antiferromagnetic, meanwhile, for $j_{i,i+1} < 0$ it is ferromagnetic.

Nevertheless, in real systems, there is always a fluctuation of the spin away from the axis of symmetry. Thus Heisenberg proposed a suitable Hamiltonian to describe all interactions **[127]**:

$$\mathcal{H}_{\mathbf{Heis}} = -J_{\parallel}\sum_{<i,j>} S_i^{z} S^{z}_j - J_{\perp}\sum_{<i,j>}(S_i^{x} S_j^{x} + S_i^{y} S_j^{y}) - B\sum_i S_i^{z}, \quad \text{with } S_{i,j} = \pm 1 \qquad \textit{II.34}$$

The symbols x, y and z represent the Cartesian axes in spin space, J and J stand for parallel and perpendicular coupling interaction energy. When $J_{\perp}$ =0, we are then in the case of the classical

Ising model. Note that the main difference between the Ising model and Heisenberg model is the fact that for the late one, the spin operators do not commute.

II.2.3. Markov chain and Importance sampling:

In statistical physics, we often want to have the most accurate value of the some quantities, e.g., the Magnetization, the internal energy or the susceptibility, etc. Hence, the most appropriate method to calculate the anticipated value (Q) of a thermodynamic quantity (Q) is by taking an average of the studied quantity over all system states in our phase space, referred to as the canonical ensemble:

$$\langle \boldsymbol{Q} \rangle = \sum_{\boldsymbol{States}} \boldsymbol{Q} e^{-\boldsymbol{\beta \mathcal{H}/Z}} \qquad \textit{II.35}$$

The summation runs over all possible states of the system. Such as:

Z: As the partition function

$\beta \equiv {}^{1}/_{K_B T}$: Represents the inverse temperature with an external heat bath.

K_B: Boltzmann's constant

H: Refer to the Hamiltonian of the system projecting all types of interactions occurring in the system (i.e. short-, medium or long-ranged).

Note that, the degrees of freedom can be either continuous or discrete field variables, such as spins.

Let's take the Ising model as an example, having two spin states, on a lattice of N sites, the above sum will run over *2N* configurations in phase space. With further calculation, this number increases rapidly, making it very difficult to analytically calculate the expectation value of our quantity. But this task can be easier if we use standard methods to evaluate integrals, such as taking a random sampling of these configurations $\{\ \sigma\}$ and weighing them accordingly.

Keep in mind that not every region in the phase space is easily targeted by the random numbers. That's why it's better and more precise to restrict the sampling on spin configurations in the

important regions. This is referred to as importance sampling **[118]**. The purpose is to build an appropriate Markov chain that projects configurations following there Boltzmann weigh:

$$\mathcal{P}^{eq}(\{\sigma_i\}) = \frac{e^{-\beta\mathcal{H}(\{\sigma_i\})}}{\mathrm{Z}} \qquad \textit{II.36}$$

Now how can we move in a Markov chain? The answer is via stochastic rules applied in the transition from one state to another. Let's take two configurations: (1) and (2), the condition here is that the probability of configuration (2) depends only on the configuration (1), such as:

$$\left\{\dots \xrightarrow{W} \{\sigma_i\} \xrightarrow{W} \{\sigma_i\}' \xrightarrow{W} \{\sigma_i\}'' \xrightarrow{W} \dots\right\} \qquad \textit{II.37}$$

The probability of transition W has to fulfill the conditions:

$$\left\{\begin{array}{c} (a) W(\{\sigma_i\} \to \{\sigma_i\}') \geq 0 \; for\ all\ \{\sigma_i\}, \{\sigma_i\}' \\ (b) \sum_{\{\sigma_i\}'} W(\{\sigma_i\} \to \{\sigma_i\}') = 1 \; for\ all\ \{\sigma_i\} \\ (c) \sum_{\{\sigma_i\}} W(\{\sigma_i\} \to \{\sigma_i\}')\, \mathcal{P}^{eq}(\{\sigma_i\}) = \mathcal{P}^{eq}(\{\sigma_i\}') \; for\ all\ \{\sigma_i\}' \end{array}\right\} \qquad \textit{II.38}$$

According to condition (c), we can notice that the Boltzmann distribution P^{eq} is just an exact point of W, taken as an eigenvalue of W. Hence, we can write the detailed balance as:

$$\mathcal{P}^{eq}(\{\sigma_i\}) W(\{\sigma_i\} \to \{\sigma_i\}') = \mathcal{P}^{eq}(\{\sigma_i\}') W(\{\sigma_i\}' \to \{\sigma_i\}) \qquad \textit{II.39}$$

Moreover, the condition (c) runs a summation over all $\{\sigma_i\}$ and using condition (b). Thus, after reaching equilibrium, one can estimate the anticipated values by taking a mean over the Markov chain of length L, for instance:

$$E = \langle \mathcal{H} \rangle = \sum_{\{\sigma_i\}} \mathcal{H}(\{\sigma_i\}) \mathcal{P}^{eq}(\{\sigma_i\}) \approx \frac{1}{n} \sum_{j=i}^{L} \mathcal{H}\left(\{\sigma_i\}_j\right) \qquad \textit{II.40}$$

Such as:

$\{\sigma_i\}_j$: Represent the spin configuration at (time) j.

II.2.4. Metropolis Algorithm:

II.2.4-a. Presentation:

The Monte Carlo (TM) Metropolis method was introduced in condensed matter physics by Metropolis et al. in 1953 [**128].** It is called because it is based on the use of random numbers. This method allows the estimation of the average physical quantities given by the Gibbs formulation of statistical mechanics in the form of multidimensional integrals.

The MC technique is in fact particularly suitable for calculating integrals larger than ten. The first simulations were performed in the canonical set (constant N, V and T), then the technique was extended to the other statistical sets. A random sequence of accessible states (Markov chain) is generated in the system configuration space. We sample by favoring the regions where the Boltzmann factor (e^{-U/K_BT}), that is to say the probability density of the canonical set in this space, is the highest (Metropolis algorithm). The probability of a particular configuration of potential energy U_i is then proportional to e^{-U_i/K_BT}), in other words the acceptance of a configuration of the Markov chain is weighted by a frequency proportional to the Boltzmann factor. A property of equilibrium is then obtained as a simple average on the accepted configurations. This exploration of the configuration space, following the Metropolis algorithm, constitutes the first case of sampling according to importance in statistical mechanics.

It is still widely used nowadays because it represents a simple and relatively efficient way to obtain averages of physical quantities in a statistical set. It is important to note that these averages are obtained despite the inability to know explicitly the standardized probability density of the set considered. Direct estimates of free energy (entropy, free energy of Helmholtz, enthalpy, free enthalpy) are therefore impossible, whereas differences in free energies (corresponding to ratios of probability densities) are accessible and are subject to particular methods. The MC method is generally limited to computation of static properties since only the configurational part of the phase space is explored and time is not an explicit variable. Dynamic properties are inaccessible and should be obtained by another technique **[129]**.

II.2.4-b. Application in Monte Carlo method:

There are various single flip algorithms that can differently fulfill the main Markov chain conditions (a) and (b). Nevertheless, the simplest and most flexible one is the classic Metropolis algorithm **[130**], It is applicable in nearly all situations, such as (discrete/continuous, lattice/off-lattice, short-range/ long-range interactions ...) in which we can suggest a state for a single degree of freedom, that is the spin, and accept this suggestion with an acceptance probability:

$$\boldsymbol{W(\{S_i\}_{old} \rightarrow \{S_i\}_{new}) = \begin{cases} 1 & E_{new} < E_{old} \\ e^{-\beta(E_{new}-E_{old})} & E_{new} \geq E_{old} \end{cases}} \qquad \textit{II.41}$$

E_{new} and E_{old}: corresponds to the energy of the new and old spin configuration $[\{S_i\}_{new}]$ and $[\{S_i\}_{old}]$ respectively.

When we move from a configuration to another, one degree of freedom is changed, this modification is the difference between the $[\{S_i\}_{old}]$ and $[\{S_i\}_{new}]$. So respecting the transition probabilities, the variation of the system goes in an asymptotic way to a stable state where the probability of a configuration is $e^{(-\beta E[S])}$.

Hence, how can we accept or deny a spin flip?

To decide that, we compare the energies, if the new energy is lower than the old configuration energy, the flip is always accepted. Hereafter, if the energy of the new configuration is higher than the old one, the flip can still be accepted with a reliable probability. Thus, we take a random number r [0, 1) which we compare to W, if W≤r, we accept the new state. Or else we maintain the old configuration and move on to the next spin. The process of the execution of the Metropolis algorithm is quite simple as show in **Figure II.9 [130]**, which we have summarized in these steps:

1- Specify the system, a spin-lattice of N sites along with the lattice size L.

2- Specify a matrix of N variables which represents the spin values.

3- Impose the periodic boundary conditions.

4- Define the temperature interval and ΔT as it's variation.

5- Choose the initial spin configuration.

6- The boucle of temperature starts from the initial state at T+ ΔT which is the equilibrium state of T.

7- Now, pick out a random or sequent spin, which will be updated, then flip it and calculate the corresponding energy, after that, calculate the energy variation $\Delta E= E_f - E_i$ and its probability W .

8- Randomly select a number r and accept the update (flip), only, if ΔE≤0 or W≤r.

9- In the case where the flip is accepted, we then compute the related changes in energy and magnetization.

10- We repeat the steps (7-9) until the thermal equilibrium is attained.

11- Now it's the production step, after the thermal equilibrium, repeat the steps (7-9) n times so as to calculate the measurements and averages.

12- Modify the temperature by ΔT and repeat the steps (6-11) until the temperature reaches its maximum, already defined.

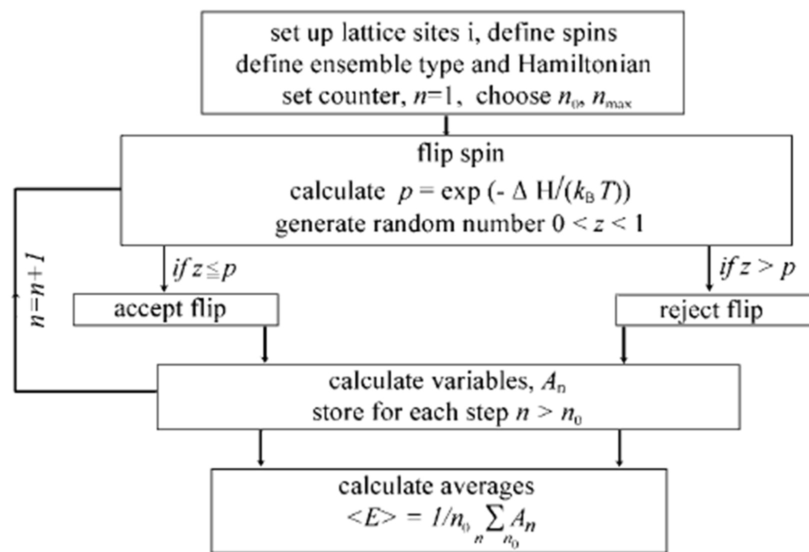

Figure II.9: Flowchart representing the basic steps in a Monte Carlo simulation for a simple spin model.

II.2.5. Critical properties:

In Monte Carlo simulation, our aim is to calculate the critical parameter of the system, these parameter are measured in the "production step". That is to say, when our system reaches equilibrium, which equals a certain number of Monte Carlo steps, we, then, calculate the most important quantities, or the thermodynamic quantities that we aim at. Namely, the magnetization, the magnetic susceptibility and the specific heat beside the hysteresis loops. In our Metropolis algorithm we've used the following expressions to compute the critical parameters:

$$\boldsymbol{m} = \frac{1}{N}\sum_{i=1}^{N} \boldsymbol{S_i} \qquad \textit{II.42}$$

$$\chi = \beta N(< m^2 > - < m >^2) \qquad II.43$$

$$C_v = \frac{\beta^2}{N}(< E^2 > - < E >^2) \qquad II.44$$

N: stands for the number of spins in our studied system which has a size L.

We evaluate the Curie temperature through the susceptibility peak with different system sizes giving more precision.

Note that in the aim to compute the magnetic properties of a real magnetic material, the exchange interaction coupling J, which can be one or multiples, beside other constants in the Hamiltonian, such as the magnetic anisotropy Δ, ought to be pre calculated via experimental methods like SQUID or theoretical methods, such as the DFT calculations to determine these terms especially the exchange coupling **[131-134]**.

II.2.6. Implementation and practical Details:

In the previous section we've defined the basis of the metropolis algorithm. So how can we use it practically?

The following part is the answer to this question. We give here, few steps to implement the Metropolis algorithm and data analysis:

First, we establish the initial configuration. Basically, there is no effect between the first and the final configuration. Add that, we can urge the system to reach equilibrium faster if we choose a convenient initial configuration.

Secondly, choose the degrees of freedom, in magnetic systems, it is the spin value of each site, we can for example update the values of all even sites and then all odd sites. Or we can sequentially update the values of the sites, until we run through all sites in our system.

Thirdly, apply the boundary conditions. We use these conditions in the system, such that we emulate an infinite system by copying the system periodically in all directions (x, y, z). Note that, free boundary conditions are used for the finite size system such as Nano-particles.

Fourthly, this step is about the finite-size effects, we repeat the Monte Carlo steps over different system sizes L, starting from a small size to larger ones and thus we can have an idea about the system magnetic behavior for an infinite size L.

Fifth, we generate random numbers, within Monte Carlo simulations; we use the random numbers generators (RNG) to generate random values between 0 and 1. There are various RNGs, a good RNG have to produce a reproducible results for testing operations in the algorithm. Namely, the energies and Boltzmann weight. Moreover one has to use only well-tested and well-documented RNGs

Finally, Statistical errors: in the aim to get trustworthy results, we must take an average over MC steps, so one should run some tests on the system to get an idea about the system's equilibrium, meaning how many MC steps the program go through in order to reach equilibrium. After that, those steps are discarded, and in that point, we starts generating the thermodynamic quantities, e. g, magnetizations, susceptibilities, ...

At last, we have to say that in statistical physics; two other spin flip (local) algorithms exist, which are amply utilized nowadays: the heat -bath and Glauber algorithms **[135]**. Alongside these types of algorithms, there is another family of algorithms named "non-local update (cluster)" algorithms such as Wolf **[136]** and Swenden- Wang **[137]**. Of course, these two algorithms verify the general Markov chain conditions (a) and (b) and both have their advantages and flaws.

II.7. Conclusion:

Here above, we presented the two main methods that we employed in our calculations, the first one being the Ab initio method, and the second one being the Monte Carlo simulation. On one hand, for the Ab initio, we gave the concept of the DFT method which is the base of the Ab initio calculations, and its importance in different theorem and condensed matter approximations. Also, we introduced the two main approximations we used: LDA and GGA approximation. In addition, we displayed an outlook regarding the AKAI code and AKAI KKR- CPA method. The details of our data implementation for the two materials: Mn-doped GaN and (Ni, Fe)-doped GaAs, were also given. On the other hand, we presented the Monte Carlo method: its advantages, its importance and the simulation models (Ising model and Heisenberg model),

noting that we employed the Ising model in our simulations. Besides, we exposed the Metropolis algorithm, on which the Monte Carlo method is based on. After that, we detailed the critical properties that we target (the magnetization, susceptibility …) and the implementation in the Monte Carlo algorithm.

Chapter III

Ab initio study of the electronic, magnetic properties and phase transitions in Ga (Mn) N with Monte Carlo Approach

Journal of Magnetism and Magnetic Materials 396 (2015) 153–159

Contents lists available at ScienceDirect

Journal of Magnetism and Magnetic Materials

journal homepage: www.elsevier.com/locate/jmmm

Ab-initio study of magnetic properties and phase transitions in Ga (Mn) N with Monte Carlo approach

Y. Sbai [a], A. Ait Raiss [a], E. Salmani [a], L. Bahmad [a,*], A. Benyoussef [a,b,c]

[a] LMPHE (URAC 12), Faculty of Science, Mohammed V University, Av. Ibn Batouta, Rabat, Morocco
[b] Institute of Nanomaterials and Nanotechnologies, MAScIR, Rabat, Morocco
[c] Hassan II Academy of Science and Technology, Rabat, Morocco

ARTICLE INFO

Article history:
Received 29 April 2015
Received in revised form
2 August 2015
Accepted 7 August 2015
Available online 11 August 2015

Keywords:
AKAI–KKR–CPA method
LDA
GaN:Mn
Ab-initio calculations
DOS
Monte Carlo simulations

ABSTRACT

On the basis of ab-initio calculations and Monte Carlo simulations the magnetic and electronic properties of Gallium nitride (GaN) doped with the transition metal Manganese (Mn) were studied. The ab initio calculations were done using the AKAI–KKR–CPA method within the Local Density Approximation (LDA) approximation. We doped our Diluted Magnetic Semiconductor (DMS), with different concentrations of magnetic impurities Mn and plotted the density of state (DOS) for each one. Showing a half-metallic behavior and ferromagnetic state especially for $Ga_{0.95}Mn_{0.05}N$ making this DMS a strong candidate for spintronic applications. Moreover, the magnetization and susceptibility of our system as a function of the temperature has been calculated and give for various system size *L* to study the size effect. In addition, the transition temperature was deduced from the peak of the susceptibility. The Ab initio results are in good agreement with literature especially for (x=0.05) of Mn which gives the most interesting results.
© 2015 Elsevier B.V. All rights reserved.

1. Introduction

In the past few years, scientists have given a huge interest to diluted magnetic semiconductors (DMS) especially when they are doped with a small concentration of magnetic impurities which are transition metals inducing ferromagnetic DMSs. In particular, DMS based on III–V and II–VI semiconductors. That type of doping has been really investigated by both theoretical and experimental scientists as said before [1–2] in the aim to use these DMSs for spintronic devices such as optical isolator, emitting diodes, spin-valve transistor, non-volatile memory, spin light, etc. Theoretically, there are lots of studies giving considerable results like Dietl et al. [1] predicting high temperature ferromagnetism in some doped semiconductors such as GaN, ZnO, GaAs and specifically GaN (Gallium nitride) for which significant interest has been devoted for the application in many and different electronic and optoelectronic applications, such as blue laser diodes, light-emitting diodes (LEDs), high power and high frequency devices [1–3]. This interest can be justified by the great qualities that possess this material GaN, a direct wide band-gap, high electron saturation velocity, high breakdown strength and good electrical properties. Moreover, as we are interested in spintronics, doping GaN with magnetic impurities(transition metals) enhance the flexibility for spin based electronic application [4]. Mn-doped GaN can be considered as a good and appropriate candidate for spintronic applications due to its promising room temperature ferromagnetism [5]. Nevertheless, it has been reported that the distribution of the Mn atoms being not uniform within (Ga, Mn)N layers form micro-precipitates and clusters, which affect negatively the efficiency and quality of the material [6,7]. Yet, the ferromagnetism (FM) noticed experimentally has still not been explained clearly and fully understood. Some of the cases where this ferromagnetism was subjected and a Curie temperature above room temperature was shown, is that of nanocrystals and thin films formed by $Ga_{1-x}Mn_x$ N. We can reverse or change that magnetic state by changing the type of doping, p- or n-. One of the principal goals of the researches is to maintain the ferromagnetism in (Ga, Mn)N up to room temperature and It was predicted theoretically [5]. There were many questionable results coming after The firsts works giving high T_c in (Ga, Mn)N, where the recorded T_c varied between 20 K and 940 K [8–9]. Zajac et al. [10] reported that the coupling between Mn ions in $Ga_{1-x}Mn_xN$ ($x<0.1$) is anti-ferromagnetic (AFM). So to conceive the FM–AFM competition, electronic structures and magnetic properties of zinc blende $Ga_{1-x}Mn_xN$ for different concentrations of dopant x were exanimated and processed in different calculations using the tight binding LMTO (Linear Muffin-Tin Orbital Method) method in the local spin density approximation by Uspenskii et al. [11]. Sanyal and Mirbt [12] worked with the ab-initio plane wave code (VASP) on Mn-doped GaAs and GaN DMS through the density functional theory (DFT). They

* Corresponding author.
E-mail address: Bahmad@fsr.ac.ma (L. Bahmad).

http://dx.doi.org/10.1016/j.jmmm.2015.08.032
0304-8853/© 2015 Elsevier B.V. All rights reserved.

III.1. Introduction:

The scientific community has given a huge focus to the study of diluted magnetic semiconductors (DMS) doped with a controlled concentration of magnetic impurities, such as, transition metals inducing ferromagnetic DMSs. particularly, DMS based on III–V and II–VI semiconductors. This DMS doping has been That type of doping has been really explored both theoretically and experimentally **[138,139]**, with the attempt to integrate these DMSs in spintronic devices such as optical isolator, emitting diodes, spin-valve transistor, non-volatile memory, spin light, etc. From a Theoretical point of view, there are many studies exhibiting interesting results like Dietl et al. **[138]** predicting high temperature ferromagnetism in doped semiconductors such as GaN, ZnO, GaAs and specifically Gallium nitride (GaN), for which significant interest has been devoted in the purpose of application in many and various electronic and optoelectronic applications, e.g, blue laser diodes, light-emitting diodes (LEDs), high power and high frequency devices **[138-140]**. This scientific interest is coming from the interesting qualities possessed by this GaN material, e.i a direct wide band-gap, high electron saturation velocity, high breakdown strength and good electrical properties. Also, since we are interested in spintronics, doping GaN with magnetic impurities such as, transition metals, increases the flexibility for spin based electronic application **[141]**. Mn-doped GaN can be considered as a good and suitable candidate for spintronic applications thanks to its promising room temperature ferromagnetism **[142]**. However, it has been reported that the non-uniform distribution of the Mn atoms within (Ga, Mn)N layers, forms micro-precipitates and clusters, which affects negatively the efficiency and quality of the material **[143,144]**. Still, the ferromagnetism (FM) noticed experimentally has yet to be explained clearly and fully understood. There are certain cases where this ferromagnetism was subjected and a Curie temperature above room temperature was shown, namely in nanocrystals and thin films formed by $Ga_{1-x}Mn_xN$. Note that, we can control the magnetic state either reverse or change that magnetic state by switching the type of doping, p- or n-. One of the main targets of these researches is to sustain the ferromagnetism in (Ga, Mn)N up to room temperature and It was theoretically anticipated **[142]**. The early studies have given some debatable results showing high T_c in (Ga, Mn)N, where the recorded T_c varied between 20K and 940K **[145,146]**. Zajac et al. [**147**] reported that the coupling between Mn ions in Ga_{1-x} Mn_xN ($x < 0.1$) is anti-ferromagnetic (AFM). So to understand the FM–AFM competition ,electronic structures and magnetic properties of zinc blende $Ga_{1-x}Mn_xN$ for different

concentrations of dopant x were exanimated and processed in different calculations using the tight binding LMTO (Linear Muffin-Tin Orbital Method) method in the local spin density approximation, by Uspenskii et al. **[148]**. Sanyal and Mirbt **[149]** used the ab-initio plane wave code (VASP) on Mn-doped GaAs and GaN DMS through the density functional theory (DFT). They calculated the interatomic exchange interactions by substituting Mn atoms in specific positions within the unit cell and attributed the origin of the ferromagnetism in (Ga,Mn)N to a double-exchange mechanism associating the hopping of Mn–d electrons. Raebiger et al. **[150]** studied all possible configurations formed by the two Mn atoms on a Ga sublattice for 5% of magnetic impurities using the full potential linearized augmented plane wave (FP-LAPW) method in order to investigate the correlation between clustering and exchange coupling in the magnetic semiconductor $Ga_{1-x}Mn_xN$. We point out an interesting conclusion that is the clustering of Mn atoms at near neighbor Ga sites is energetically preferred. This can be very useful in order to have the best output from these materials.

Hereafter, regarding Monte Carlo approach, as far as we are concerned we are not aware of any work in which we perform Monte Carlo Simulating for GaN doped with Mn. Where Mn^{3+} is the only present high spin magnetic ion, S =2, and this is where comes our motivation for this work, to lighten and clear up data about MCs simulation for Ga(Mn)N. We study the variation of the thermal magnetization, susceptibility as a function of the temperature for a spin S=2 and for different lengths by Monte Carlo simulations (MCS). The critical temperature (T_c) is deduced from the susceptibility graph. In addition, the ab-initio calculations were performed to investigate the magnetism in Ga(Mn)N.

III.2.Crystal structure and Calculation Methods:

In this ab initio study we exploited the AKAI-KKR-CPA code MACHIKANEYAMA2002v08 package designed and made by Akai **[98]**, for our GaN system. Within the Korringa- Kohn-Rostoker method combined with the coherent potential approximation (KKR-CPA) with the parameterization of Moruzzi, Janak and Williams (MJW), and Vosko, Wilk, and Nusair (VWN) **[88]**, **[99]**. The MJW and VWN functional showcase a band gap of approximately 2.72 eV for bulk GaN. This result is compared with the experimental value of 3.507 eV. We apply the LDA technic as approximation since we have a disordered system. This method is the most convenient to study this kind of system. KKR-CPA was developed by Akai and Dederichs for DMSs doped

with a transition metal see Ref **[100]** about KKR-CPA method. Also for oxide semiconductors, ZnO based DMSs **[101]**.

The density of states (DOS) were calculated and plotted for $Ga_{1-x}Mn_xN$ for different doping concentrations which are Mn magnetic impurities. For better understanding of the upcoming figures, the syntax "Total" represents the total density of spins up and down, located in the valence and band conduction in the system structure. The Total density must not change from a figure to another. But the partial DOS curves will change, when varying the doping concentrations. These concentrations are x(Mn)=0.10, x(Mn)=0.15 and x(Mn)= 0.20. After the doping operation, the Mn atoms are placed in the Ga sites in the wurtzite structure at any concentration. We've used in our code 250 K-point in the first Brillouin zone and took into account that the magnetic impurities (Mn) replace randomly Ga atoms in the structure. Our system has a wurtzite crystal structure with a = 3.180 Å, and c = 5.166 Å as lattice constants and u= 0.377 **[102]**. Since the unite cell is hexagonal with two lattice parameters, our atoms in this system are disposed as each Ga atom is encircled by four N atoms on the corners and vice versa as we will see next for more details about the model.

III.3. Results and discussions:

III.3.a.Band structures and density of states:

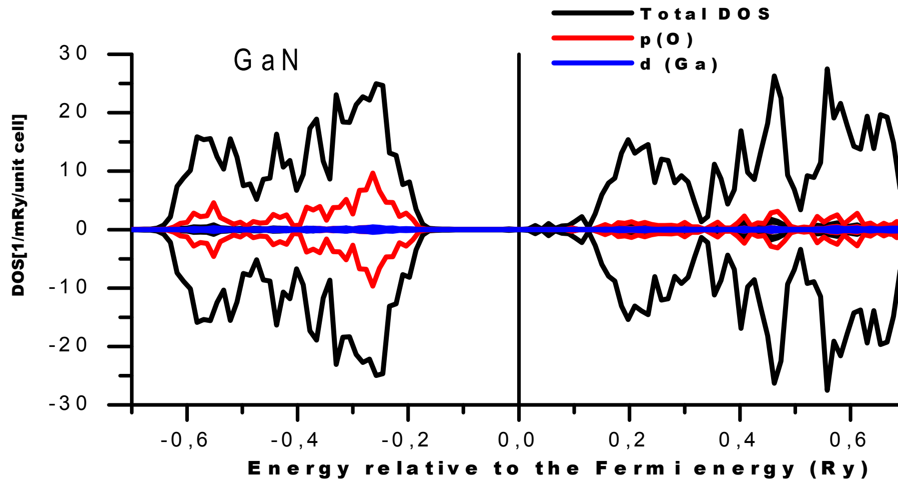

Figure III.1: The density of states (DOS) for GaN without any transition metal impurities.

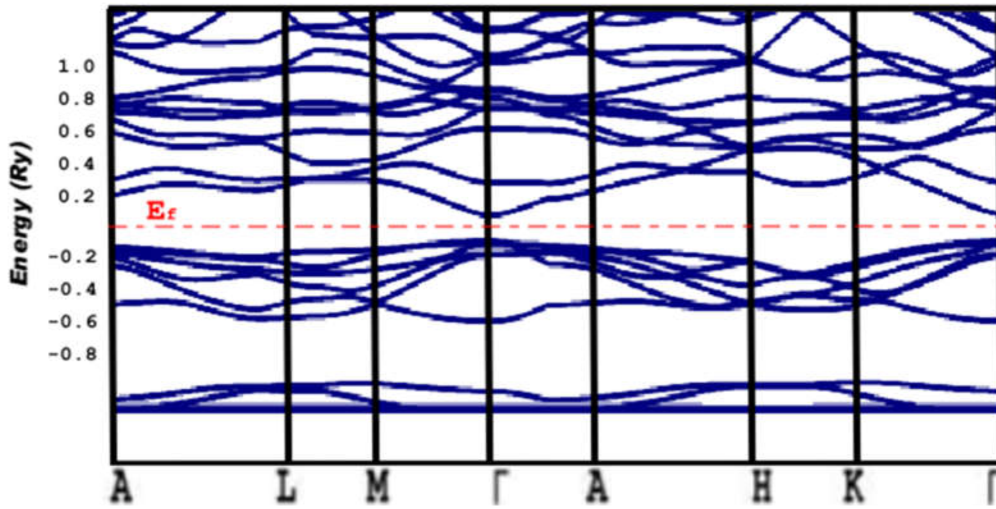

Figure III.2: The band structure (E-k curve) for non-doped GaN (1Ry =13.605 ev)

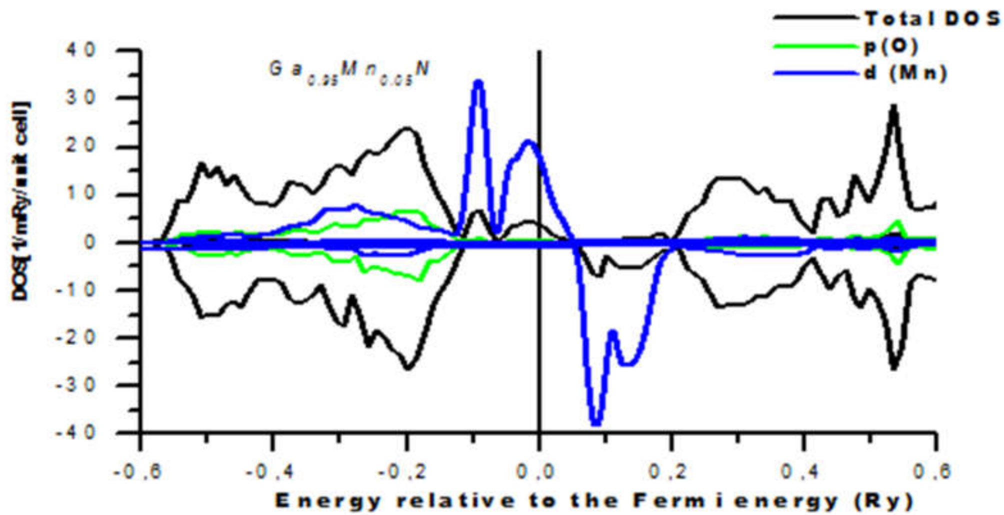

Figure III.3: Total d and p state projected density of stat (DOS) of Mn, doped GaN.$Ga_{0.95}Mn_{0.05}N$, the total DOS is denoted by a thick solid black line,3d-states of Mn by a blue line and 2p-states of N by a Green line.

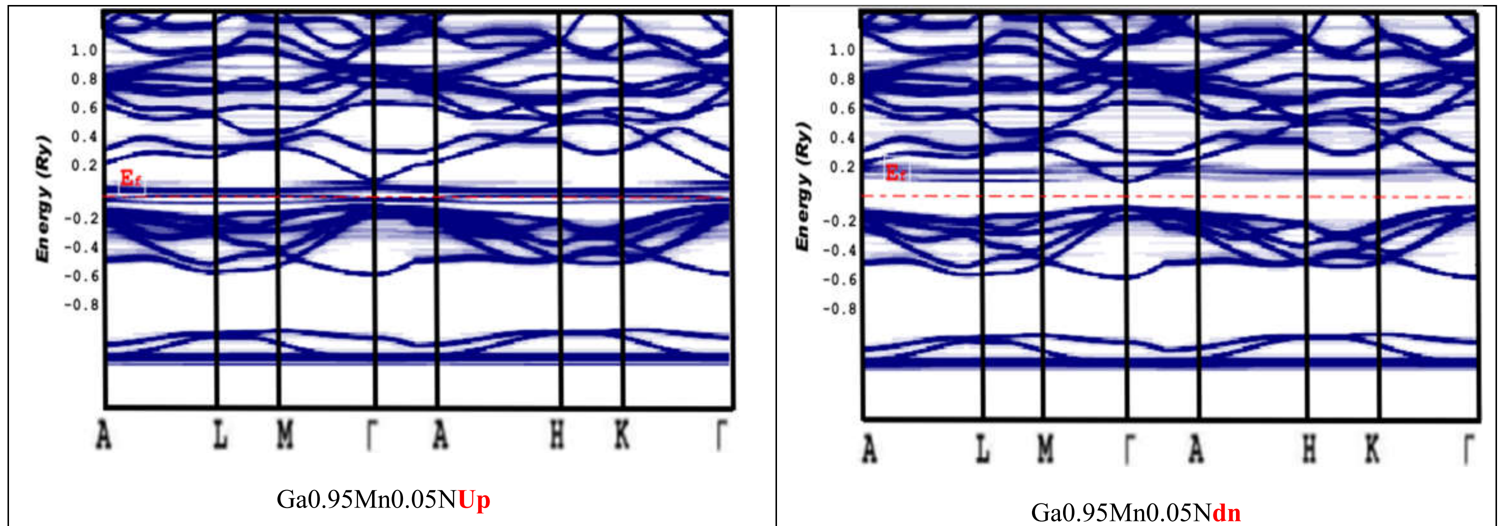

Figure III.4: The Band structure (E-k curve) in the case $Ga_{0.95}Mn_{0.05}N$ for up spins $Ga_{0.95}Mn_{0.05}N$**Up** and down spins $Ga_{0.95}Mn_{0.05}N$**dn**

The total density of states for GaN before doping with Mn atoms is given in **Figure III.1** as we can see in the DOS, we don't have any impurities bands in the gap, the corresponding band structure is given in **Figure III.2**. It shows a direct band gap .As a result there no magnetism in GaN so it is not interesting for spintronics applications that's why we are in the necessity of doping it with a metal transition which is Mn, that's when we proceeded with the doping of our material using various concentrations of magnetic impurities, Mn atoms, to determine the effect of the amount of magnetic atoms on the Density of State of our system, and then on magnetic properties.

Since low concentration of Mn does not exhibit interesting results, we started with x(Mn)=0.05, see **Figure III.3**. This illustrates the total and partial density of states (DOS) for this case: $Ga_{0.95}Mn_{0.05}N$. The DOS is divided into two parts: a first one corresponding to the spin up states and a second one indicating the spin down states. Preliminary results show that when adding magnetic impurities in our structure, this causes the appearance of a magnetic band in the gap. Also when we are doping with a transition metal, these bands are 3d bands. This result is confirmed by **Figure III.3**. The 3d bands of Mn are thin and localized in the gap of the spin up part. Furthermore, these bands are not hybridized with the valence band. To better understand the magnetic behavior, we considered the electronic structure. As we mentioned before, every Mn atom replaces a Ga atom, and as Mn has 7 valence electrons and Ga has 3. These 3 electrons

(from 7 electrons) create a bond and replace the 3 electrons of Ga in the valence band. In the other hand, the 4 remaining electrons, belonging to the Mn valence, are located in the band gap, corresponding to new localized d states. As a result, the electronic structure of Mn transition metal impurity in DMS is dominated by the d-states which represent the impurity bands in the Gap. The 3d states for the spin up in the gap have a little lower energy than those of the spin down part, each Mn atom have 4 nearest-neighbor atoms of nitrogen (N) that have 2p states. These surrounding atoms generate a crystal field that splits the impurity bands (3d states) into two bands. These bands are: a double degenerated band (e band), and a triple degenerated band (t_a band). Each one has 3d orbitals with different symmetry. As it is seen in the DOS, see **Figure III. 3**. The d (t_a) band is higher than the d (e) band. The bands d (t_a) have higher energy than d (e) band. This is due to the fact that the d(t_a) orbitals are situated closer to the N atoms than those of d(e), increasing the interaction between these atoms. The strong interaction between the 3d(t_a) states and the 2p states of N splits the d(t_a) bands in two part. A bonding and anti-bonding parts arises and the second part (anti-bonding) is located above the d(e) band. This is in good agreement with the results of Sato et al. **[151,152]**.

The above considerations explain the fact that the d(e) band are fully situated under the Fermi level, as well as the fact that d(t_a) band have two parts: a part situated under the Fermi level and another above the Fermi level. This leads to the fact that the 3d (e) spin up is completely filled by electrons, whereas the 3d(t_a) spin up is partially empty. The magnetic state of our system is ferromagnetic, as it is seen in the DOS, see **Figure III.3**, with a small width of the triple degenerated state (t_a). In order to stabilize this ferromagnetic state, we have to add carriers in t_a states. Since the d(e) band is totally filled, and d(t_a) band is still partially empty, the e state electrons are localized and will not participate in the interaction mechanism .

In the other hand, a stable magnetic state has the lowest energy. This is why the itinerant electrons participate to the double exchange mechanism leading to the apparition of a lower ferromagnetic energy state.

The origin of the ferromagnetism has been subject of a great debate. Other researchers, see Ref. **[102]**, outlined that the increasing of the doping concentrations of magnetic impurities, leads to a larger partially filled band in the gap (t_a). This indicates that the coupling is a ferromagnetic double exchange. It’s clear that the ferromagnetism is caused by the double exchange interaction

mechanism between different Mn atoms (Mn-Mn). The double exchange interaction occurs between the magnetic atoms Mn, of different valences, with the assistance of a non-magnetic atom, which is the Ga atom **[102]**. This result is in good agreement with what we have found, as it is illustrated in **Figure III.5** and **Figure III.7**. Moreover, the band structure corresponding to the case of $Ga_{1-x}Mn_xN_x$ =0.05, 0.10, 0.15, 0.20 are given in **Figure III.4** and **Figure III.6**. We have found a half–metallic behavior which is reinforced by increasing the concentration values of the magnetic impurities Mn, see **Figure III.5**. This represents the evolution of the density of spin states as a function of the energy level including the Fermi level. From this figure, the density of states (DOS) of Ga and N doesn't change because these atoms do not contribute to the magnetic interactions. The Mn dopant is the only magnetic atom. As a result, the Mn impurity is the only responsible of the appearing magnetism in the studied system.

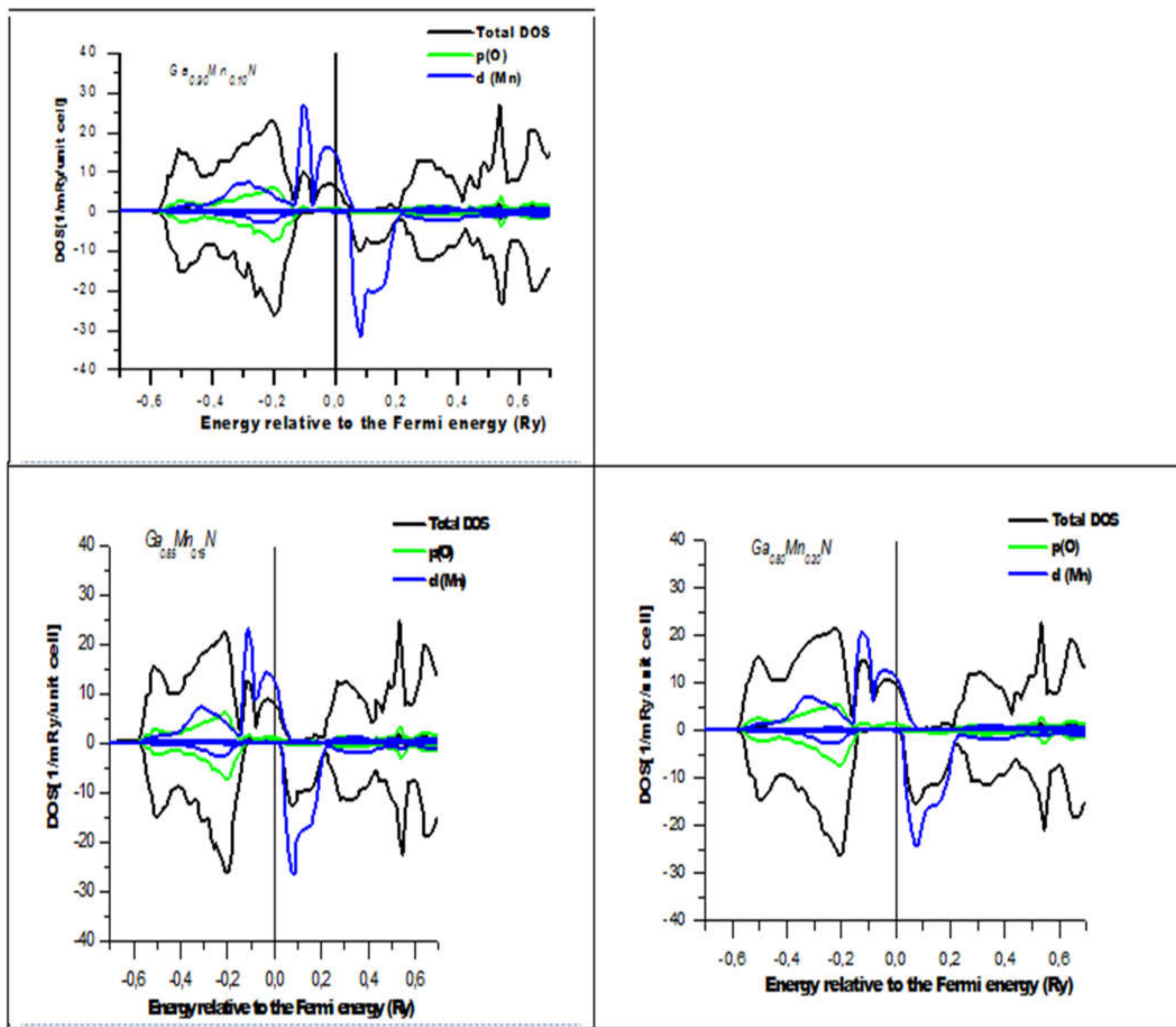

Figure III.5: Total d and p state projected density of stat (DOS) of Mn, doped GaN, for different concentrations of Mn impurities, x(Mn)=0.10, x(Mn)=0.15 and x(Mn)= 0.20.

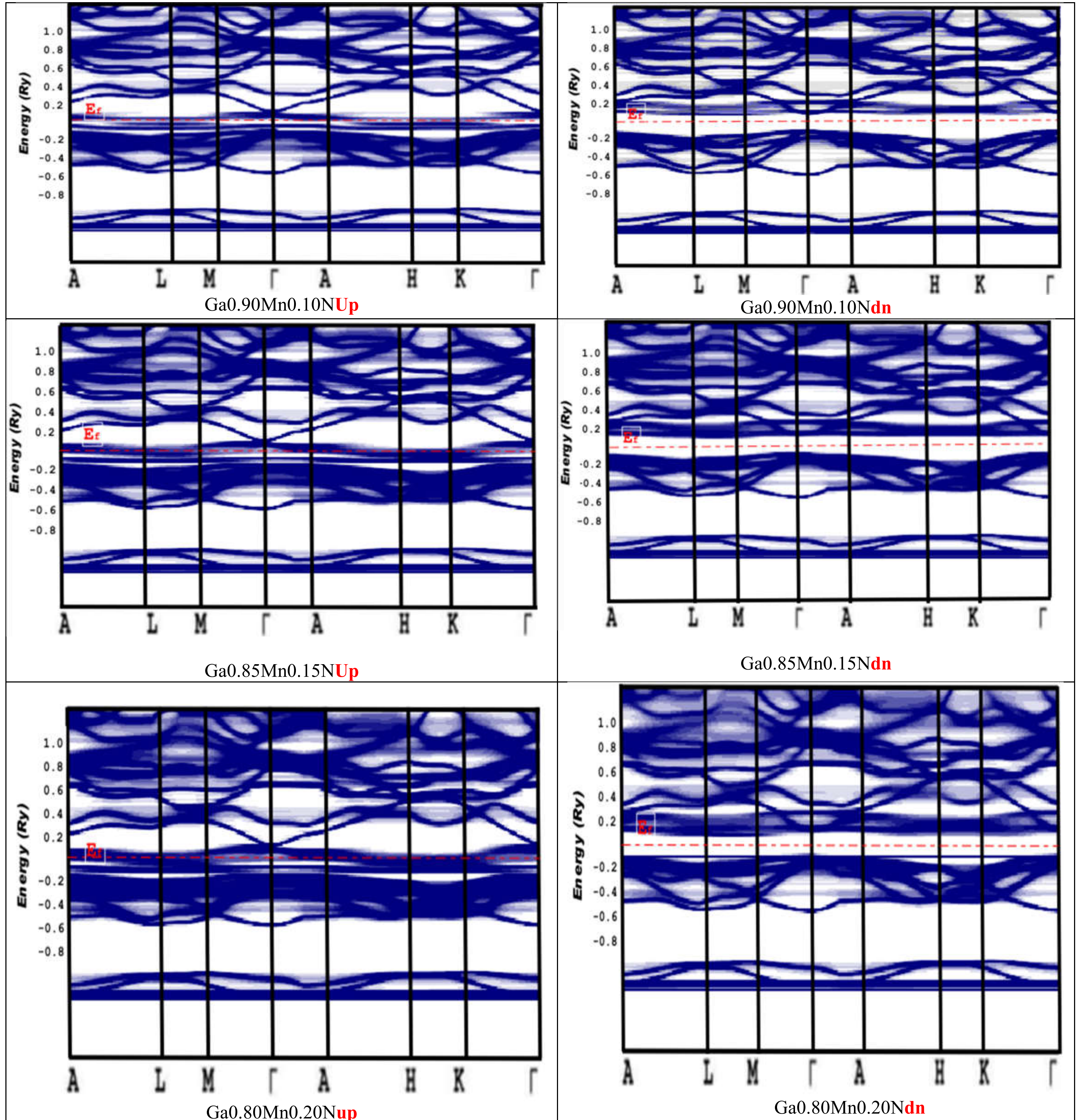

Figure III.6: The Band structure (E-k curve) for $Ga_{0.90}Mn_{0.10}N$, $Ga_{0.85}Mn_{0.15}N$, $Ga_{0.80}Mn_{0.20}N$ for up spins and down spins.

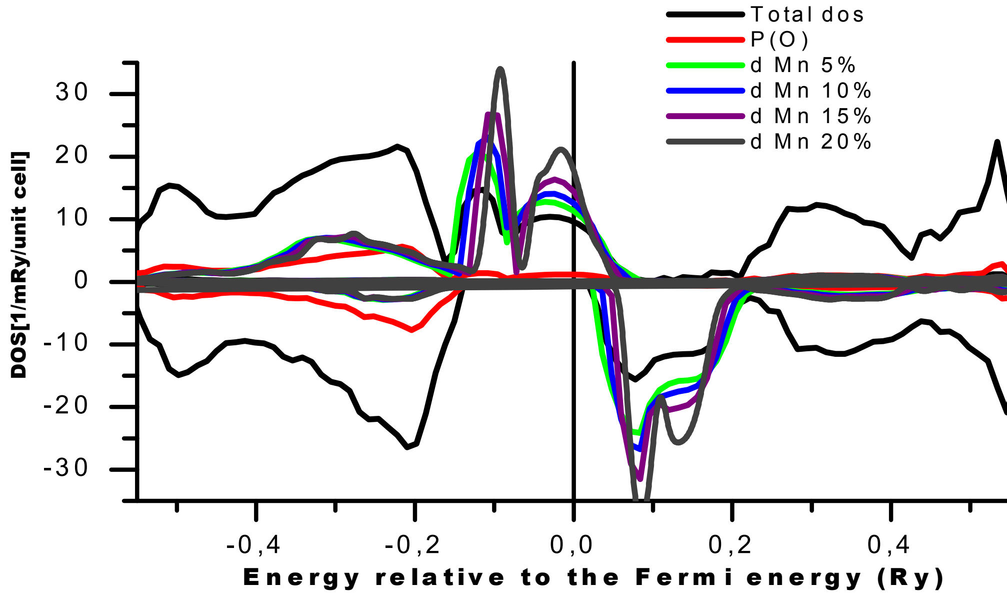

Figure III.7: The DOS of GaN doped with various concentrations of Mn plotted simultaneously.

III.3.b. Monte Carlo Simulation:

In our calculations we have used a wurtzite structure for which the primitive GaN unit cell contains 4 atoms. The corresponding space group is $P6_3mc$. We will define the structures as follows: The shape of the wurtzite cell is a vertically oriented prism with the base defined by the primitive lattice vectors 'a' and 'b' (a=b) separated by an angle of 60°; 'a' and 'b' both lies in the horizontal (xy)-plane. The height of the cell is defined by the vector c which is oriented vertically at 90° to both 'a' and 'b'. In the ``ideal" wurtzite structure $c = 2\sqrt{\frac{2}{3}}a$. This is not necessarily the case in the real structure. To specify the positions of atoms within the cell we usually use fractional coordinates. If a point in space (r) has Cartesian coordinates, (x,y,z), then its fractional coordinates, (x',y',z'), are defined as that :

$$\boldsymbol{r} = \boldsymbol{x'a} + \boldsymbol{y'}\mathbf{b} + \boldsymbol{z'c} \qquad \textbf{\textit{III.1}}$$

The Ga atoms are positioned such as one is at the origin (0,0,0) and the other is at (1/3,1/3,1/2). The N atoms are positioned directly above the Ga atoms. In the (ideal) wurtzite structure, these

are at (0,0,3/2) and (1/3,1/3,7/8). The length of each Ga-N bond is the same if $c = 2\sqrt{\frac{2}{3}}a$; a graphical representation of the wurtzite cell is shown in **Figure III.8**:

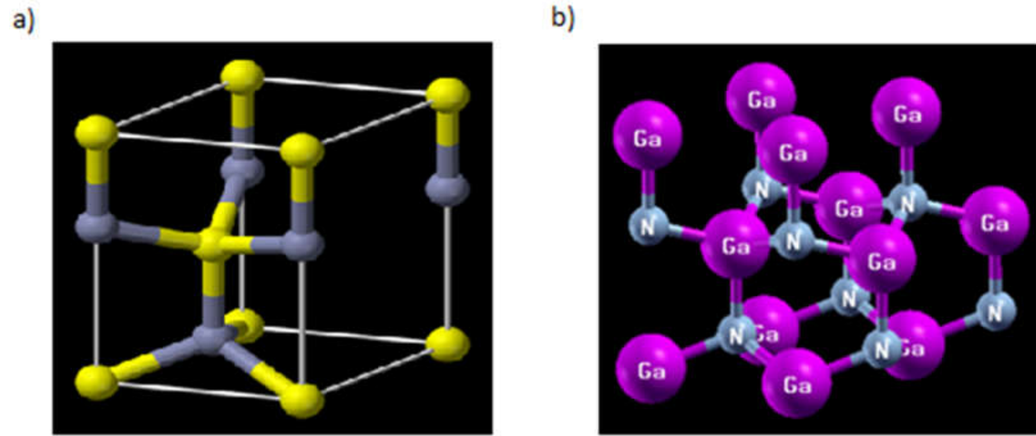

Figure III.8: a) The Wurtzite-unit-cell-3D and b) The Wurtzite-unit-cell that we have obtained using "XCrySDen".

The geometry of the studied structure is displayed in **Figure III.9**, with Ns=6 spins for the distance D_1 corresponding to the coupling J_1 and Ns=6 for D_2 corresponding to J_2 and Ns= 12 spins for D_3 corresponding to J_3. The size of our system is N= L^x L^x L with L =5(number of layers) that we increase it in our simulation to see the effect of the size on the magnetization and susceptibility. We have applied Standard sampling method under the Metropolis algorithm to simulate the Hamiltonian given by equation ***III.4***. The boundary conditions on the structure lattice were imposed and configurations were generated by sequentially visiting all the sites of our system and making single-spin flip trial. The flips are accepted or rejected according to conditions and probability function imposed in the algorithm. In our program, data were generated with 10000 Monte Carlo steps per spin, discarding the first 7000 Monte Carlo simulations, starting from initial conditions. We performed the average of each parameter and estimate the Monte Carlo simulations. We calculate the following parameters, namely:

The magnetization per site:

$$\boldsymbol{M_S = \frac{1}{N}\sum_i^N S_i} \qquad \textbf{\textit{III.2}}$$

N = L^3 : total number of sites , it's the size of the system.

The magnetic susceptibility is given by:

$$\chi = \frac{1}{K_B T}\left(< {M_S}^2 > - < M_S >^2\right) \qquad \textbf{\textit{III.3}}$$

And $\beta=\frac{1}{K_B T}$, K_B the Boltzmann's constant and T denotes the temperature.

The Hamiltonian of the Ising model includes the nearest neighbors interactions and the external magnetic field and is given as follow:

$$\mathcal{H} = -(\sum_{<ij>1} J_1\, SiSj) - (\sum_{<ij>2} J_2 SiSj) - (\sum_{<ij>3} J_3 SiSj) - H\sum_i Si \qquad \textbf{\textit{III.4}}$$

where <i,j> stands for nearest neighbors spins $S_{i,j}$. J_1 , J_2 and J_3 denotes the coupling constants between Si and Sj spins respectively, H represents the magnetic field.
Since the spin amplitude is S=2 ,the spin S_i introduced in our Hamiltonian takes the values [+2,+1,0,-1,-2] and The corresponding energy E_i is defined as follows :

$$E_i = -S_i \sum_j J_{1,2,3} S_j \qquad \textbf{\textit{III.5}}$$

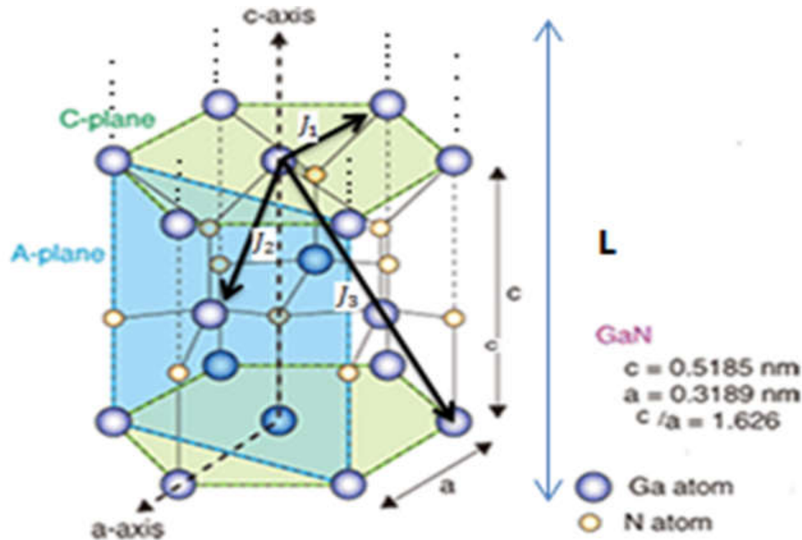

Figure III.9: The wurtzite structure of GaN with the 3 coupling interactions between atoms.

We calculated and plotted the ground state representing our system at zero temperature at the lowest energy state. It corresponds to an Ising model with a value of spin S=2 that gives rise to

five states (+2, +1, 0, -1, -2) using our Hamiltonian, as illustrated in **Figure III.10**. The plotted ground state diagram is separated into five phases; each phase is separated from the other by a line obeying to a certain equation. We have calculated the equation for each line, beginning with the (phase -2) which is separated from the (phase -1) by the equation H= -12J -1/10.The (phase -1) is separated from (phase 0) by the equation H=-4J – 1/8 , by symmetry on the axe H=0 we find the two equations separating the phases (0 , +1 and +2): H=4J - 1/8 and H=12J -1/10 respectively. On one hand, the stable phases are (phase +2), (phase -2) for positives values of the coupling interactions J referring to the ferromagnetic state. On the other hand, the (phase-1), (phase0) and (phase+1) are the stables phases for negatives values of the coupling interaction indicating anti-ferromagnetic state. In the **Figure III.11.a)** and **Figure III.11.b)** we present the thermal variation of the magnetization M_S and the magnetic susceptibilityχ_S, respectively. We've calculated the variation of the magnetization as a function of the temperature for different size of the system (L≥4). The magnetization becomes lower and takes smaller values with the increasing of temperature, until a temperature T=27K and the magnetization M remain nearly constant (M_s=0,18 emu g^{-1}) indicating that the transition is of second order. This behavior of the magnetization stays the same for the others values of the lattice size L but as we increase L, the value of M_S for which we have the stability of the system get lower. The magnetization vanishes continuously at the critical temperature indicating a second order transition as we mentioned. Therefore, as we increase the size of our system the occurrence of this second order transition get delayed. Moreover, the susceptibility is calculated and plotted in **Figure III.11.b)** .The peak of the susceptibility and its corresponding temperature increase by increasing the system size L. The variation of susceptibility χ_S takes a maximum value for a T_c= 29K, then it decreases until it reaches a minimum value of χ_S = 0,1.

As we increase L, the susceptibility peak becomes thinner and the value of T_c can be evaluated more precisely. In **Figure III.12**, we plotted both the magnetization and susceptibility in the same graph, when the fluctuations of the magnetization (χ_S) are at there maximum M_S take the minimum value between 0,18 and 0,17 emu g^{-1} .

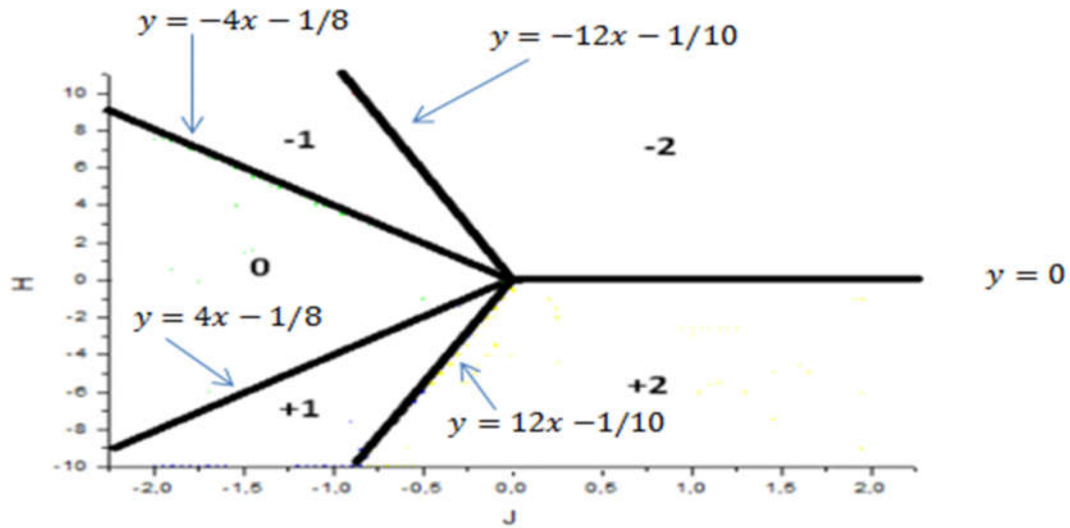

Figure III.10: The ground state phase diagram in the plan (J,H) for an Ising system corresponding to our spin configuration.

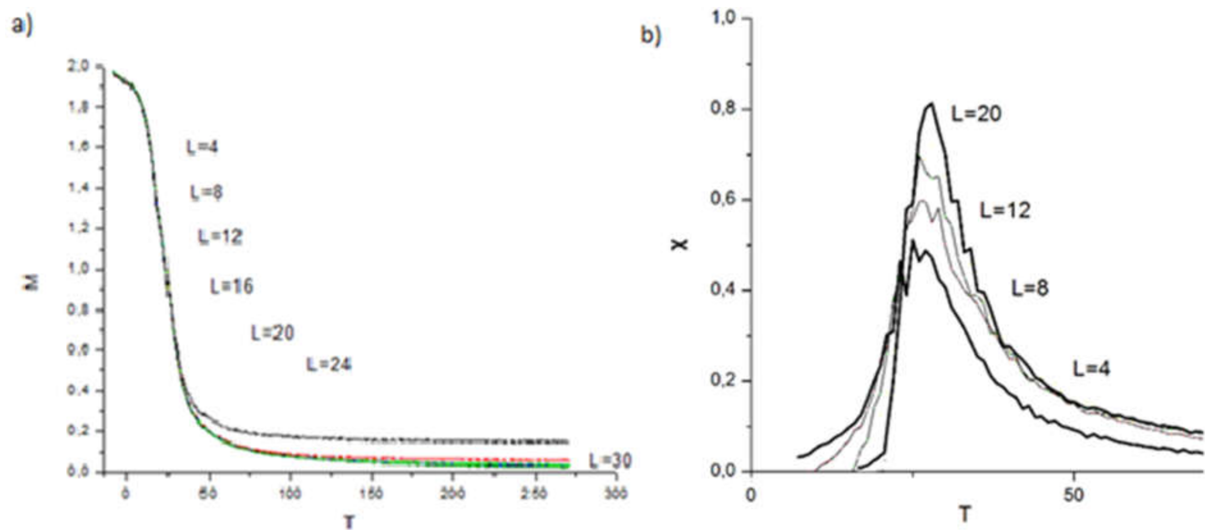

Figure III.11: a) The magnetization and b) The susceptibility as a function of the temperature for different size ranges L= 4 to L= 30

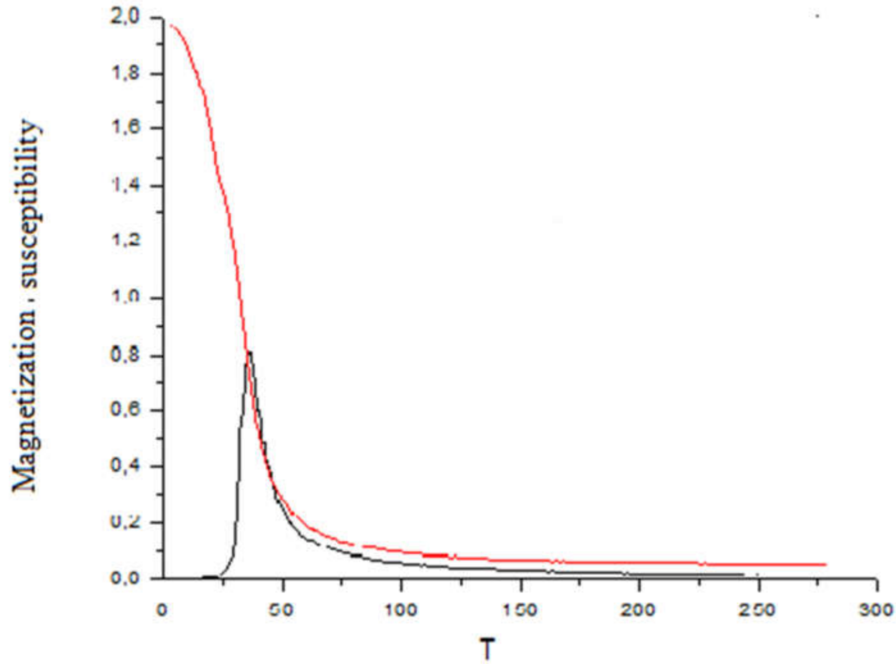

Figure III.12: The magnetization M_s and magnetic susceptibility χ_S versus the temperature plotted simultaneously.

III.4. Conclusion:

The Total Density of state for our DMS Ga(Mn)N was calculated for different doping concentrations of magnetic impurities. We obtained a half-metallic behavior which is reinforced by increasing the concentration of the doping impurities (Mn atoms) taking into account not to exceed a certain concentration where the structure can be broken. Moreover, the magnetic state is ferromagnetic and the mechanism responsible for this magnetic state is the Double exchange confirmed by the DOS calculated for doping concentration x ≥0.05. In addition to that, the ferromagnetism can be stabilized by adding itinerants carriers in the semi-filled band of Mn 3d-state, in good agreement with other ab initio calculations about GaN doped system.

The ground state phase diagram was determined and plotted in the plan (H,J) for our Ising system , it corresponds to the spin configuration Si. The ground state shows five separated phases (phase (+2), phase (+1), phase (0), phase (-1) and phase (-2). For the positives values of the coupling interaction J, the two phases [(+2) and (-2)] are the stable ones and for negatives values of J, the phases [(+1),(0) and (-1)] are the stables phases. Moreover, the magnetic properties were investigated by Monte Carlo simulations using Ising model applied on a wurtzite

structure system.The magnetization decreases with the increasing of the temperature then it vanishes and maintain a value of 0,18 emu g^{-1} at a temperature T= 27K, it indicates a second order transition. The same behavior of the magnetization is obtained when increasing the size lattice L, except the fact that the value of the magnetization corresponding to the second order transition gets lower. The magnetic susceptibility increases when the temperature gets higher until it reaches a peak and vanishes after that to take the lowest value. The peak of the susceptibility and its corresponding temperature T_c increases by increasing the lattice size L, its peak is at maximum at the transition temperature.

Chapter IV

Ab initio investigation of (Fe, Ni) doped GaAs: Magnetic, electronic properties and Faraday rotation

Superlattices and Microstructures 106 (2017) 163–169

Contents lists available at ScienceDirect

Superlattices and Microstructures

journal homepage: www.elsevier.com/locate/superlattices

Ab initio study of (Fe, Ni) doped GaAs: Magnetic, electronic properties and Faraday rotation

Y. Sbai [a,*], A. Ait Raiss [a], L. Bahmad [a], A. Benyoussef [a,b]

[a] Laboratory of Magnetism and High-energy Physics (LMPHE), Faculty of Sciences, University Mohammed-V, Av. Ibn Battouta, B. P. 1014, Rabat, Morocco

[b] Resident Member in Hassan II Academy of Science and Technology, Rabat, Morocco

ARTICLE INFO

Article history:
Received 21 February 2017
Accepted 27 March 2017
Available online 30 March 2017

Keywords:
Ab-initio calculations
Density of state (DOS)
Akai-KKR-CPA method
GGA approximation
Magneto-optical property

ABSTRACT

The interesting diluted magnetic semiconductor (DMS), Gallium Arsenide (GaAs), was doped with the transition metals magnetic impurities: iron (Fe) and Nickel (Ni), in one hand to study the magnetic and magneto-optical properties of the material Ga(Fe, Ni) As, in the other hand to investigate the effect of the doping on the properties of this material, the calculations were performed within the spin polarized density functional theory (DFT) and generalized gradient approximation (GGA) with AKAI KKR-CPA method, the density of states (DOS) for different doping concentrations were calculated, giving the electronical properties, as well as the magnetic state and magnetic states energy, also the effect of these magnetic impurities on the Faraday rotation as magneto-optical property. Furthermore, we found the stable magnetic state for our doped material GaAs.

© 2017 Elsevier Ltd. All rights reserved.

1. Introduction

These last twenty years, diluted magnetic studies (DMS) have been the subject of many and considerable studies and researches leaded by different laboratories and institutes around the world, these DMSs can be divided into various categories: III-V DMSs, II-VI DMSs ..., this attention has been given because of their interesting properties and applications in Spintronic devices [1,2] (II, Mn)VI diluted magnetic semiconductors (DMS) with a strongly enhanced paramagnetic behavior have been investigated [3–7]. Doped GaAs, and other DMSs of the group III–V [8,9]. The doping of these DMSs has been the key for their various applications because of the magnetism inducted by the injection of the magnetic impurities, e. g, transition metals: Mn, Ni, Fe, Co ... [1,10], predicting high temperature ferromagnetism in some doped semiconductors such as GaN, ZnO, GaAs. One of the most studied and interesting DMS is GaAs, various studies has targeted this material, it has been studied from many aspects, e.g, spin-orbit interaction in GaAs wells [11], and the interface contribution of this spin-orbit interaction in the GaAs/AlGaAs [12] Udson C. Mendes et al. [13] have studied the electronic and optical properties of InGaAs wells with Mn delta doping GaAs barriers, also there are some few Ab initio calculations on GaAs, precisely, on the Mn-doped GaAs digital ferromagnetic heterostructures [14], a remarkably high Tc about 250 K has been reported in a P-type selectively doped III-V hetero-structured composed of Mn delta-doped GaAs/p-AlGaAs [1]. There are not many theoretical studies about the Fe-doped GaAs and Ni-doped GaAs. I.R. Harris et al. [15] worked on the phase identification in Fe-doped GaAs single crystals and reported a ferromagnetic phase with a curie temperature about 100 °C, along with some

* Corresponding author.
E-mail address: YSbai.2011@gmail.com (Y. Sbai).

http://dx.doi.org/10.1016/j.spmi.2017.03.042
0749-6036/© 2017 Elsevier Ltd. All rights reserved.

IV.1. Introduction:

In recent years, many laboratories and institutes around the world have given noticeable attention, in their studies and researches, to diluted magnetic studies (DMS). These DMSs can be divided into various categories: III-V DMSs, II-VI DMSs…, and this scientific attention comes from their interesting properties and potential applications in Spintronic devices **[153,154]**. Namely, (II, Mn)VI diluted magnetic semiconductors (DMS) with a strongly enhanced paramagnetic behavior have been investigated **[155,156]**. As well as doped GaAs, and other DMSs of the group III–V **[157,158]**. The doping of these DMSs has opened the door for their different applications because of the magnetism inducted by the injection of magnetic impurities, e. g, transition metals: Mn, Ni, Fe, Co…**[153]**, predicting high temperature ferromagnetism in certain doped semiconductors such as GaN, ZnO, GaAs. Among these DMSs, one attracts lots of interest, which is Gallium Arsenide (GaAs). Various studies has targeted this material, it has been studied from many aspects, e,g , spin-orbit interaction in GaAs wells **[159]**, and the interface contribution of this spin-orbit interaction in the GaAs/AlGaAs **[160]** Udson C. Mendes et al. **[159]** have investigated the electronic and optical properties of InGaAs wells with Mn delta doping GaAs barriers, also there are some few Ab initio calculations on GaAs, precisely, on the Mn-doped GaAs digital ferromagnetic heterostructures **[161]**. Also, a remarkably high Curie temperature (Tc) about 250 K has been reported in a P-type selectively doped III-V hetero-structured composed of Mn delta-doped GaAs/p-AlGaAs **[153]**. Meanwhile, there are not many theoretical studies about the Fe-doped GaAs and Ni-doped GaAs. I.R. Harris et al. **[162]** worked on the phase identification in Fe-doped GaAs single crystals and reported a ferromagnetic phase with a curie temperature about 1000C. Further experimental works have been carried on for Fe-doping in GaAs **[163-166]**. As mentioned before, our interest comes from the lack of data concerning the magnetic and magneto-optical properties of Ga(Fe, Ni)As. Along with the interesting properties that the Fe doping can show and the effect on the magneto-optical aspect as reported in **[166]**. While regarding Ni-doping in GaAs, Nickel diffuses rapidly into GaAs and acts as a deep acceptor **[164]**. It has often been used as a contact material on GaAs devices **[165]**. The outline of this paper is as follows: In section 2 we present the calculation method and approximation. In section 3 we investigate and discuss the Ab initio results and then we conclude by a summarizing conclusion.

IV.2. Crystal structure and Calculation Methods:

In the following Ab initio calculations we utilized the AKAI-KKR-CPA code MACHIKANEYAMA2002v08 package designed and made by Akai. Korringa- Kohn-Rostoker method **[98]** combined with the coherent potential approximation (KKR-CPA). The method is based on the density functional theory (DFT), the KKR-CPA method was developed by Akai and Dedrichs to trait transition metal alloys, with the parametrization of Vosko, Wilk and Nusair (VWN) **[88]**, e.g. in our case we have GaFeAs and GaNiAs alloys. The host material is GaAs and the transitions metals used are Iron (Fe) and Nickel (Ni). The doping with these impurities is done randomly since the Fe and Ni atoms in each case replace and take the cation atoms (Ga) sites randomly. Therefore, we have employed the Generalized Gradient Approximations (GGA) approximation, Perdew–Wang functional, (GGA91) [**92]**, to treat this disordered system since it is one of the most accurate and precise approximation to deal with this disorder. In our previous works we have used the local density approximation LDA approximation also **[166,167].**

The density of states (DOS) were calculated and plotted for both systems $Ga_{1-x}Fe_xAs$ and $Ga_{1-y}Ni_yAs$ for different doping concentrations which are the Fe, Ni magnetic impurities. To better understand the upcoming figures, the syntax "Total" represents the total density of spins up and down, located in the valence and conduction bands in the system structure. The Total density must not change from a figure to another. But the partial DOS curves will change, when varying the doping concentrations. These concentrations are x (Fe) =0.01, 0.02, 0.03, 0.04, 0.05, 0.06, 0.07, and y (Ni) = 0.01, 0.02, 0.03, 0.04, 0.05, 0.06, 0.07. As mentioned above, the Fe atoms are placed in the Ga sites inside the structure of GaAs. We've used in our code 300 K-point in the first Brillouin zone. Our system is a III-V direct bandgap semiconductor with a zinc blende crystal structure. See **Figure IV.1.** With a = b= c= 5.65325 Å, as lattice constants and T_d^2-F43m as a space group. Since we have a zinc blend structure with one lattice parameter, our atoms in this system are disposed as each Ga atom is encircled by four As atoms on the corners and vice versa.

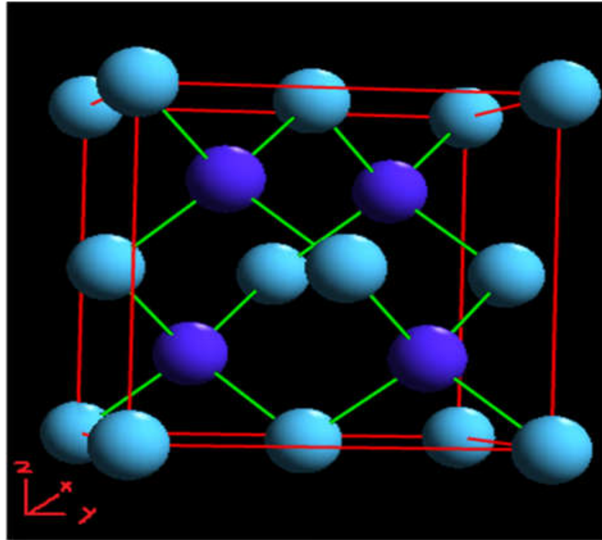

Figure IV.1: GaAs zinc blende structure where Ga atoms are presented in Blue color and As atoms in purple one**,** via “XCrySDen”.

IV.3. Results and discussions:

IV.3.a. Density of states:

We calculate the Density of state for different cases in our system, **Figure IV.2** represents the Density of state (DOS) corresponding to the pure GaAs, without any doping impurities. The Fermi level is close to the conduction band and there is no impurities bands in the gap beside the symmetry between the spins up and down for both valence and band conduction, Thus our material in this case is n-type showing no magnetism as clear in the **Figure IV.2**.

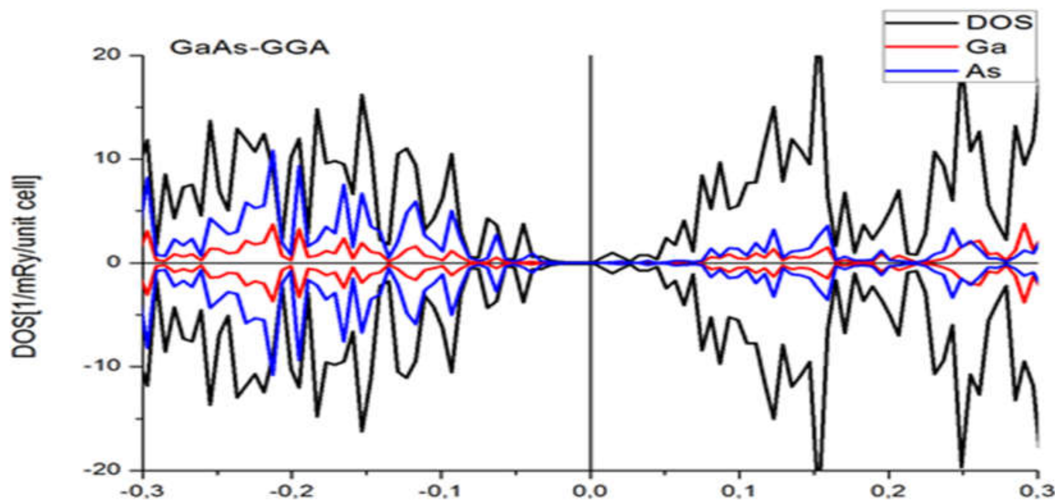

Figure IV.2. Density of states by GGA approximation for the pure GaAs without any doping impurities

It’s obvious that DMSs are more interesting when they’re doped with magnetic impurities which are in our case, transition metals atoms, irons (Fe) and Nickel (Ni). These transition metals contribute with their 3d bands electrons. For this purpose we proceeded by the doping of our host material, GaAs, with Fe atoms and Ni atoms separately. We’ve applied doping concentrations from 0.01 to 0.07 for each doping impurities. We did not reach higher concentration, taking into consideration not to exceed the solubility rate of GaAs, to not break the symmetry of the structure. Below, in **Figure IV.3** are the corresponding DOS for each concentration. From **Figure IV.3** we notice that doping with the Ni impurities changes the type of the semi-conductor from n-type to p-type which indicates in this case the abundance of the holes carriers in the material. This is clear for every concentration as in **Figure IV.3 a)…g)**. The injection of the magnetic impurities causes the appearance of impurities band which are 3d-band as clear in both **Figure IV.3** and **Figure IV.4**. Beside that, in **Figure IV.2 a)** Ni 3d-bands are degenerated and located in the gap below the Fermi level. As we increase the doping concentration the degeneracy is lifted progressively. From **Figure IV.3 b)** to **g)**.the peaks of the Ni bands have the highest density of states of electrons as it reaches approximately (748 ev/unit cell) in comparison with the Arsenide (As) bands which have a really weak magnetic moment. In **Figure IV.3 a)** we have two Ni 3d-band in the Fermi level, one for the up-spins and the other in the down-spins region. In on hand, the majority of the first band (up-spins) is located below Fermi level. Therefore, the electrons bands are empty. In the other hand, the major part of the second band (down-spins) is above Fermi level, thus, the electrons bands are contains Ni electrons and their spins are down. This is an interesting information to have, because it can help in some GaAs spintronic application, e.g. Data memory….There is a shift between the magnetic 3d-up-spins band and down spins, **Figure IV.3a)** and **Figure IV.3b)**.As the we inject more magnetic impurities, the shift disappears.

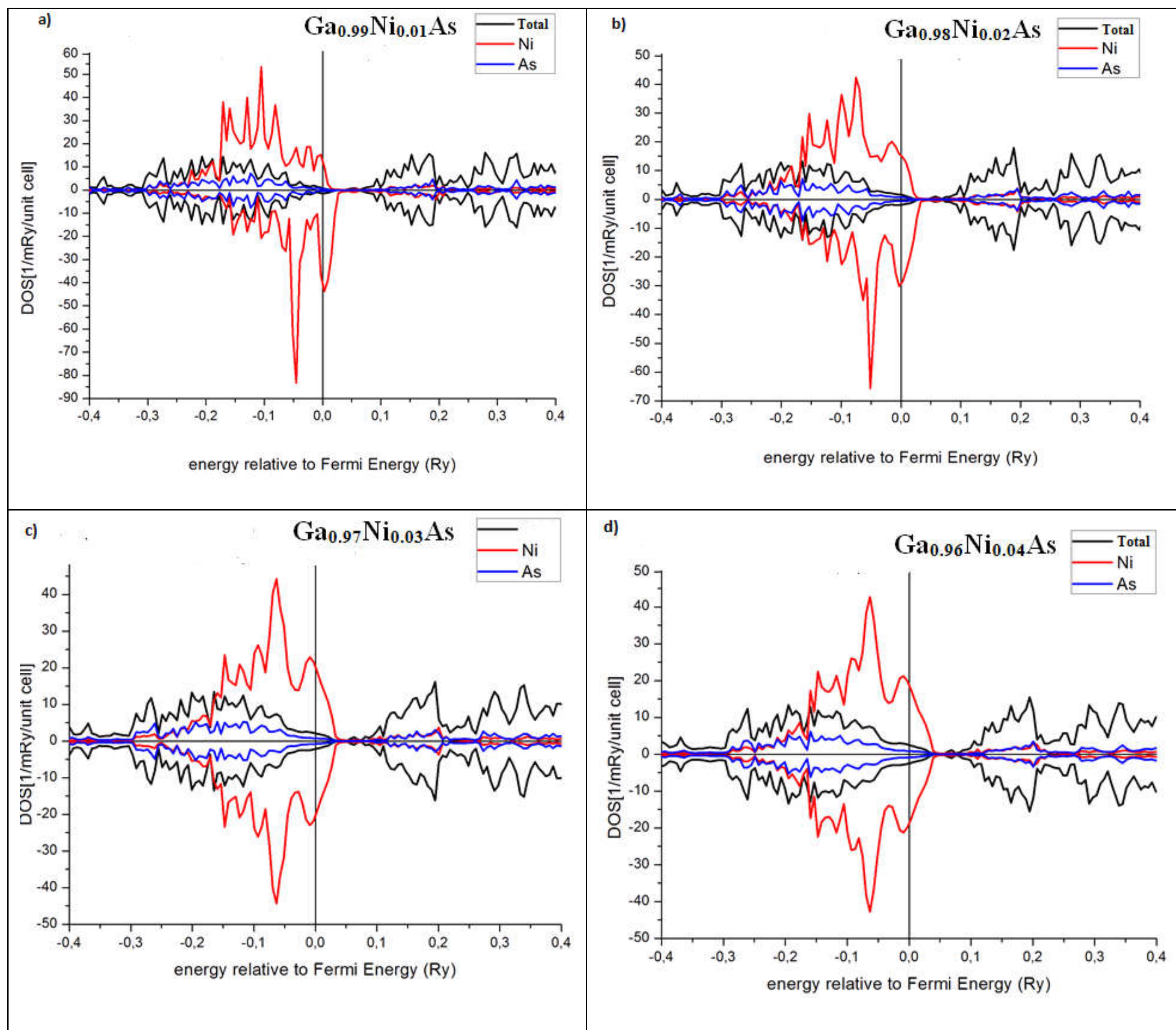
a)
$Ga_{0.99}Ni_{0.01}As$
Total
Ni
As
DOS[1/mRy/unit cell]
energy relative to Fermi Energy (Ry)
b)
$Ga_{0.98}Ni_{0.02}As$
Total
Ni
As
DOS[1/mRy/unit cell]
energy relative to Fermi Energy (Ry)
c)
$Ga_{0.97}Ni_{0.03}As$
Ni
As
DOS[1/mRy/unit cell]
energy relative to Fermi Energy (Ry)
d)
$Ga_{0.96}Ni_{0.04}As$
Total
Ni
As
DOS[1/mRy/unit cell]
energy relative to Fermi Energy (Ry)

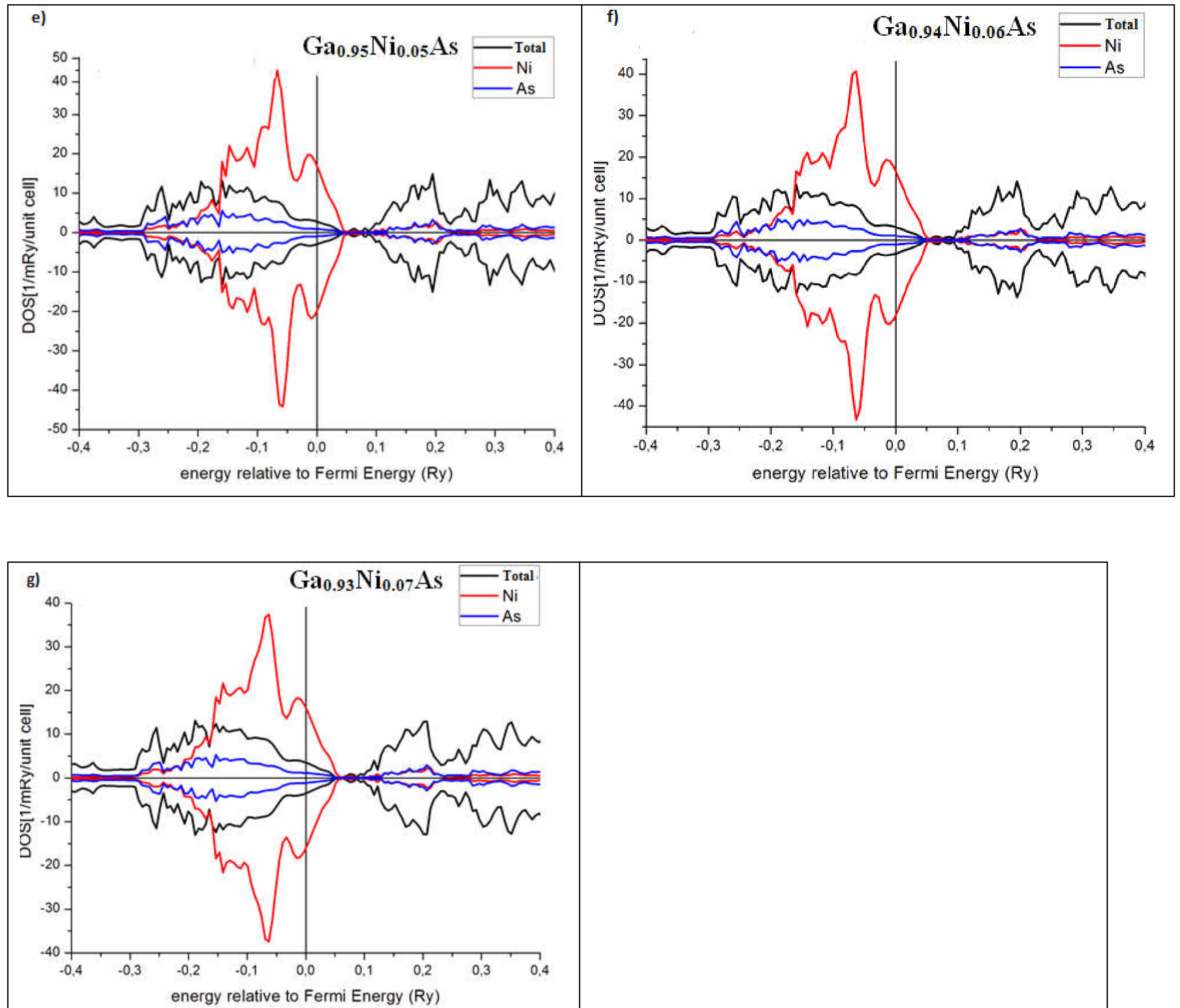

Figure IV.3. Total and Partial density of states for the case of $Ga_{1-x}Ni_xAs$ for various doping concentrations: a)x=0.01, b)x=0.02, c)x=0.03, d)x=0.04, e)x=0.05, f)x=0.06, g)x=0.07.

As well as Ni doping, we performed Fe doping with the same range of concentrations. The doping with Fe atoms changes the type of the semiconductor from n-type to p-type. See **Figure IV.4**. In the first DOS, **Figure IV.4a)**, the 3d-bands in the gap are triple degenerated. This degeneracy is lifted slowly with the increasing of the doping rate. The down-spins electrons have the highest density of state as clear in **Figure IV.4a)**. With this low concentration of Fe, a half metallic behavior appears in our material. As we increase the concentration this half metallic behavior become stable this can be explained by the injection of carriers, which are the holes in this case. Moreover, the 3d-bands get wider as the percentage of magnetic atoms, Fe, increases,

indicating a double exchange mechanism responsible for the magnetism appearing in the material.

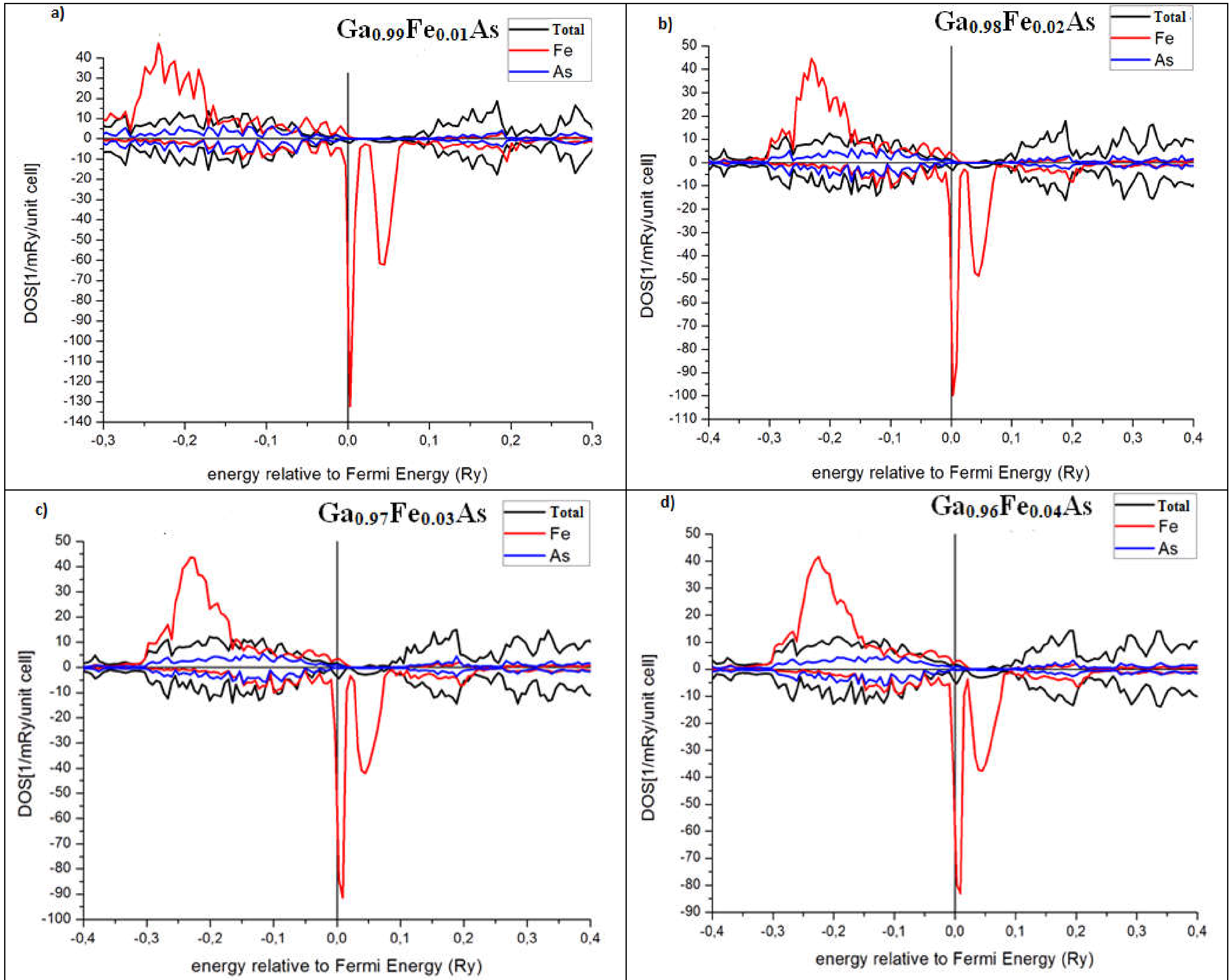

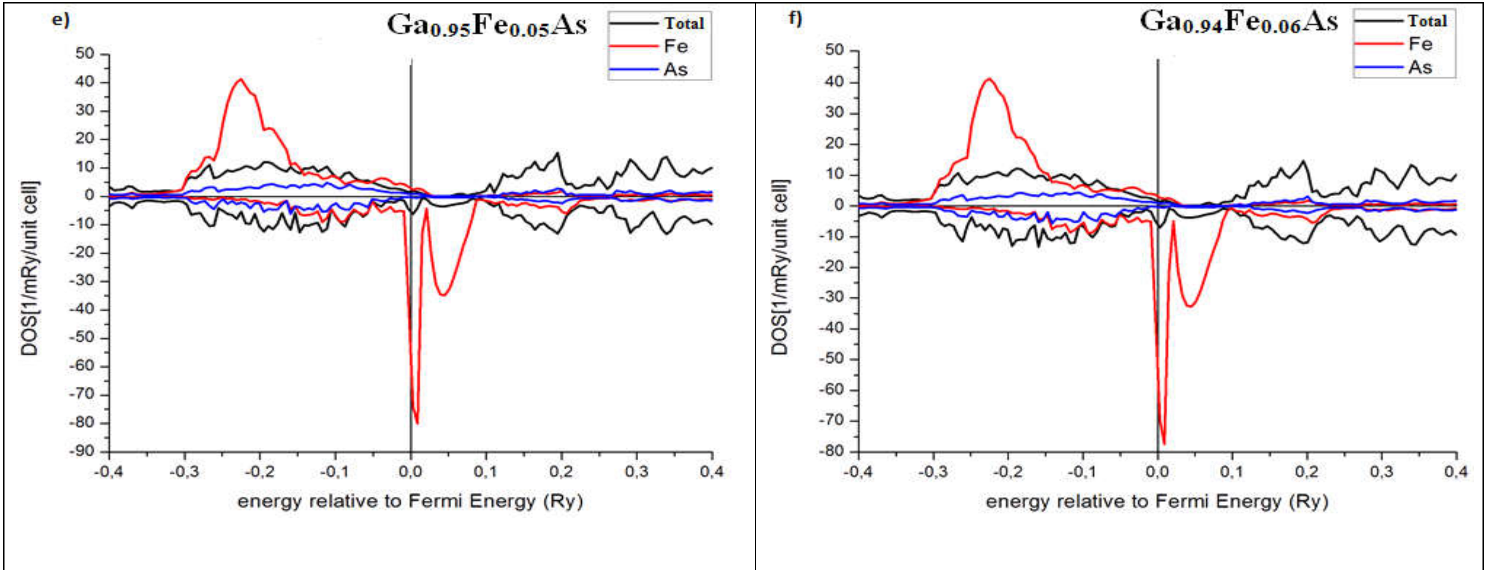

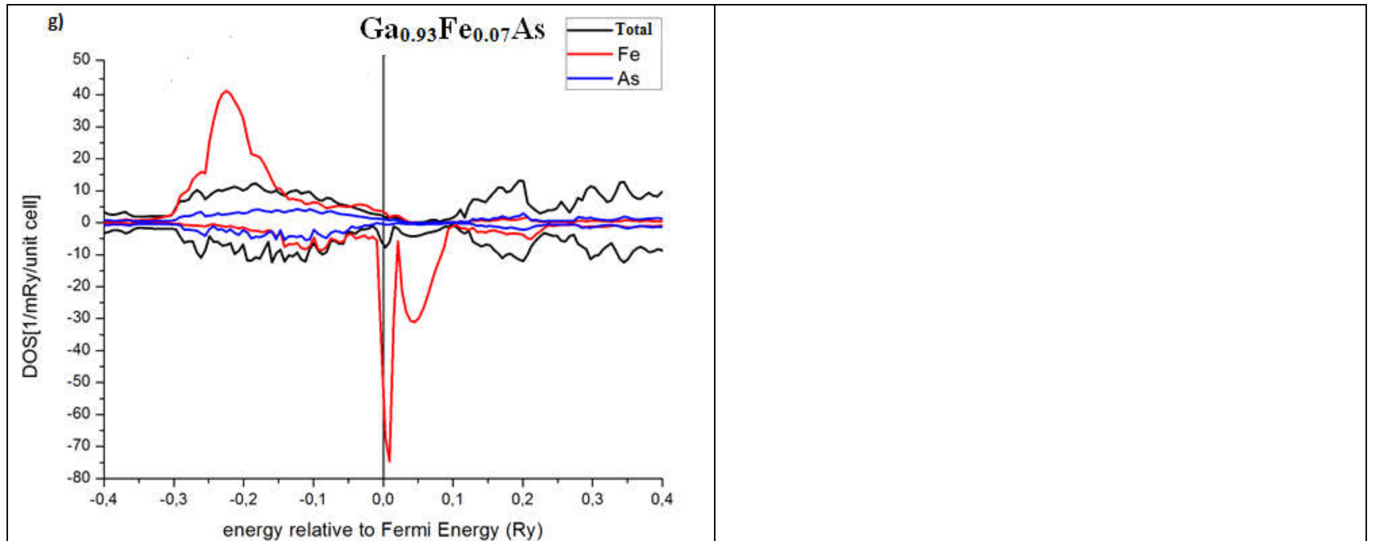

Figure IV.4: Total and Partial density of states for the case of $Ga_{1-y}Fe_yAs$ for various doping concentrations: a) y=0.01, b) y=0.02, c) y=0.03, d) y=0.04, e) y=0.05, f) y=0.06, g) y=0.07.

IV.3.b. Magnetic stability and Faraday rotation:

We calculated the magnetic state energy for each concentration of the magnetic impurities (Fe, Ni).In the aim to study the competition between the DLM and Ferromagnetic state. See **Table IV.1** and **Table IV.2**. In the first case, Ni doping, $Ga_{1-y}Ni_yAs$, from y= 0.01 of Ni to 0.04, the DLM is the stable magnetic state; since it has the lowest energy. For $0.04 \leq y < 0.07$, the energy of the ferromagnetic state becomes the lowest and then the ferromagnetic state becomes the stable one. Above 0.07 the stability goes to the DLM state. **Table.2** corresponds to the case of

$Ga_{1y}Fe_yAs$, for $0.01 \leq x \leq 0.03$, our material is ferromagnetic. Above x= 0.03 the stable magnetic state changes to DLM state. This is very interesting since we have an idea about the stable magnetic state and then we can us the material in the appropriate application.

Table.1: The Values of the ferromagnetic and Dlm energy for $0.01 \leq x(Ni) \leq 0.07$ in the case of $Ga_{1-x}Ni_xAs$.

$Ga_{1-x}Ni_xAs$	E_{Ferro}(Ry)	E_{DLM}(Ry)	E_{DLM}- E_{Ferro} (Ry)
$Ga_{0.99}Ni_{0.01}As$	-8403.2666199	-8403.2667263	-0.0001064
$Ga_{0.98}Ni_{0.02}As$	-8394.7944555	-8394.7946326	-0.0001771
$Ga_{0.97}Ni_{0.03}As$	-8386.3275106	-8386.3314842	-0.0039736
$Ga_{0.96}Ni_{0.04}As$	-8377.8640770	-8377.8640917	-0.0000147
$Ga_{0.95}Ni_{0.05}As$	-8369.3933444	-8369.3933223	0.0000221
$Ga_{0.94}Ni_{0.06}As$	-8360.9262415	-8360.9262183	0.0000232
$Ga_{0.93}Ni_{0.07}As$	-8352.4621321	-8352.4621451	-0.0000130

Table.2: The Values of the ferromagnetic and Dlm energy for $0.01 \leq y(Fe) \leq 0.07$ in the case of $Ga_{1-y}Fe_yAs$.

$Ga_{1-y}Fe_yAs$	E_{Ferro}(Ry)	E_{DLM}(Ry)	E_{DLM}- E_{Ferro} (Ry)
$Ga_{0.99}Fe_{0.01}As$	-8386.1335411	-8386.1332684	0.0002727
$Ga_{0.98}Fe_{0.02}As$	-8354.6879312	-8354.6875709	0.0003603
$Ga_{0.97}Fe_{0.03}As$	-8434.1576544	-8434.1573928	0.0002616
$Ga_{0.96}Fe_{0.04}As$	-8344.2837491	-8344.2839433	-0.0001942
$Ga_{0.95}Fe_{0.05}As$	-8330.8692579	-8330.8693447	-0.0000868
$Ga_{0.94}Fe_{0.06}As$	-8317.4546271	-8317.4547431	-0.0001160
$Ga_{0.93}Fe_{0.07}As$	-8304.0399780	-8304.0401350	-0.0001570

Note that, GaAs material has various domains of application and consequently different types of properties have to be studied, namely, the Faraday rotation as an important magneto-optical property in this case, see ref **[167]**.The following equation represents the equation of the Faraday rotation:

$$\theta_F = \frac{\sqrt{F0}\,d}{2\pi c} \cdot \frac{E^2}{(E_0^2 - E^2)3/2} . N0(\alpha - \beta).x. < Sz > \qquad IV.1$$

Such as: F_0, is a constant, E is the photon energy and E_0, is the "exciton" energy, d is the sample thickness in our case the sample is composed by GaAs. Note that, θ_F is proportional to the value of <Sz> and $N0(\alpha - \beta)$. Therefore, we introduce the equations ***IV.2*** below, See Ref **[166]**:

$$\left(\boldsymbol{N_{0\alpha}} = \frac{\mathbf{\Delta Ec}}{\mathbf{x.}<\boldsymbol{S}>}, \boldsymbol{N_{0\alpha}} = \frac{\mathbf{\Delta Ev}}{\mathbf{x.}<\boldsymbol{S}>}\right) \qquad \textbf{\textit{IV.2}}$$

We exploited the results of the density of states (DOS) that we obtained for different doping concentration. ΔE_c and ΔE_v are the spin splitting of the difference between the up-spins and down-spins in both the conduction and valence bands. $N_{0\alpha}$ and $N_{0\alpha}$ represent the exchange constants in the valence and conduction bands, as clear in equation IV.1,the Faraday rotation depends on the exchange interactions in the valence and the conduction bands, then, it depends on $N0(\alpha - \beta)$. Which is illustrated in the DOS **[167]**, by the spin splitting in both of the valence and conduction bands. In our case, For Fe doping we have a weak splitting in the valence band whereas the injection of Ni causes no splitting in the valence or conduction band. Which indicate that the appropriate doping with Fe can help and increase the magneto optical properties for GaAs.

IV.4. Conclusion:

We performed and Ab initio calculations for the magnetic and magneto-optical properties of GaAs in two case, the doping with Ni atoms and the doping with Fe atoms. For the first case, $Ga_{1-x}Ni_xAs$, the degenerated 3d-band are near the Fermi level. As we increase the doping concentration the degeneracy is lifted progressively. The stable magnetic state is the Dlm state for the range of concentration $0.01 \leq x \leq 0.04$, for 0.04 and 0.05 the ferromagnetic state is the stable magnetic state. For the case of $Ga_{1-y}Fe_yAs$, as well as Ni, the degeneracy is lifted by the increasing of the doping concentration. For the lower concentrations $0.01 \leq y \leq 0.03$, the ferromagnetic state is stable, for higher range of concentrations $y \geq 0.04$, the Dlm state becomes the stable magnetic state. It is very interesting since we can have an idea about the stable magnetic state and then we can us the material in the appropriate application. Also Ni doping does not present magneto-optical properties, the Faraday rotation, but for the Fe doping, the Faraday rotation exists and the Fe doping increases the magneto-optical properties. Hence, GaAs doped with Fe can be used for Faraday rotation based applications such as: optical isolator, telecommunications via optic fiber cables, Modern ultra-high field permanent magnet and special

paramagnetic glasses. Furthermore, when doped with the right and accurate concentration of magnetic impurities GaAs is an interesting semiconductor and a huge candidate for spintronic applications and photovoltaic cells also.

General Conclusion

In this work, we utilized ab-initio methods, such as the linearized augmented plane waves method (FP-LAPW) and the KKR method in the framework of density functional theory (DFT), to study doped Dilute magnetic semiconductors (DMS) and there application in Spintronic field so as to have new spintronic technologies and new electronic devices.

These DMSs are divided into families: IV, IV-VI and the principal ones are the II-VI(ZnTMO, CdTMTe...) and the III-V(GaTMAs, GaTMN,...) types with TM = ion from the series of transition metals.

In our cases, we used Mn, Fe and Ni as transition metals. We, as a team, worked with both II-VI and III-V Types, but in the part of our work within this PhD thesis, we focused on the Mn-based III-V based DMS. The III—V DMS can be more attractive than II—VI materials, as they are probably much more usable for spintronic device fabrication. That's why over last two decades, diluted magnetic semiconductors based on III—V compounds have been of considerable interest, in the aim to find semiconductors that show ferromagnetism at room temperature or even higher.

Note that, we study the magnetic and electronic properties of two important semiconductor compounds: GaN and GaAs and precisely, GaMnN and Ga(Fe/Ni)As, with a small Monte Carlo approach for GaN, that will be much more elucidated in future work.

The Ab initio calculations were performed within the AKAI code, using two approximations: Beginning with LDA approximation which became the main approximation for the calculation of physical properties related to different semiconductors. Then, GGA approximation for Ga(Fe/Ni)As material .

We calculated and plotted both total and partial Density of states and there magnetic and electronic properties, compared with other literature works. In GaMnN and Ga(Fe/Ni)As materials respectively, we discuss the doping with Mn impurity on one hand and Fe, Ni on the other hand. Different magnetic impurity concentrations are considered and analyzed suggesting the dominating role of Mn ($3d^5$) configuration. Then we analyze s, p—d exchange, together with resulting magnetooptical properties (in particular Faraday rotation for GaFe/NiAs). Also the

coupling between Mn ions (d—d exchange) and ferromagnetic ordering observed in our material. We propose a potential mechanism responsible for this ferromagnetism.

For GaN material, we found a half-mettalic behavior which is reinforced by increasing the concentration of the TM impurities (Mn atoms) taking keeping in mind not to exceed a certain concentration otherwise the structure could be broken. In addition, the magnetic state observed is ferromagnetic and the possible mechanism responsible for this magnetic state is the double exchange confirmed by the DOS calculated for the Mn doping concentrations of $x \geq 0.05$. Besides that, the ferromagnetism can be stabilized by adding itinerants carriers in the semi-filled band of Mn 3d-state.

For the Monte Carlo approach, we calculated and presented the ground state diagram (H,J) for an Ising model showing five possible phases and there stability. Also, the magnetization and susceptibility behavior with the temperature was studied for different system sizes.

For GaAs material, we incorporated the magnetic impurities iron (Fe) and Nickel (Ni) in our system with a controlled rate, so that we can study the magnetic and magneto-optical properties of Fe/Ni-based GaAs, beside the doping effect on our DMS. By mean of polarized density functional theory (DFT) and generalized gradient approximation (GGA) with AKAI KKR-CPA method, we calculated the Density Of State related to different doping concentration ($Ga_{1-x/y}$ Fe_x Ni_y As). Also, we studied the magnetic state stability which can be very useful and therefore, apply the material conveniently in the industry. We give the calculated the magnetic state energy. The effect of Fe and Ni on the Faraday rotation in the system was also investigated, in the aim to find which one triggers the Faraday rotation on the system. It was found that, Ga_{1-x} Fe_x N is the one which can be used in Faraday rotation based applications, e.g., telecommunications via optic fiber cables, Modern ultra-high field permanent magnet, optical isolator, and special paramagnetic glasses, etc. Hence, if we control the doping concentration of magnetic impurities and apply it accurately, Ga(Fe/Ni)As will present itself a very intriguing and huge candidate for spintronic applications and DMS-based photovoltaic cells.

This DMS domain is expanding and still in progress, with each published paper we know more about DMS materials and whether or not they can be applicable in spintronic devices. The aim is to have a semiconductor that shows Ferromagnetic behavior at Room temperature or higher.

Both theoretical and experimental studies are complimentary supporting obtained results and refining them. The interest for this domain is rising and DMS-based devices will be more and more available in the industrial market in the near future.

As perspectives, there are still many tasks to focus on; In upcoming work we'll investigate the ferromagnetism stability and how to sustain this ferromagnetism beside increasing the Curie temperature. We're focusing also on Monte Carlo method in our actual DMS studies since we've not fully exploited it yet, it can be a strong asset. Also, we're interested in the study of DMS-based material for photovoltaic applications.

References

[1] P. Nemec, Charles University, Prague, Czech Republic, http://www.rpip.tohoku.ac.jp (2017)

[2] M. N. Baibich, J. M. Broto, A. Fert, F. N. Van Dau, F. Petroff, P.Etienne , G.Creuzet, A. Friederich, and J. Chazelas, Giant magnetoresistance of(001)fe/(001)cr magnetic superlattices. Phys. Rev. Lett. 61, 21 (1988), 2472–2475.

[3] G. Binasch, P.Grünberg, F. Saurenbach, and W. Zinn. Enhanced magnetoresistancein layered magnetic structures with antiferromagnetic interlayer exchange. Phys. Rev.B 39, 7 (1989), 4828–4830.

[4] Jacques Derrien, Vinh Le Thanh, Erich Kasper ,Thin Solid Films; Vol 517, Issue 1, 3 (2008) 2-5.

[**5**] M. marins de castro suza, “Commutation précessionelle de mémoire magnétique avec polariseur à anisotropie perpendiculaire”, Thèse de doctorat, Université de Gronoble (2011).

[6] P.M. Tedrow, R. Meservey, “Spin-dependent tunnelling into ferromagnetic nickel”, Phys. Rev. Lett. 26 (1971), 192-195.

[7] M. Julliere. “Tunneling between ferromagnetic films”, Phys. Lett. A, 54 3 (1975), 225-226.

[**8**] J.S. Moodera, L. R. Kinder, T. M. Wong, R. Meservey, “Large magnetoresistance at room temperature in ferromagnetic thin film tunnel junctions”, Phys. Rev. Lett.74 (1995), 3273-3276.

[9] W. H. Butler, X. G. Zhang, T. C. Schulthess and J. M. MacLaren Spin-dependent tunneling conductance of Fe|MgO|Fe sandwiches Phys. Rev. B 63, (2001) 054416.

[**10**] J. Mathon and A. Umerski Theory of tunneling magnetoresistance of an epitaxial Fe/MgO/Fe(001) junction Phys. Rev. B 63, (2001) 220403.

[11] C. Chappert, A. Fert, F. Nguyen Van Dau, Nature Materials, 2007, pp813 – 823.

[12] G. Lampel,”Nuclear dynamic polarization by optical electronic saturation and optical pumpingin semiconductors”, Phys. Rev. Lett. 20 10 (1968), 491-493.

[13] S. Sugahara and J. Nitta, Spin Transistor Electronics: An overview and outlook. Proceeding of the IEEE, 98(12) (2010) 2124-2154.

[14] K. Uchida, J. Xiao, H. Adachi, J. Ohe, S. Takahashi, J. Ieda, T. Ota, Y. Kajiwara, H. Umezawa, H. Kawai, G. E.W. Bauer, S. Maekawa, and E. Saitoh, Nature Mater. 9, (2010) 894.

[15] A. Brataas, Yu. V. Nazarov, and G. E. W. Bauer, Phys. Rev. Lett. 84, (2000) 2481; Eur. Phys. J. B 22, (2001) 99.

[**16**] Y. Kajiwara, K. Harii, S. Takahashi, J. Ohe, K. Uchida, M. Mizuguchi, H. Umezawa, H. Kawai, K. Ando, K. Takanashi, S. Maekawa, and E. Saitoh, Nature 464, (2010) 262.

[17] X. Jia, K. Liu, K. Xia, and G. E. W. Bauer, Europhys. Lett. 96, (2011) 17005.

[18] C. Burrowes, B. Heinrich, B. Kardasz, E. A. Montoya, E. Girt, Y. Sun, Y. Y. Song, and M. Wu, Appl. Phys. Lett. 100, (2012) 092403.

[19] R. Janisch, P. Gopal and N. A. Spalding, "Transition metal-doped TiO2 and ZnO –present status of the field", J. Phys.: Condens. Matter 17 (2005) R657, and references therein.

[20] Luzhao Sun, Guowen Yuan, et al. NATURE REVIEwS | MeTHODS PRIMeRS | Article citation ID: (2021) 1:5

[21] Y. Ziat, A. Slassi, Z. Zarhri, M. Hammi, M. Houmad, A. Ait raiss, Y. Sbai, S. Echihi, A. El kenz, A. Benyoussef. J Supercond Nov Magn DOI 10.1007/s10948-016-3609-9.

[22] N. Theodoropoulou, A. F. Hebard, S. N. G. Chu, M. E.Overberg, C. R. Abernathy, S. J. Pearton, R. G. Wilson, J. M. Zavada, and Y. D. Park, J. Vac. Sci. Technol. A, 20, (2002), p.579.

[23] H. Ohno, H. Munekata, T. Penny, S. Von Molnar, and L. L. Chang, "Magnetotransport Properties of p-type (In, Mn) As Diluted Magnetic III-V semiconductors".. Phys. Rev. Lett.,68, (1992) 2664.

[24] Y.-J. Zhao, T. Shishidou, and A. J. Freeman, Phys. "Ruderman-Kittel-Kasuya-Yosida–like Ferromagnetism in Mnx Ge1-x ". Rev. Lett., 90 (2003) 047204.

[25] H. Munekata, H. Ohno, S. Von Molnar, A. Segmuller, L. L. Chang, and L.Esaki, « Diluted magnetic III-V semiconductors » .Phys. Rev. Lett., 63 (1989) 1849.

[26] G. Kioseoglou, A. Hanbicki, C. Li, S. Erwin, R. Goswami, and B. Jonker, condmat/0302231 (submitted to Appl. Phys. Lett., (2003). "Epitaxial Growth of the Diluted Magnetic Semiconductors CryGe1-y and CryMnxGe1-x-y".

[27] H. Ohno, A. Shen, F. Matsukura, A. Oiwa, A. Endo, S. Katsumoto and Y. Iye, Appl. Phys.Lett., 69 (1996) 363.

[**28**] K. Furdyna, "Diluted magnetic semiconductors", J. Appl. Phys. 64 (1988) R29.

[**29**] D. Ferrand, J. Cibert, A. Wasiela, C. Bourgognon, S. Tatarenko, G. Fishman, T. T. Andrearczyk, J. Jaroszynski, S. Kolesnik, T. Dietl, B. Barbara and D. Dufeu, "Carrier induced ferromagnetism in p-Zn1-xMnxTe", Phys. Rev. B 63 (2001) 085201.

[30] Y. Nagai, K. Nagasaka, Infrared Physics & Technology, 48 (2006) 1-15.

[31] I. T. Yoon, T. W. Kang, D. J. Kim,Journal of Magnetism and Magnetic Materials 320 (2008) 662-665.

[32] H. Munekata, T. Penney, L. L. Chang, Surface Science, 267 (1992) 342-348.

[33] T. Jungwirth, J. Sinova, J. Masek, J. Kucera and A. H. MacDonald, “Theory of ferromagnetic (III,Mn)V semiconductors”, Rev. Mod. Phys. 78 (2006) 809.

[34] K. W. Edmonds, K. Y. Wang, R. P. Campion, A. C. Neumann, N. R. S. Farley, B. L.Gallagher and C. T. Foxon, “High-Curie-temperature $Ga_{1-x}Mn_xAs$ obtained by resistancemonitored annealing”, Appl. Phys. Lett. 81 (2002) 4991.

[35] « The Economist, No Moore, A golden rule of mcrochips appears to be coming to an end » http://www.economist.com (2013).

[36] https://shop19.shopsoutlet2021.ru/

[37] Coronado E., Tsukerblat B.S., Georges R. (1996) Exchange Interactions I: Mechanisms. In: Coronado E., Delhaès P., Gatteschi D., Miller J.S. (eds) Molecular Magnetism: From Molecular Assemblies to the Devices. NATO ASI Series (Series E: Applied Sciences), vol 321. Springer, Dordrecht. https://doi.org/10.1007/978-94-017-2319-0_3

[38] H. Kramers, Physica 1, 182 (1934).

[39] G. W. Pratt, Phys. Rev. 97, 926 (1955).

[40] G. Jonker, J. Van Santen, “Ferromagnetic compounds with manganese and perovskites structure”, Physica 16 3 (1950), 337-349.

[41] C. Zener, “Interaction between the d-shells in the transition metals. II. Ferromagnetic compounds of manganese with perovskite structure”, Phys. Rev. 82 (1951), 403-405.

[42] C. Zener, “Interaction between the d shells in the transition metals”, Phys. Rev. 81 (1951), 440-444.

[43] J.B. Goodenough, A. Wold, R.J. Arnot, N. Menyuk, “Relationship Between Crystal Symmetry and Magnetic Properties of Ionic Compounds Containing Mn3+”, Phys.Rev. 124 (1961), 373-384.

[44] Xueyang Li, Hongyu Yu, et al. Molecules, 26(4), (2021) 803.

[45] E Janke et al, J. Phys. C: Solid State Phys. 16 (1983) 5959.

[46] Z. Ben Ayadi et al. Nanotechnology 18 (2007) 445702.

[47] M. A. Ruderman, C. Kittel, Physical Review 96 (1954) 99–102.

[48] T. Kasuya, Progress of Theoretical Physics 16 (1956) 45–57.

[49] K. Yosida, Physical Review 106 (1957) 893–898.

[50] X. L. Wang et al. EPL 87 (2009) 47001.

[51] K. Sato, H. K.Yoshida, Physica E 10 (2001) 251–255.

[52] K. Sato et al. Europhys. Lett. 61 (2003) 403.

[53] K. Sato, H. K. Yoshida, Semicond. Sci. Technol. 17 (2002) 367.

[54] K. Sato, P. H. dederichs and H. K. Yoshida, Europhys. Lett. 61 (2003) 403.

[55] G. Bouzerar, J. Kudrnovsky, L. Bergqvist and P. Bruno, Phys. Rev. B 68 (2003) 81203(R).

[56] Kudrnovsky J, Turek I, Drchal V, Maca F, Weinberger P and Bruno P 2004 Phys. Rev B69 115208.

[**57**] https://slidetodoc.com/origin-of-ferromagnetism-in-co-doped-zn-o.

[58] J. Li, T. Ikegami, T. Mori, Acta Mater. 52 (2004) 2221–2228.

[59] M. Cyrot et all, Magnétisme, I-Fondement, EDPscience (2000).

[60] A.M. Panich, V. Yu. Osipov, K.Takai, New Carbon Materials, 29 (2014) 392-397.

[61] M. Reis, Fundamentals of Magnetism (2013) 74-92.

[62] X. Oudet, Journal of Magnetism and Magnetic Materials, 98 (1991) 307-332.

[63] D.V.Metelin, A.Yu.Kazansky, V.Yu.Bragin, V.A.Tsel'movich, A.V.Lavrenchuk, L.V.Kungurtsev, Russian Geology and Geophysics, 48 (2007) 185-198.

[64] L. B. Kong, L. Liu, Z. Yang, S. Li, T. Zhang, C. Wang, Magnetic, Ferroelectric, and Multiferroic Metal Oxides, Metal Oxides (2018) 287-311.

[65] E. ChitraDevi, I. Soibam, Journal of Magnetism and Magnetic Materials, 469 (2019) 587-592.

[66] D. Benea, R. Gavrea, M. Coldea, O. Isnard, V. Pop, Journal of Magnetism and Magnetic Materials, 475 (2019) 229-233.

[67] X. Jiang, X. Zhang, Z. Hua, D. Han, W. Zhao, Z. Wang, S. Yang, Physics Letters A, 383 (2019) 2097-2101.

[68] M. D. Asham, A. H. Phillips, Physica E: Low-dimensional Systems and Nanostructures, 113 (2019) 97-102.

[69] N. Suganthi, K. Pushpanathan, Transactions of Nonferrous Metals Society of China, 29 (2019) 811-820.

[70] X-L. Wu, R-S. Wang, J. Cheng, G-H. Zhong, X-J. Chen, Y. Gao, Z-B. Huang, Carbon, 136 (2018) 125-129.

[71] G. Cao, S. Chikara, X.N. Lin, E. Elhami and V. Durairaj ,Physical review. B, Condensed matter, 3 (2005) 71.

[72] M. B. Jungfleisch, W. Zhang, Axel Hoffmann, Physics Letters A, 382 (2018) 865-871.

[73] A. Patsopoulos, D. Kechrakos, N. Moutis, Journal of Magnetism and Magnetic Materials, 475 (2019) 171-175.

[74] Y.Y. Wang, C. Song, J.Y. Zhang, F. Pan, Progress in Natural Science: Materials International, 27 (2017) 208-216.

[75] A. C. Sreekantan, B. George, Smart Sensors and MEMs (Second Edition), (2018) 131-150.

[76] D. Bang, P. Van Thach, H. Awano, Journal of Science: Advanced Materials and Devices, 3 (2018) 389-398.

[77] H-W. Zhang, Z-R. Wei, Z-Q. Li, G-Y. Dong, Materials Letters 61 (2007) 3605-3607.

[78] K. Sato, H. K-Yoshida, “First principles materials design for semiconductor spintronics”, Semicond. Sci. Technol. 17 (2002), 367-376.

[79] H. K-Yoshida, K. Sato, “Spin and charge control method of ternary II–VI and III–V magnetic semiconductors for spintronics: theory vs. experiment”, J. Phys. Chem. Solids. (2003), 1447-1452.

[80] M. Born, J.R. Oppenheimer, Ann Physik, 84 (1927) 457.

[81] S. T. Epstein and C. M. Rosenthal The Journal of Chemical Physics 64, 247 (1976)

[82] W. Kohn, L.J. Sham “Self-Consistent Equations Including Exchange and Correlation Effects”, Phys. Rev. 140 (1965) 1133-1138.

[83] D.R. Hartree, ‘the wave mechanics of an atome with noncooulombic central field’, 24 (1928) 89-110.

[84] D. R. Hartree, ‘The Calculation of Atomic Structures ‘, Wiley, New York, (1957).

[85] T. Tsuneda, K. Hirao, The Journal of Chemical Physics 140 (2014) 18-513 .

[**86]** D. Ceperley, « Ground state of the fermion one-component plasma: A Monte Carlo study in two and three dimensions », Phys. Rev. B, 18 (1978) 3126-3138.

[87] D.M. Ceperly, B. J. Alder, “Ground State of the Electron Gas by a Stochastic Method”, Phys. Rev. Lett. 45 (1980), 566-569.

[88] S.H. Vosko, L. Wilk, M. Nusair, “Accurate spin-dependent electron liquid correlation energies for local spin density calculations: a critical analysis”, Can. J. Phy., 58 (1980), 1200-1211.

[89] J. P. Perdew and A. Zunger, « Self-interaction correction to density-functional approximations for many-electron systems», dans Phys. Rev. B, vol. 23 (1981) 5048-5079.

[90] L Hedin and B I Lundqvist, J. Phys. C: Solid State Phys. 4 (1971) 2064.

[91] W. Kohn, Reviews of Modern Physics, Vol. 71, No. 5 (1999) 1253.

[92] J.P. Perdew , J.A Chevary ,S.H. Vosko, K.A. Jackson, M.R. Pederson, D.J. Singh and C Fiolhais, Phys. Rev. B 46 (1992) 6671.

[93] J.P. Perdew, K. Burke, and M. Ernzerhof: Phys. Rev. Lett. 77 (1996) 3865.

[94] J.P. Perdew, J.A. Chevary, S.H. Vosko, A. Jackson, M.R. Pederson, D.J. Singh, C. Fiolhais, Phys. Rev B, 48 (1993) 4978.

[95] O.K.Andersen, Phys.Rev. B12 (1975) 3060.

[**96]** K.Schawarz, Density functional theory (DFT) and the concepts of the augmented plane wave plus local orbital (L) APW+lo metod, Institute for Material Chemistry, 2010.

[97] D.Singh, Phys.Rev.,B43 (1991) 6388.

[98] MACHIKANEYAMA2002v08: Akai H., Department of Physics, Graduate School of Science, Osaka University, Machikaneyama 1-1, Toyonaka 560-0043, Japan, akai@phys.sci.osaka-u.ac.jp.

[99] A. H. MacDonald, J. P. Perdew, S. H. Vosko, Solid State Communication 18 (1976) 85.

[100] H. Akai, P.H. Dederichs, Phys. Rev. B 47 (1993) 8739.

[101] H. Akai, Phys. Rev. Lett. 81 (1998) 3002.

[102] E. Salmani, A. Benyoussef, H. Ez-Zahraouy, E.H. Saidi, Chin. Phys. B 20 (8) (2011) 086601.

[103] P. SOVEN , Phys. Rev. 156 (1967) 809.

[104] H. SHIBA, Progr. Theor. Phys. 46 (1971) 77.

[105] M. E. J. Newman, G. T. Barkema, Monte Carlo Methods in Statistical Physics. Oxford: Clarendon Press , 1999.

[106] D. P. Landau and K. Binder, A Guide to Monte Carlo Methods in Statistical Physics. Cambridge: Cambridge University Press, 2000.

[107] B. A. CIPRA, "The Best of the 20th Century: Editors Name Top 10 Algorithms," SIAM News, vol. 33 (2000) 4.

[108] J. Dongarra and F. Sullivan, Comp. in Sci. Eng, vol. 2 (2000) 22.

[109] N. Boccara, Phys. Lett.A. vol. 94, (1983) 185.

[110] A. Benyoussef and N. Boccara, J. Appl. Phys , vol. 55, (1985) 1667.

[111] K.G. Wilson, Phys. Rev. B, vol. 4, (1971) 3184.

[112] J. Oitmaa, Phys. Lett. A, vol. 33, (1970) 230.

[113] K. Binder and P.C. Hohenberg, Phys. Rev. B, vol. 9, (1974) 2194.

[114] I. Syozi, Progr. Theor. Phys. vol. 6, (1951) 341.

[115] C. Domb, Phase Transitions and Critical Phenomena, M. S. Green, J. Lebowitz C. Domb, Ed. London: Academic Press, vol. 1-20, 1974-2000.

[116] H. E. Stanley, Introduction to Phase Transitions and critical phenomena. Oxford: Oxford University Press, 1971.

[117] M. Yeomans, Statistical Mechanics of Phase Transitions. Oxford: Oxford University Press,1993.

[118] W.Janke, Computational Many-Particle Physics, in: Lect. Notes Phys, R. Schneider, A. Weiße H. Fehske, Ed. Berlin Heidelberg: Springer, (2008) vol. 739.

[119] W. Lenz, Physikalische Zeitschrift, vol. 21 (1920).

[120] R. J. Baxter, Exactly solved models in statistical mechanics.: Academic Press Inc, 1982.

[121] E.Z. Ising, Phys. vol. 31 (1925) 253.

[122] R. B. Potts, Proc. Camb. Phil. Soc., vol. 48, (1952) 106.

[123] J. Ashkin and E. Teller, Phys. Rev., vol. 64, (1943) 5.

[124] H. E. Stanley, Phys. Rev. Lett., vol. 20, (1968) 589.

[125] L. Onsager, Phys. Rev., vol. 65, (1944) 117.

[**126**] N.W. Ashcroft and N.D. Mermin .Solid state physics .W. B. Saunders Company (1976).

[**127**] P.A .M. Dirac .Proceeding of the royal society A123 (1929) 714.

[128] N. Metropolis, A. Rosenbluth, A. Teller, E. Teller, J. Chem. Phys., vol.21 (1953) 1087.

[129] J. Hammersley and D. Handscomb, Monte Carlo Methods. London, New York: Chapman and Hall, 1964.

[130] S. Naji, A. Belhaj, H. Labrim, M. Bhihi, A. Benyoussef, A. El Kenz, J. Phys. Chem.C, vol.118, no. 9, (2014) 4924.

[131] K. Binder and D.W. Heerman, Monte Carlo Simulation in Statistical Physics.: Springer Verlag, 1988.

[132] S. Naji, A. Belhaj, H. Labrim, M. Bhihi, A. Benyoussef, A. El Kenz, Int. J. Quantum Chem. , vol. 114, (2014) 463.

[133] S. Naji, A. Benyoussef, A. El Kenz, H. Ez.Zahraouy, M. Loulidi, physica A, vol. 391,(2012) 3885.

[134] F. El Hallani, S. Naji, H. Ez-Zahraouy and A. Benyoussef, J. Appl. Phys. , vol. 114, (2013) 163909.

[135] R. Glauber, J. Math. Phys., vol. 4, (1963) 294.

[136] U. Wolff, Phys. Rev. Lett., vol. 62, (1989) 361.

[137] R. Swendsen and J.S.Wang, Phys. Rev. Lett., vol. 58, (1987) 86.

[138] T. Dietl, H. Ohno, F. Matsukura, J. Cibert, D. Ferrand, Science 287 (2000) 1019.

[139] O.D. Jayakumar, et al., Physica B 381 (2006) 194.

[140] S. Nakamura, GaN I, Semiconductors and Semimetals, in: J.N. Pankov, T. D. Moustakas (Eds.), GaN I, Semiconductors and Semimetals, Academic, New York, 1998, pp. 431–437.

[141] P. Kung, M. Razeghi, Opt. Electron 201 (2000) (Rev. 8).

[142] S. Das Sharma, Am. Sci. 89 (2001) 516.
[143] N. Hasuike, H. Fukumura, H. Harima, K. Kisoda, M. Hashimoto, Y.K. Zhou, H. Asahi, J.Phys.: Condens. Matter 16 (2004) S5811.
[144] H. Harima, J. Phys.: Condens. Matter 16 (2004) S5653.
[145] M.L. Reed, N.A. El-Masry, H.H. Stadelmaier, M.K. Ritums, M.J. Reed, C.A. Parker, J.C. Roberts, S.M. Bedair, Appl. Phys. Lett. 79 (2001) 3473.
[146] K. Ando, Appl. Phys. Lett. 82 (2003) 100.
[147] M. Zajac, J. Gosk, M. Kaminska, A. Twardowski, T. Szyszko, S. Podsiadlo, Appl. Phys. Lett. 79 (2001) 2432.
[148] Y. Uspenskii, E. Kulatov, H. Mariette, H. Nakayama, H. Ohta, J. Magn. Magn. Mater. 248 (2003) 258.
[149] B. Sanyal, S. Mirbt, J. Magn. Magn. Mater 1408 (2005) 290.
[150] H. Raibiger, A. Ayuela, R.M. Nieminen, J. Phys.: Condens. Matter 16 (2004) L457.

[151] K. Sato, H. Katayama-Yoshida, Jpn. J. Appl. Phys. 40 (2001) L334.
[152] K. Sato, H. Katayama-Yoshida, Jpn. J. Appl. Phys. 39 (2000) L555.

[153] H. Ohno, Science 281 (1998) 951.
[154] O. Goede, W. Heimbrodt, Phys. Stat. Sol. B 146 (1988) 11.
[155] F. Matsukura, A. Oiwa, A. Shen, Y. Sugawara, N. Akiba, T. Kuroiwa, H. Ohno, A. Endo, S. Katsumoto, Y. Iye, Appl. Surf. Sci. 113e114 (1997) 178.
[156] D. Chiba, A. Werpachowska, M. Endo, Y. Nishitani, F. Matsukura, T. Dietl, H. Ohno, Phys. Rev. Lett. 104 (2010) 106601.

[157] Jiyong Fu, J. Carlos Egues, Phys. Rev. B 91 (2015) 075408.

[158] Zh.A. Devizorova, A.V. Shchepetilnikov, Yu. A. Nefyodov, V.A. Volkov, I.V. Kukushkin, JETP Lett. 100 (2014) 102.
[159] Udon C. Mendes, M. A. G. Balanta, Maria J. S. P. Brasil, Jose A. Brum. arXiv:1509.07136 [cond-mat.mes-hall] (2015).
[160] P. Roma, D. Sangalli, G. Onida, A. Debernardi. (in press). PACS numbers: 71.45.Gm ; 75.70.Cn ; 75.50.Tj ; 78.20.Ls (2015).

[161] T. Kobayashi, I. Kuru, A. Hojo, T. Sugita, Nucl. Sci. IEEE Trans. 23 (1) (2007) 97e101, 0018-9499.

[162] I.R. Harris, N.A. Smith, B. Cockayne, W.R. MacEwan, J. Cryst. Growth 82 (1987) 450.

[163] V.W. Rampton, M.K. Saker, Phonon Scattering in condensed Matter V, in: Proceeding of the Fifth International Conference Urbana, 1986, pp. 138e140. M. Kleverman et al. Journal of Applied Physics 54, (1983) 814.

[164] W.E. Bron, Rep. Prog. Phys. 43 (1980) 301.

[165] W.E. Bron, Nonequilibrium phonon dynamics, Nato Asi B 124 (1985) 1.

[166] A. Ait Raiss, Y. Sbai, Z. Zarhri,L. Bahmad , A. Benyoussef, J Supercond Nov Magn DOI 10.1007/s10948-015-3179-2.

[167] Y. Sbai , A. Ait Raiss , E. Salmani , L. Bahmad , A. Benyoussef , Journal of Magnetism and Magnetic Materials 396 (2015) 153–159.

List of publications

- **Sbai, Y**., Ait Raiss, A., Bahmad, L., Benyoussef, A. Superlattices and Microstructures, 2017, 106, pp. 163-169
- **Sbai, Y**., Ait Raiss, A., Salmani, E., Bahmad, L., Benyoussef, A.Journal of Magnetism and Magnetic Materials, 2015, 396, pp. 153-159, MAGMAD1500798
- **Y. Sbai**, A. Ait Raiss, R. Bouachraoui , L. Bahmad, A. Benyoussef, Journal of Magnetism and Magnetic Materials (2020) MAGMA-D-20-00828.
- Bouachraoui, R., Ziat, Y., **Sbai, Y.**, ...Goumrhar, F., Bahmad, L. Journal of Alloys and Compounds, 2019, 809, 151785
- Raiss, A.A., **Sbai, Y.**, Bahmad, L., Benyoussef, A.Journal of Superconductivity and Novel Magnetism, 2018, 31(8), pp. 2661-2667
- Raiss, A.A., **Sbai, Y.**, Bahmad, L., Benyoussef, A.Journal of Superconductivity and Novel Magnetism, 2018, 31(8), pp. 2661-2667
- Ait Raiss, A., **Sbai, Y.**, Bahmad, L., Benyoussef, A.Journal of Superconductivity and Novel Magnetism, 2017, 30(10), pp. 2883-2889
- Hammi, M., Ziat, Y., Raiss, A., **Sbai.Y.**, Rhazouani, O.E., Slassi, A. Optik, 2017, 131, pp. 399-405
- Ziat Y., Slassi A., Zarhri Z., **Sbai Y.** Kenz A.E., Benyoussef A. Journal of Superconductivity and Novel Magnetism, 2016, 29(11), pp. 2979-2985
- Ait Raiss, A., **Sbai, Y.**, Zarhri, Z., Bahmad, L., Benyoussef, A. Journal of Superconductivity and Novel Magnetism, 2015, 28(12), pp. 3545-3552
- Ait Raiss, A., **Sbai, Y.**, Bahmad, L., Benyoussef, A. Journal of Magnetism and Magnetic Materials, 2015, 385, pp. 295-301, 59960
- Sbai S., Elyahyaoui A., **Sbai Y**., Bentayeb F. and Bricha M. R., J. Environ. Res. Develop, Vol.11 No. 03, January-March 2017.

ROYAUME DU MAROC
Université Mohammed V - RABAT - جامعة محمد الخامس - الرباط -
Faculté des sciences
كلية العلوم
CENTRE D'ETUDES DOCTORALES - SCIENCES ET TECHNOLOGIES

Résumé

La spintronique connait actuellement un avancement qui vise à améliorer les nouvelles hétérostructures semi-conductrices pour augmenter la densité des composants, améliorer les performances et baisser les prix. L'objectif est de fusionner des matériaux magnétiques avec des semi-conducteurs afin de trouver des matériaux pouvant fonctionner à une température supérieure à la température ambiante et d'avoir un couplage d'échange ferromagnétique. Dans cette thèse, nous avons réalisé, d'une part, une étude théorique utilisant des calculs Ab initio via le code (AkaiKKR) basée sur la méthode (DFT) avec les deux approximations LDA et GGA. Les principaux matériaux utilisés dans nos calculs sont le Nitrure de Gallium (GaN) et l'Arséniure de Gallium (GaAs), les deux dopé avec des métaux de transition (Mn, Fe and Ni) dans le but d'étudier leur propriétés électroniques, magnétiques et magnéto-optiques. Pour GaN, les DOS et les diagrammes de bands d'énergie ont été calculés, le ferromagnétisme a été observé avec un comportement half- métallique pour une concentration de 5% de Mn avec un gap direct. Tandis que pour GaAs les DOS ont été calculé aussi ainsi que les états magnétiques et la stabilité magnétique du matériau pour différents pourcentages de dopage, la rotation de Faraday a été aussi observé pour le dopage avec le fer (Fe). Confirmant ainsi ces deux DMS comme candidats principaux pour les applications spintroniques.

Mots-Clés : DMS; Calcules Ab initio ; Simulation Monte Carlo ; Propriétés magnétiques ; DOS ; structures de bandes ; Ferromagnétisme.

Abstract

There is currently a huge advancement in the spintronic field aimed at improving new semiconductor heterostructures in order to increase the components density, improve the performance and lower the prices. The objective is to fuse magnetic materials with semiconductors in order to find new materials that can operate above room temperature and have a ferromagnetic exchange coupling. In this thesis, we carried out a theoretical study using Ab initio calculations via (AkaiKKR) code based on the (DFT) method with the two approximations LDA and GGA. The main materials used in our calculations are Gallium Nitride (GaN) and Gallium Arsenide (GaAs), both doped with transition metals (Mn, Fe and Ni) so as to study their electronic, magnetic and magneto-optical properties. For GaN, the DOS and energy band diagrams were calculated and plotted, ferromagnetism was found with half-metallic behavior for a concentration of 5% (Mn) with a direct gap. While for GaAs the DOS were calculated as well as the magnetic states and the magnetic stability of the material for each (Fe) and (Ni) doping concentrations. The Faraday rotation was also observed for Ga(Fe)As. Thus, asserting these two DMSs as main candidates for spintronic applications.

Keywords: DMSs; Ab initio calculations; Monte Carlo simulation; Magnetic properties; DOS; Band Structures; Ferromagnetism.

✉ Faculté des Sciences, avenue Ibn Battouta, BP. 1014 RP, Rabat –Maroc
☎ 00212(05) 37 77 18 76 ☏ 00212(05) 37 77 42 61; http://www. fsr.um5.ac.ma